ARC-HEATED GAS FLOW EXPERIMENTS

FOR HYPERSONIC PROPULSION

APPLICATIONS

by

CHRISTOPHER MATTHEW ROSEBERRY

Presented to the Faculty of the Graduate School of

The University of Texas at Arlington in Partial Fulfillment

of the Requirements

for the Degree of

DOCTOR OF PHILOSOPHY

THE UNIVERSITY OF TEXAS AT ARLINGTON

December 2005

ACKNOWLEDGEMENTS

First and foremost, thanks go to my wife, Rosemary, for standing by me through this odyssey. Without her support, I would have had little choice but to abandon this effort, many times over. I have also been fortunate to have the love and support of my parents, Jerry and Bettye, and my brother Michael. My children, Daniel and Caitlyn, have encouraged me by showing interest in my work.

I probably learned as much from Jim Holland as anyone else on campus. Jonathon Liu was an excellent partner in the early facility development work and is one of the most loyal friends I have ever had. I am also thankful to have worked with Zack Boonjue. I received vital advice from John Poole. Contacting him was like finding the Rosetta Stone. I have great admiration for my friend, George Matsumoto, who made an enormous contribution to the ARC by developing the Supersonic Wind Tunnel. I have enjoyed working with Rod Duke, who has been an important asset to my research over the last few years. The courtesy of Dr. Gary Kinsel of the Chemistry Department in allowing free access to the gas chromatograph was very helpful. Dr. Frank Lu has been a great resource of information and advice. Finally, I appreciate Dr. Donald Wilson for his guidance, patience, and cheerfulness.

November 15, 2005

ABSTRACT

ARC-HEATED GAS FLOW EXPERIMENTS

FOR HYPERSONIC PROPULSION

APPLICATIONS

Publication No. _____

Christopher Matthew Roseberry, PhD.

The University of Texas at Arlington, 2005

Supervising Professor: Donald R. Wilson

Although hydrogen is an attractive fuel for a hypersonic air-breathing vehicle in terms of reaction rate, flame temperature, and energy content per unit mass, the substantial tank volume required to store hydrogen imposes a drag penalty to performance that tends to offset these advantages. An alternative approach is to carry a hydrocarbon fuel and convert it on-board into a hydrogen-rich gas mixture to be injected into the engine combustors. To investigate this approach, the UTA Arc-Heated

Wind Tunnel facility was modified to run on methane rather than the normally used nitrogen. Previously, this facility was extensively developed for the purpose of eventually performing experiments simulating scramjet engine flow along a single expansion ramp nozzle (SERN) in addition to more generalized applications. This formidable development process, which involved modifications to every existing subsystem along with the incorporation of new subsystems, is described in detail. Fortunately, only a minor plumbing reconfiguration was required to prepare the facility for the fuel reformation research. After a failure of the arc heater power supply, a 5.6 kW plasma-cutting torch was modified in order to continue the arc pyrolysis experiments. The outlet gas flow from the plasma torch was sampled and subsequently analyzed using gas chromatography. The experimental apparatus converted the methane feedstock almost completely into carbon, hydrogen and acetylene. A high yield of hydrogen, consisting of a product mole fraction of roughly 0.7, was consistently obtained. Unfortunately, the energy consumption of the apparatus was too excessive to be feasible for a flight vehicle. However, other researchers have pyrolyzed hydrocarbons using electric arcs with much less power input per unit mass.

TABLE OF CONTENTS

LIST OF ILLUSTRATIONS

LIST OF TABLES

CHAPTER 1

INTRODUCTION

1.1 Fuel Storage Issues for Hypersonic Vehicles

Hydrogen has often been cited as the fuel of choice for hypersonic air-breathing vehicles. One of the principal advantages offered by hydrogen is its very fast rate of reaction. Particularly for a scramjet vehicle, the fuel-air mixture flows rapidly though the combustion chamber, allowing only milliseconds for the mixture to react. In addition, hydrogen produces a higher flame temperature than most fuels. To add heat to the engine flow the flame temperature must be higher than the shock-heated air coming though the inlet system. In terms of energy output per unit mass, hydrogen has the highest output of any fuel. Accordingly, because specific impulse is defined as the uninstalled thrust divided by the fuel weight flow rate, the low mass of hydrogen, and the high exhaust velocity tend to yield higher specific impulse than other fuels. However, the key disadvantage of hydrogen is its low density. In fact, the energy content per unit volume of liquid hydrogen is considerably lower than any liquefied hydrocarbon (Table 1.1). For an equal volume, liquid methane actually contains 1.5 times more hydrogen atoms than liquid hydrogen. Figure 1.1 illustrates how the choice of fuel strongly affects the vehicle frontal area and overall size (Ref. 1).

Table 1.1 Energy Content of Various Fuels

Fuel	Lower Heating Value, kJ/kg	Energy Density, kJ/m^3
Hydrogen	120,000	8,491,000
Methane	50,200	20,920,000
Propane	45,600	23,490,000
Gasoline	44,500	31,150,000
Jet Fuel	42,800	34,560,000
Methanol	18,050	15,800,000

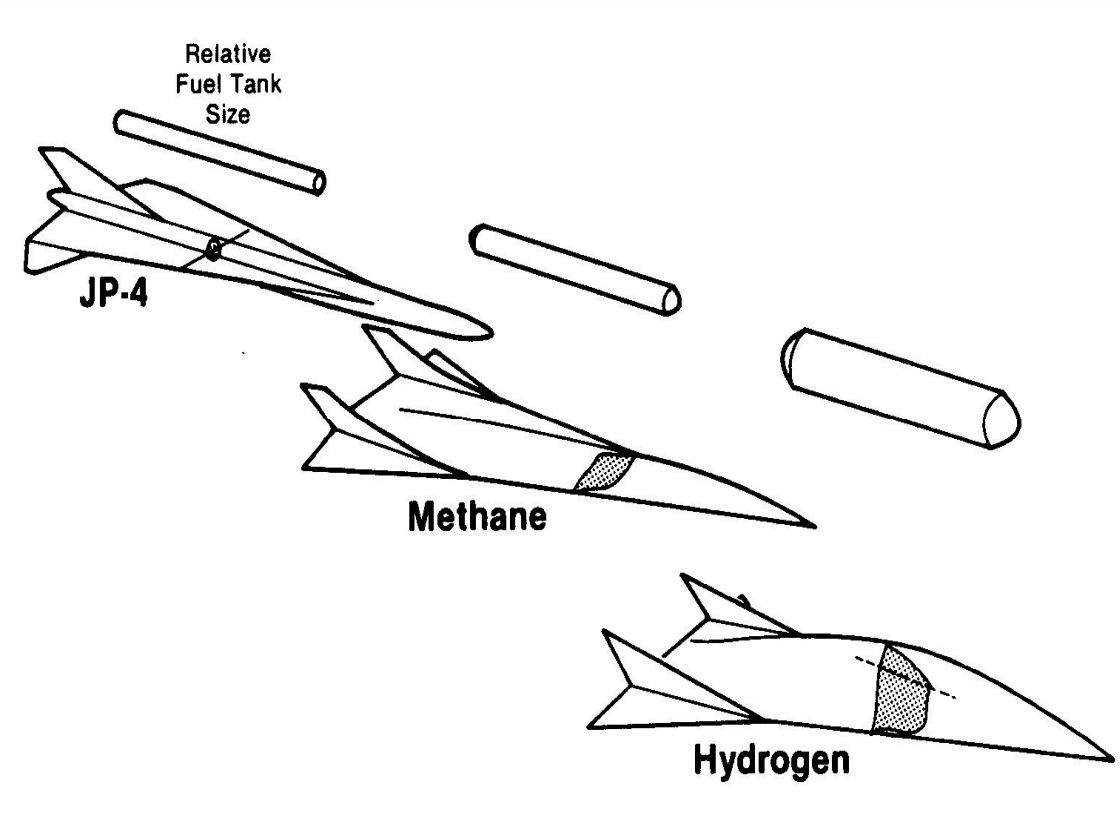

Figure 1.1 Relative Fuel Volume Requirements

Emanuel (Ref. 2) has argued that although hydrogen may be good choice for a rocket launch system, it is a poor choice for an air-breathing single-stage-to-orbit vehicle. This argument is based on the following points. For a rocket vehicle, the force opposing the engine thrust is mainly the vehicle weight. In contrast, the thrust of an air-breathing vehicle is primarily opposed by aerodynamic drag. Because drag depends strongly on frontal area, fuel volume has a much more significant effect on performance of an air-breathing vehicle than fuel weight. For the case of a hydrogen-fueled vehicle cruising in the atmosphere, much of the advantage in increased uninstalled thrust derived from using hydrogen rather than a hydrocarbon fuel, would be offset by the increased drag resulting from the bulkiness of the airframe due to the stowage of a low-density fuel. From Ref. 2, the dependence of drag on volume may be illustrated by the simple example of a symmetrical diamond-shaped airfoil at zero angle of attack with an attached bow shock and centered Prandtl-Meyer expansions (Fig.1.2). For this case, the drag per unit depth of the airfoil is

$$d = \tfrac{1}{2}\gamma p_\infty M_\infty^2 \frac{t}{\tan\phi} c_d$$

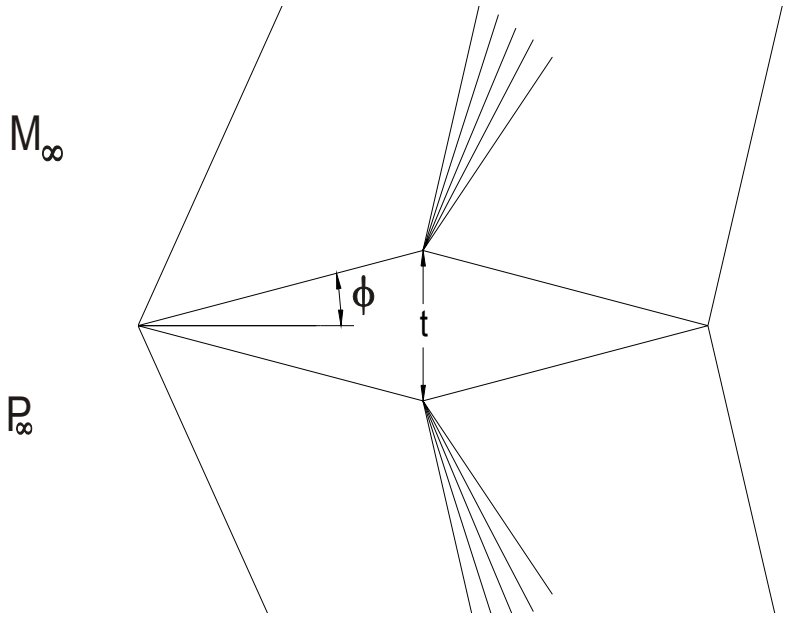

Figure 1.2 Diamond Airfoil at Zero Angle of Attack

The drag is directly proportional to the thickness, *t*. The same influence for projected frontal area would be expected in general for three-dimensional vehicle geometries. In addition, the drag coefficient of a vehicle generally tends to depend strongly on the fineness ratio, the length relative to the thickness. Accordingly, a large fuel volume results in either a large vehicle frontal area, which will produce excessive wave drag, or a very long slender vehicle, which tends to create excessive skin friction drag. Furthermore, a large frontal area is particularly disadvantageous for transiting the transonic regime. Another consideration is that over the course of its mission, a vehicle's weight will diminish as its fuel is consumed; however, the volume will stay constant unless drop tanks are used.

Although, drag is not as much of a factor for rocket launch vehicles as it is for air-breathing vehicles due to a rocket's lower dynamic pressure trajectory, some studies

have shown hydrocarbon fuels offer a small advantage in performance over hydrogen for the first stage (Ref. 3).

The difficulty involved with the storage and handling of 20 K cryogenic hydrogen is a secondary disadvantage to its use as a fuel. Many metals lose their strength at these temperatures. Moreover, some metals can also be embrittled by hydrogen. There is a historical case pertaining to the difficulties involved with a hydrogen-fuel aircraft: the Lockheed Skunk Works CL-400 "Suntan" project (Ref. 4). This project was eventually cancelled due to a shortfall in the projected range and the severe logistical difficulties in transporting and handling liquid hydrogen. The mission requirements for the CL-400 project were subsequently fulfilled by the hydrocarbon fueled A-12 and SR-71 aircraft. The Skunk Works' development data on handling, tank construction and materials for hydrogen were transferred to the Centaur program, the first liquid hydrogen-fueled space vehicle.

In contrast to hydrogen, methane only has to be cooled to 110 K to be liquefied and presents few difficulties in regard to material compatibility. Furthermore, the other hydrocarbons listed in Table 1.1 are easily stored as liquids at ambient temperatures. Propane requires a pressure vessel with a working pressure of only 45 psi, whereas the others do not need to be significantly pressurized. Ethane, the intermediate hydrocarbon between methane and propane requires a vessel rated to 600 psi to store as a liquid at ambient temperature, if not otherwise liquefied by refrigerating to 184 K. Pressurized and/or cryogenic fuel storage tends to restrict the parts of the airframe that may be utilized for fuel storage. For example, the cancelled CL-400 aircraft could only store its

liquid hydrogen in the fuselage, whereas the SR-71 can store its liquid JP-7 jet fuel in both the wings and the fuselage. Furthermore, in-flight refueling is commonplace with liquid hydrocarbons, but in-flight refueling with liquid hydrogen has not been openly demonstrated.

1.2 Fuel Reforming On-Board Hypersonic Vehicles

The on-board reformation of a hydrocarbon into a hydrogen-rich gas mixture is a concept that attempts to exploit the fast reaction rate and high flame temperature of hydrogen combustion while retaining the lower volumetric requirements of a hydrocarbon. Two methods of obtaining hydrogen from a hydrocarbon are steam reforming and pyrolysis. Industrial steam reforming of methane involves the following two reactions:

$$CH_4 + H_2O \rightarrow CO + 3H_2 \quad \Delta H^\circ = 206\,\text{kJ/mol}$$

$$CO + 3H_2 + H_2O \rightarrow CO_2 + 4H_2$$

Steam reforming also requires a catalyst. Using this process would require the vehicle to carry water, which may add undesirable weight to a vehicle. According to Ref. 5, 4.43 kg of water would be needed for each kg of methane.

Methane pyrolysis takes place in the absence of an oxidizer by the following endothermic reaction:

$$CH_4 \rightarrow C + 2H_2 \quad \Delta H^\circ = 75.6\,\text{kJ/mol}$$

The equation above is simplified; in practice other products are usually formed depending on conditions. The conventional approach to pyrolyze methane would be to

heat the gas to a temperature of 700 to 1200 °C. However, if a heat exchanger is used for this process, the hydrocarbon flow passages may become fouled with carbon or solid hydrocarbons. This problem is commonly known as coking. One approach to preventing coking is to use a partially oxidized fuel, such as methanol, which would tend to form gaseous CO instead of solid carbon or soot (Ref. 6). Coking is not only a problem in regard to heat exchanger blockage and heat transfer, but (at the very least) the substantial mass of the carbon needs to be ejected out of the vehicle to reduce the weight over the course of the mission. Moreover, if the carbon can be burned very rapidly, then it could contribute drastically to the combustion heat output. For example if methane were pyrolyzed, 30,200 kJ of heat would be released from hydrogen combustion, and 24,500 kJ would be released from carbon combustion for every kilogram of methane.

An alternative approach to thermally pyrolyzing a hydrocarbon in a heat exchanger is to use an electric arc heater to pyrolyze the fuel. This approach is the subject of the portion of this investigation sponsored by MSE Technology Applications. MSE-TA's interest in fuel reformation is part of their efforts to analyze the Russian vehicle concept known as AJAX. The complete details of the AJAX concept have not been publicly revealed by it originators. For this reason, much of the research published by others on AJAX involves some degree of speculation. In regard to fuel reformation, MSE-TA was interested in examining the premise that arc heaters act as fuel injectors for the AJAX combustor. Using an arc heater to pyrolyze a hydrocarbon offers two potential advantages over more conventional techniques. First of all, coking of the fuel

passages would not occur. Secondly, the non-hydrogen pyrolysis products would be heated to the extent that they would tend to burn rapidly. The injector configuration was believed to be very similar to a Linde (Huels-type) arc heater with the hydrocarbon gas being injected between the electrodes (Fig. 1.3). The hot flow of pyrolysis products would expand though the arc heater nozzle directly into the combustor. This idea behind this premise is not entirely peculiar; hydrocarbon-fed plasma injectors have also been proposed for scramjet engines as a source of ignition-promoting radicals (Ref. 7).

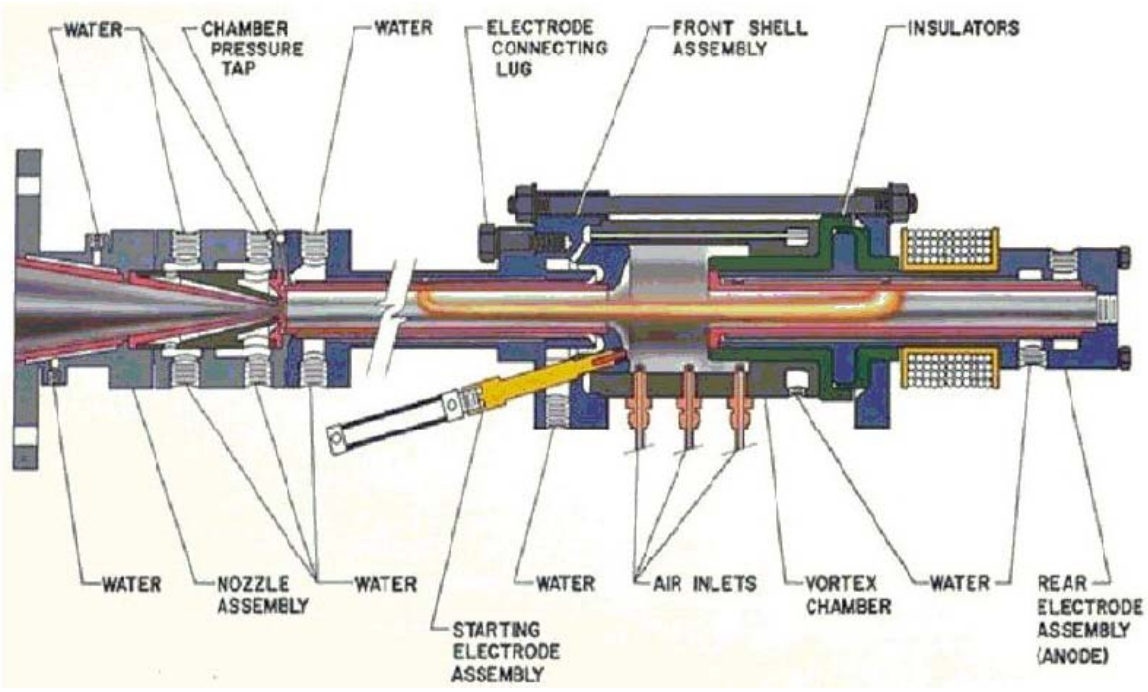

Figure 1.3 Linde Arc Heater

The AJAX concept was first proposed by Vladimir Fraishtad, of the Leninetz Holding Company, during the late 1980's (Ref. 8). The main idea of the AJAX concept is to use a magnetohydrodynamic (MHD) generator to extract kinetic energy from the inlet flow and then introduce this energy back into the flow leaving the combustor with

an MHD accelerator (Fig. 1.4). This is referred to as an MHD energy bypass injector ramjet engine. For an ordinary ramjet, the limiting operating speed is due to the inlet compression and fuel combustion heating the flow to the point that the energy goes into air molecule dissociation rather than being converted into useful energy for propulsion. The approach used with a scramjet to address this difficultly is to keep the static temperature of the air entering the combustor lower by keeping it supersonic rather than having it flow at a low subsonic Mach number. The inlet system of a ramjet or scramjet converts kinetic energy into enthalpy that (apart from heat transfer to the airframe and surroundings) remains in the flow. In contrast, the AJAX inlet converts a sizable portion of the kinetic energy into electricity that flows through conductors to the MHD accelerator (and other electric-powered subsystems). In this manner, the AJAX concept

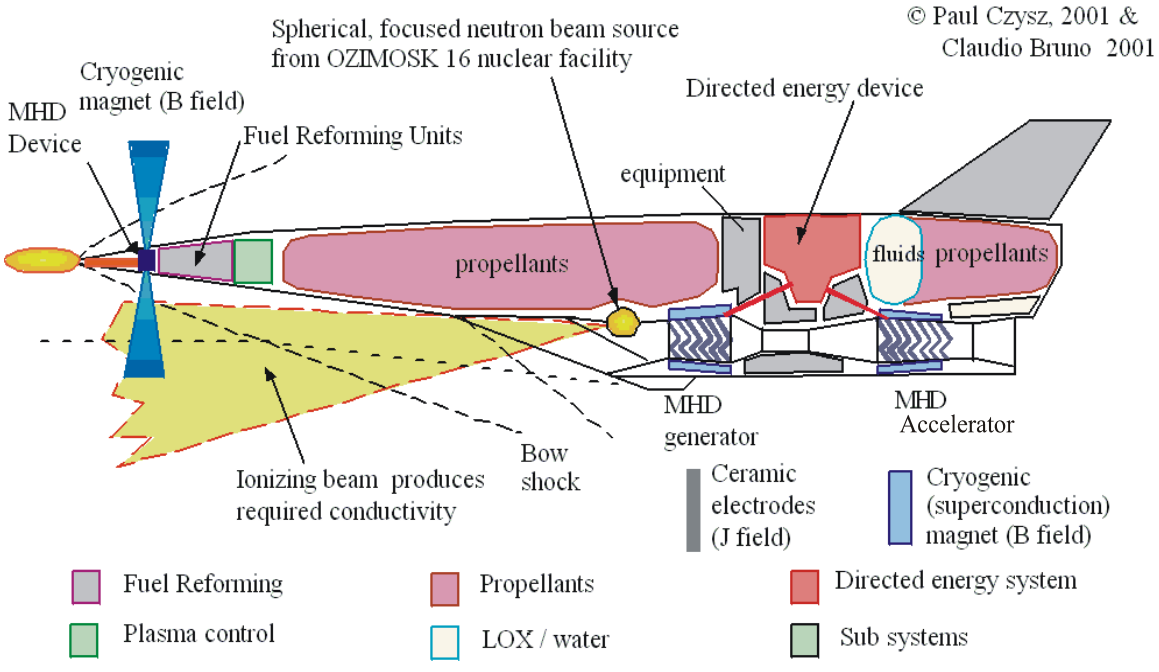

Figure 1.4 AJAX Schematic

alleviates much of the difficulty that is encountered with a ramjet or scramjet combustor. The air may be heated over a greater temperature difference before dissociation takes place and the fuel injection, mixing and combustion can take place at subsonic conditions for much higher flight Mach numbers than is possible for a ramjet.

The AJAX MHD bypass potentially makes the engine more adaptable to off-design flight conditions, which is highly advantageous considering the difficulty of making geometrical adjustments to actively cooled inlet or nozzle surfaces. In terms of the number and kinds of interacting subsystems, the AJAX concept is considerably more complex than a basic scramjet vehicle. However, these innovations have the potential of significantly relieving some of the extreme physical demands imposed by hypersonic air-breathing flight. The AJAX concept includes manipulation of the flow approaching the nose of the vehicle, by an energy or particle beam. This technique creates a disturbance in the flow further upstream of where a shockwave would normally form in front of a vehicle. The literature suggests that wave drag reductions of approximately 50% are possible using this technique (Ref 9).

The very high heat sink capacity of cryogenic hydrogen is an important justification for its use as a fuel for a scramjet. In regard to airframe and engine cooling, the heat sink capacity ($C_p\Delta T$) of liquid hydrogen exceeds that of most fuels. The specific heat of hydrogen is quite high and it can be heated from 20 K up to the material limits of the plumbing, giving a very large ΔT. Hydrocarbon fuels can potentially provide a heat sink for airframe and engine heating, by using this energy to thermally

pyrolyze (crack) the fuel. However, this issue of heat sink capability is outside the scope of this study.

According to Ref. 5 for an atmospheric cruise mission, an AJAX vehicle using a reformed hydrocarbon fuel can potentially equal or exceed the performance of a hydrogen-fueled vehicle. Figure 1.5 from Ref. 5 compares the propellant weight of a reformed hydrocarbon-fueled vehicle with a hydrogen-fueled vehicle. Apparently, the lower drag of the AJAX vehicle, due to both its reduced volume and flow manipulation, results in a vehicle with about the same propellant weight as a hydrogen-fueled vehicle. Figure 1.6 shows the huge difference in the volume requirements for the two cases. The size of a vehicle is usually a major factor influencing its manufacturing cost. If on-board hydrocarbon pyrolysis proves feasible, then a hydrocarbon-fueled hypersonic vehicle would possess substantial advantages in cost and performance over a hydrogen-fueled vehicle.

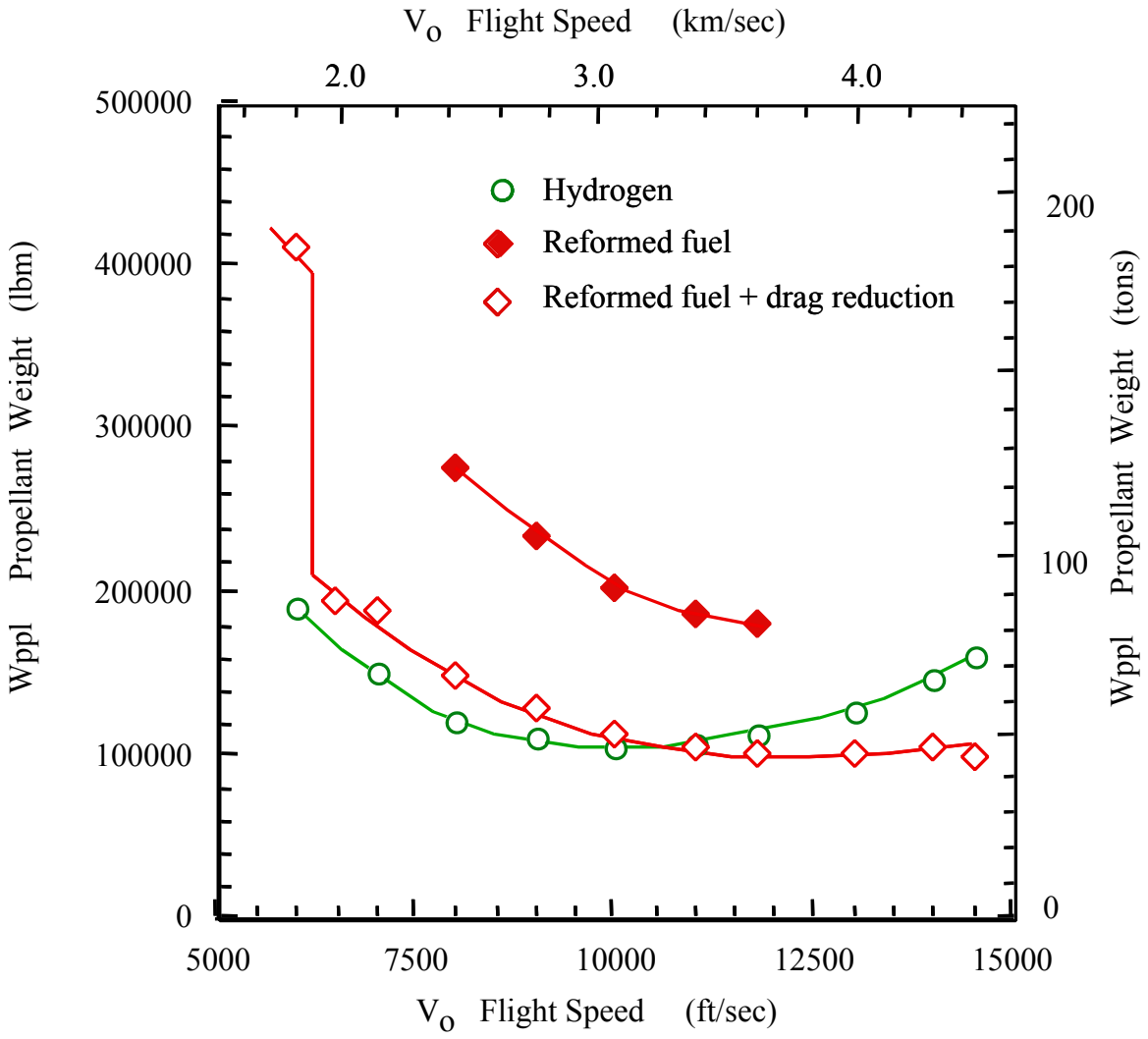

Figure 1.5 Propellant Weight Predictions

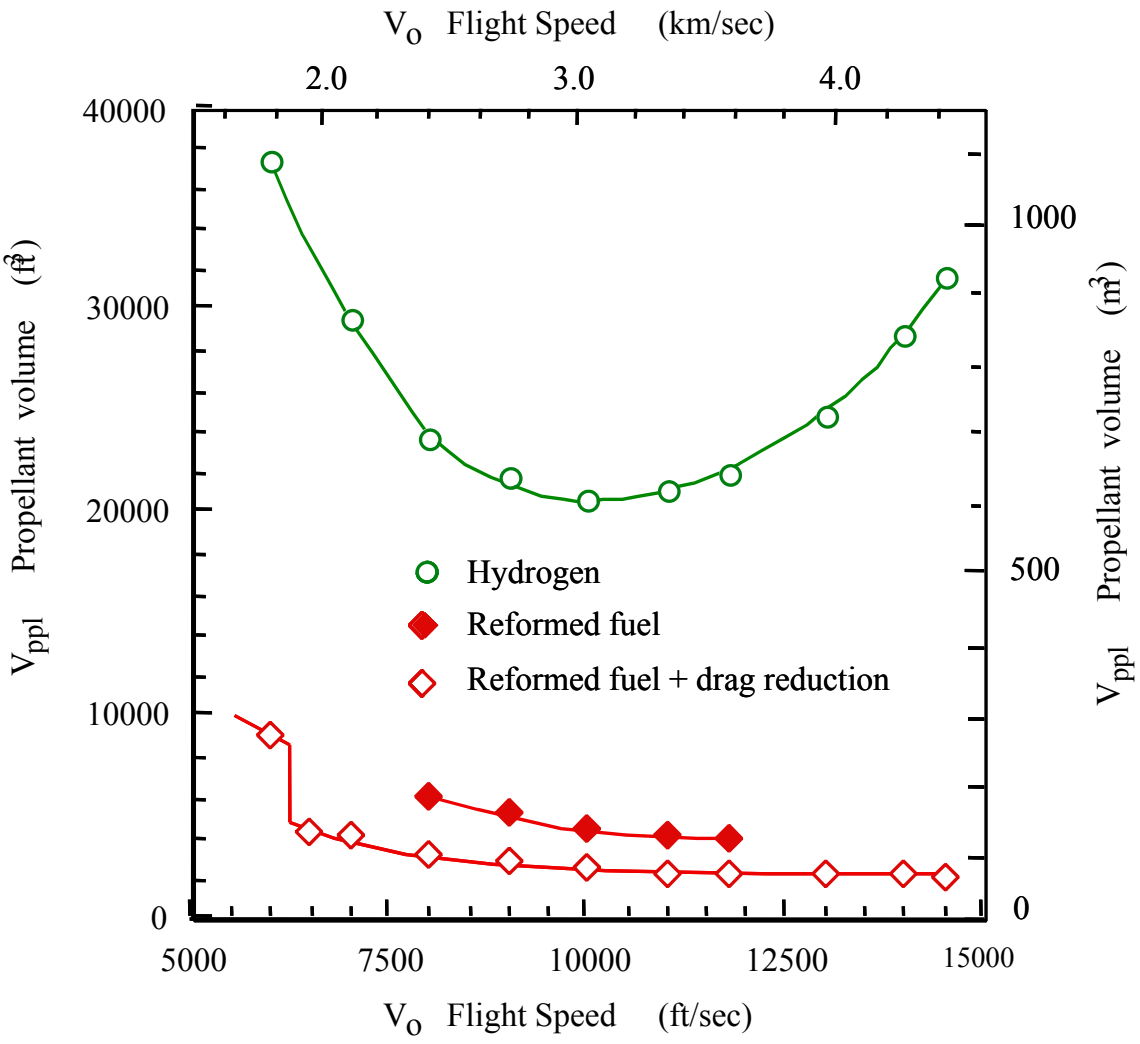

Figure 1.6 Propellant Volume Predictions

1.3 Objectives of the Fuel Reformation Investigation

The first of the original objectives of the study was to modify the facility to inject methane rather than nitrogen into the arc heater, to allow it to function as a chemical processing device. The next objective was to develop an instrumented diagnostic apparatus in order to verify that pyrolysis occurs, determine the chemical composition at the arc heater nozzle exit and also give some indication of the hydrogen yield. If these measurements proved successful, the next goal was to examine the factors (such as pressure, mass flow, current, and voltage) that influence the chemical composition and process efficiency. Another important objective in regard to studying the feasibility of the technique was to determine the power requirements for the process.

Once the experiments actually began the approach had to be adjusted to address the problems that were encountered, but the remaining objectives of determining product composition and power consumption were still pursued.

CHAPTER 2

FACILITY DEVELOPMENT

2.1 Research Motive for Facility Development

The original goal of the arc heater research was to develop a hot-flow technique to more accurately simulate single expansion ramp nozzle (SERN) flows. During the National Aero-Space Plane (NASP) program, the companies designing the scramjet vehicles encountered difficulty in predicting performance. For much of the trajectory, the net thrust of the vehicle was reportedly only a marginal difference between the nozzle thrust and the overall drag of the vehicle. For instance, suppose 1,000,000 pounds of predicted gross thrust is opposed by 900,000 pounds of drag. This would give 100,000 pounds of net thrust to accelerate the vehicle. But what if the gross thrust was over-predicted by 2%? This would result in a 20% error in the net thrust of the vehicle with a corresponding shortfall in performance. Moreover, it is important to accurately predict the moment resulting from the nozzle pressure distribution to correctly analyze the stability and controllability of a scramjet vehicle. Unfortunately, there are issues that complicate the prediction of the nozzle flow for this situation. First of all, the flow, which consists of products of hydrogen-air combustion, is not likely to be in thermal or chemical equilibrium. Rizkalla (Ref. 10) found that in numerical simulations, the resulting nozzle force and moment coefficients were strongly influenced by the

underlying assumption of either finite-rate chemistry or frozen chemistry of the flow. Experimental studies of SERN flows have relied primarily on cold flow tests using either air or a simulant argon-freon mixture. This approach has some inherent inadequacies in that the properties of the hot exhaust gas in the actual case would differ considerably from a cold-flow simulation.

In order to provide a more accurate SERN simulation, oxygen and hydrogen were to be added to the arc heater's primary flow of nitrogen to obtain the same basic chemical species that would result from hydrogen combustion in shock-heated air. In this manner, the arc heater could potentially match both the gas dynamic state of the actual flow as well as the flow chemistry. Until April 2003, when the investigation shifted to fuel reformation, the arc-heated wind tunnel facility was developed with the goal of eventually conducting the hot flow SERN simulation (Fig. 2.1). When the opportunity was presented to conduct the fuel reformation research, the existing facility fortunately only required minor plumbing reconfiguring to accommodate this new investigation. The facility changes are completely reversible, so with a little more development, the hot-flow simulation technique could be attempted.

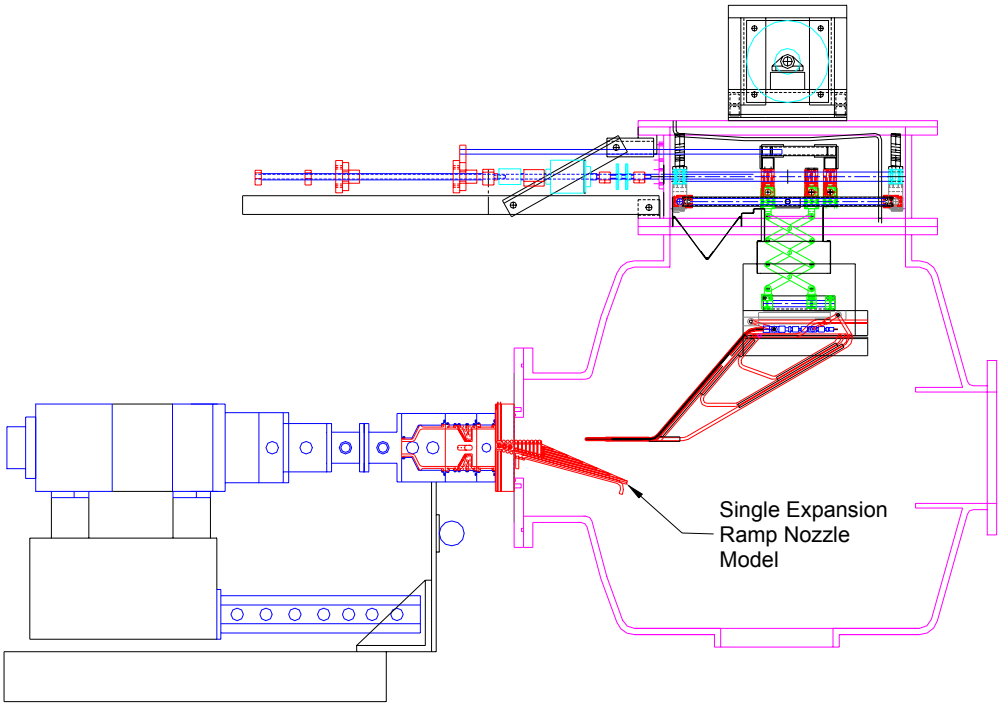

Figure 2.1 Arc Heater Configured for SERN Experiment

2.2 The Thermal Dynamics F-5000 Arc Heater

The Thermal Dynamics F-5000 arc heater is vortex-stabilized and nominally rated at 2.0 MW. A cross-sectional view of the heater is shown in Figure 2.2. The anode, cathode, plenum chamber, and nozzle inserts are fabricated from tellurium-copper, and mounted in a brass housing that provides the necessary cooling water passages. The anode and cathode sections are electrically separated by a boron nitride insulator ring at the N_2 injection station. The anode section, as well as the subsequent downstream components, are grounded, whereas the cathode section is electrically floating. High-pressure nitrogen gas is injected tangentially into the arc chamber through a swirl plate at the anode/cathode interface. This provides an intense vortex

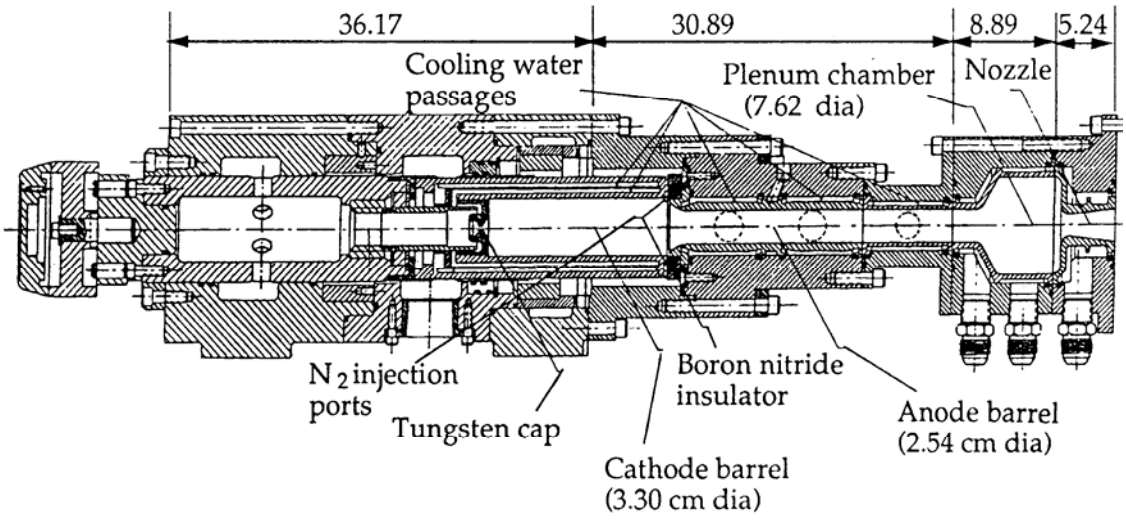

Note: All dimensions in cm

Figure 2.2 Cross-Sectional View of Thermal Dynamics F-5000 Arc Heater

flow field within the arc chamber that centers the arc between a tungsten electrode at the base of the cathode barrel and the rotating arc termination point at the entrance to the plenum chamber downstream of the anode barrel. The F-5000 that is now at the ARC (Fig 2.3) was originally used at the US Air Force Arnold Engineering Research Center (AEDC) during the LORHO program to investigate the feasibility of using MHD-augmented, electric arc heaters for hypersonic test facilities (Ref. 11). After delivery to AEDC, the basic design was upgraded in order to increase the power rating to 3 MW. The depth of the cathode was increased to 11.75" and supplemental gas injection ports were added to the anode barrel.

This F-5000 was eventually donated to UTA, where it sat in storage for several years. Eventually, a 1.6 MW DC power supply was purchased to power the arc heater. Sometime after this, the F-5000 was moved to the ARC and connected to water,

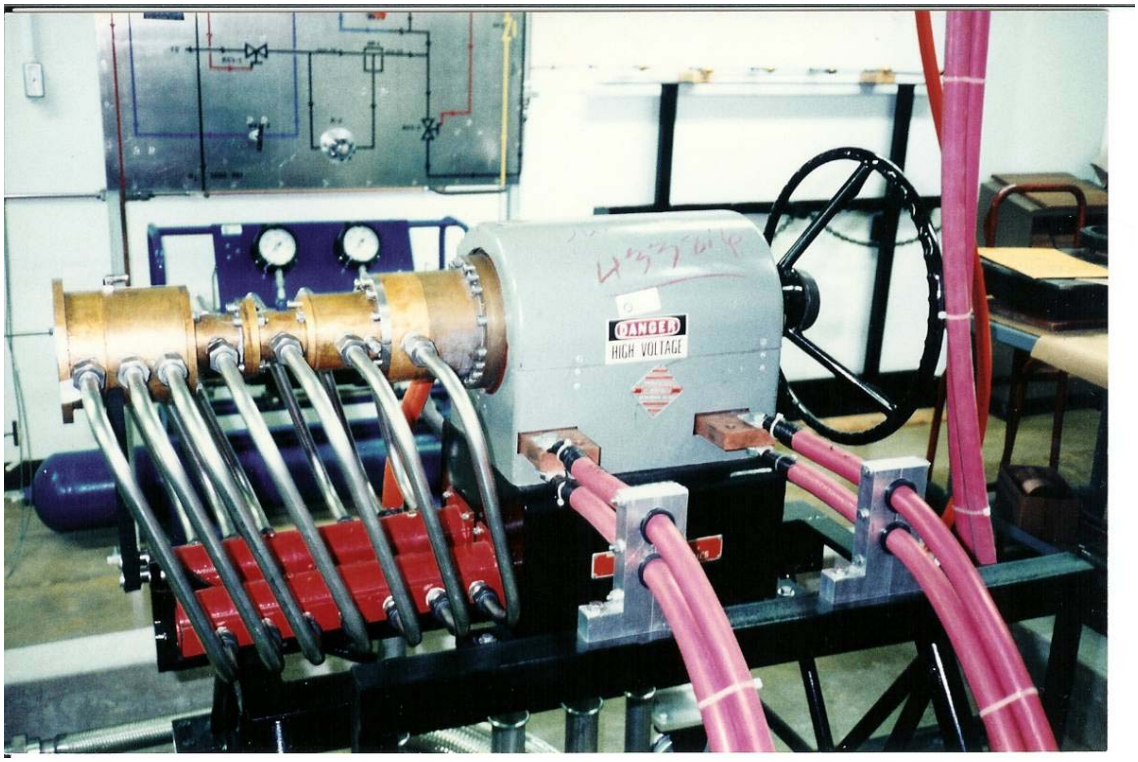

Figure 2.3 F-5000 Arc Heater Circa 1994

nitrogen and high voltage lines. Although all of this occurred before 1994, there was a substantial amount of facility development necessary to eventually get the arc heater to the point were it could be operated in the fall of 1996. Although the arc heater was already connected, the cooling water system and power supply were far from being operational. Accordingly, the F-5000 sat idle while these other systems were worked-on.

Before the leak testing process began, there was a strong hesitation to take the F-5000 apart due to the assumption that it was assembled correctly, and the lack of any detailed instructions for doing so. However, the issue of cooling passage leaks due to

missing or damaged o-rings eventually made this action compulsory. The arc heater had to be disassembled and reassembled a few times to finally eliminate all of the leaks.

There came a time when the facility finally seemed to be ready to test fire the arc heater, but this was followed by dozens of unsuccessful attempts. After months of fruitless effort, a former Thermal Dynamics engineer, John Poole, was contacted for consultation. Much of the difficulty was due to unapparent problems with the ignition system (which are discussed in Chapter 2.3). However, there was still one mysterious problem with the arc heater itself that was finally solved with John Poole's advice. The arc heater had failed to start due to there being too large of a gap between the electrodes. The F-5000 features a screw mechanism, turned with an automotive steering wheel, for moving the cathode to or away from the anode. Before the high frequency ignitor was introduced, a brave technician would actually start the arc by making the cathode touch the anode and then rapidly rotating the wheel to pull it back. Although this starting method was discontinued, the adjustment mechanism was retained in the design. The Thermal Dynamics manual gave instructions for setting the electrode gap: turn the steering wheel carefully until the electrodes bump together and then turn it back two turns. When this was tried, it felt as if the electrodes were bumping together when in fact the resistance was actually due to the cathode assembly pushing against an o-ring seal. It was discovered from measurements with the anode section taken off, that the electrodes had been about an inch apart rather than the proper 0.02-inch gap width. Considerable strength was required to turn the wheel to move the cathode beyond the o-

ring seal to the vicinity of the anode. Once the gap was properly adjusted, the arc heater ran on the very next attempt.

Since this time, the arc heater itself has rarely been a source of problems (Fig. 2.4). A thoriated tungsten cathode cap did fail during the shakedown testing, but this went unnoticed until John Poole saw video footage of some test runs. According to John

Figure 2.4 F-5000 Firing During Shakedown Testing

Poole, the failure was probably due to a faulty silver braze joint between the tungsten and copper. Fortunately there were spares available to replace this piece. There have also been instances in which the boron nitride insulator rings have been damaged or broken. The recent purchase of a borescope has made it possible to inspect the electrodes without disassembling the arc heater. A performance map was created to summarize the results of the shakedown testing (Fig. 2.5).

The F-5000 is protected by a set of analog circuits that monitor each critical process (primarily cooling water and gas flow) in order to automatically turn-off the

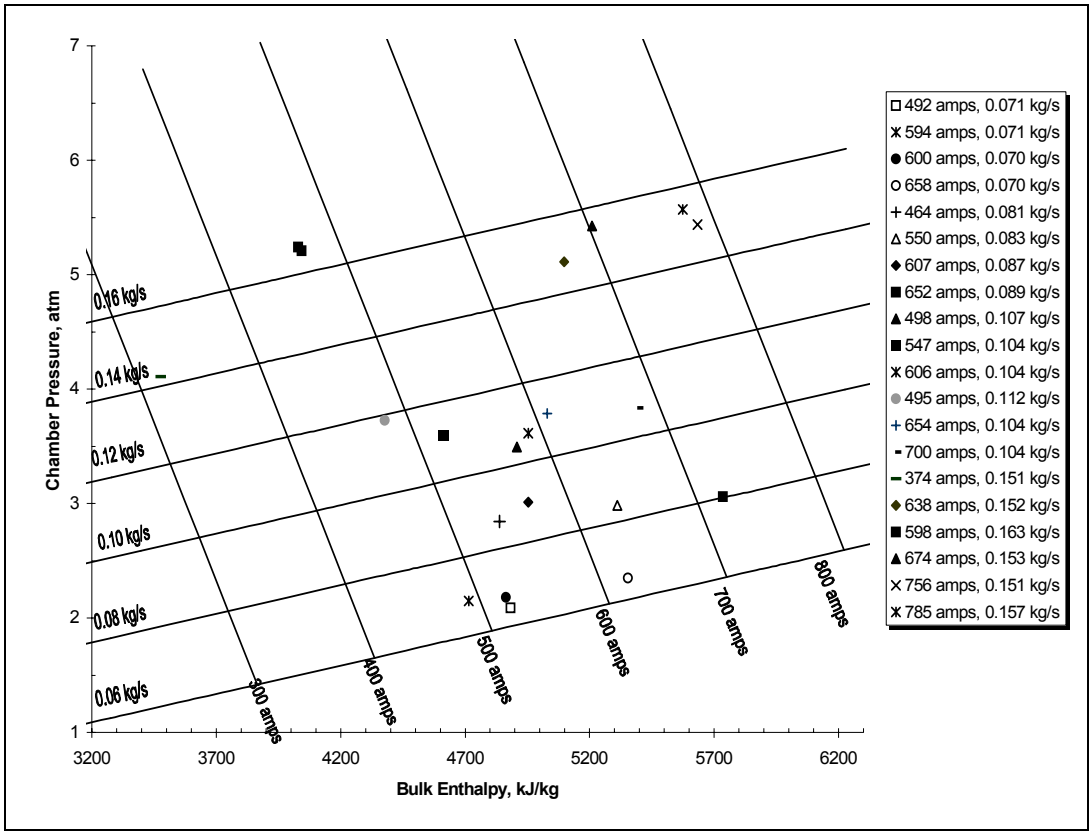

Figure 2.5 F-5000 Performance Map

power to the arc heater within 20-30 milliseconds. These circuits also are very effective in preventing damage due to an operator error. In fact, there have probably been at least three or four instances of damage being prevented by the power being kept off when there was insufficient (if any) gas flow to the arc heater. These "safeguard" circuits were designed and assembled by Sarrat Boonjue and are described in detail in Ref. 12.

The only difficulty with the safeguard circuits has been reliability. The circuits have actually worked properly about 90% of the time during test run operations. However, for those days when they did malfunction, it was very hard to resist the temptation to disable them by attaching a jumper wire across the master shutdown relay. Because of this issue, pressure switches have been purchased for the purpose of

eventually incorporating a redundant protective interlock system into the facility. The advantages to this approach would be simplicity and robustness. One possible disadvantage to a switch-based system is that it may be somewhat slower responding than the safeguard circuits. Ideally, both the safeguard circuits and the redundant switch based interlock system would be enabled in preparation for a test run. However, for those times when the primary protective circuits are not working, and it is imperative to conduct a test run, a selector switch could be installed to enable only the back-up interlocks.

2.3 Halmar 1.6 MW DC Power Supply

The Halmar 1.6 MW DC power supply was purchased and installed in 1989, prior to this author's involvement with the facility, which began in 1994. Operational testing of the power supply had to wait until the cooling system was functioning properly. As may be seen in Figure 2.6, the power supply, which is housed in a walk-in enclosure, is the largest component of the facility. The power supply was the most difficult facility system to work on, due to the dazzling quantity of electronics it involves. The power supply converts three-phase 2400V AC to DC output at levels up to 800 Amps and 2000 V. The rectification is accomplished with a 12-SCR bridge connected to the transformer. The power supply controls are capable of stabilizing an arc (which is not naturally stable) and holding it at a constant current level by making dynamic adjustments.

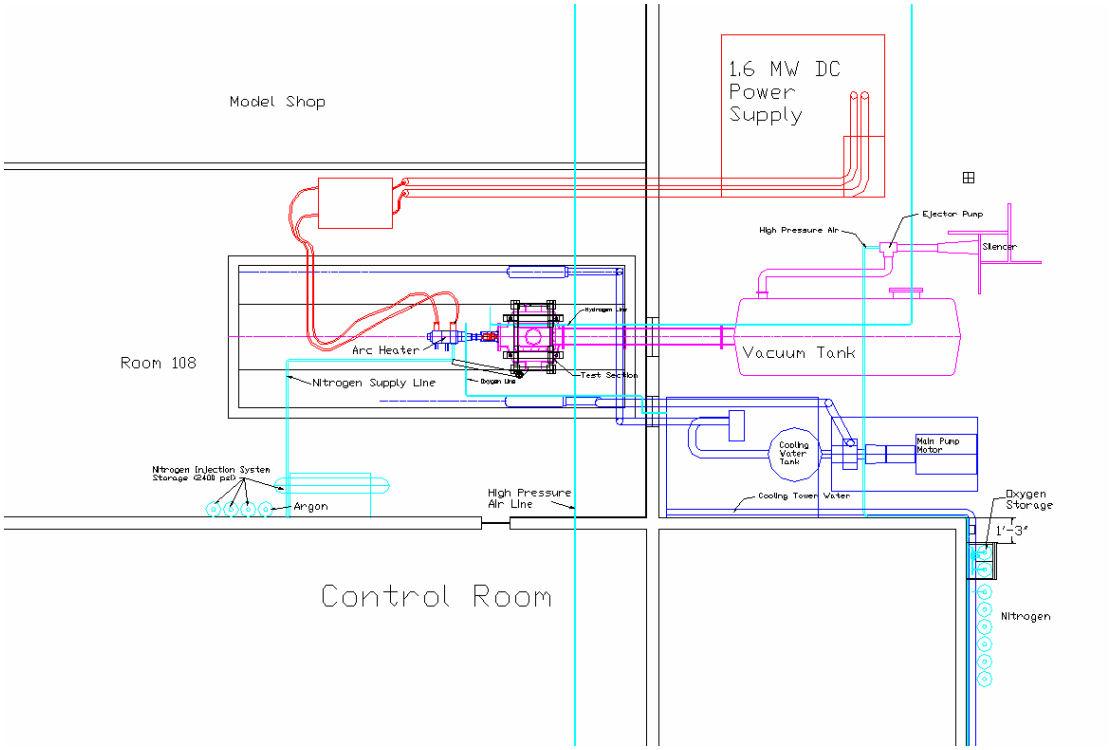

Figure 2.6 Top View of the UTA Arc-Heated Wind Tunnel Facility

Unfortunately, in many respects, the power supply was not set-up properly to work with just the turn of a key. The purchase contract with Halmar called for a no charge set-up service visit for the power supply within a year of delivery. Unfortunately, this time period had long expired by the time cooling water was available to the power supply. At the time, it seemed reasonable to try to save thousands of dollars by calibrating and setting-up the power supply without on-site service from Robicon. (Halmar changed its name to Robicon after merging with another company. Presently, the company is known as ASI Robicon.) As far as anyone knew, the power supply was almost ready to run in its delivered condition.

One thing that had to be determined was whether the power supply was actually connected to 2400 V, three-phase power from the utility grid. Fortunately, there is a fairly safe method of checking for high voltage AC in the power supply's fuse compartment that does not require any contact with conductors. A $10 device called a "tick tracer" or AC voltage detector readily indicates the presence of alternating current by sensing the induced fluctuating magnetic field. To detect 110V in a wall socket, one has to practically insert the tip of the instrument into the socket. However, to detect 2400 V AC one only has to get the voltage detector within a few feet of the conductors to pick-up the strong magnetic fields. (This device will not detect DC voltage! The reader should understand that dangerous DC voltage will go completely unnoticed if one tries to misuse a tick tracer in this fashion.) It so happened that the power supply was not actually connected initially; fuses had to be inserted into the main switchgear by electric utility personnel to make the connection.

Once the power supply was connected to the grid, problems were then encountered in satisfying all of the power supply control interlocks. The interlocks hold the main contactor open; so as to not allow high voltage to the main transformer, until all the proper conditions are met. The power supply controls and interlocks are numerous enough to fill an entire sheet of the electrical plans. Some of the trouble in clearing the interlocks was caused by door switches not engaging properly. The door switches are there to turn off the high voltage if someone tries to enter the enclosure at an inopportune time. This problem was corrected by remounting some of the door switches. Another malfunction was one of the water flow switches not making contact

when there was actually sufficient flow. This flow switch had to be taken apart, and readjusted to get it working properly. Finally, a switch that is depressed when the manual disconnect lever is put in the closed position had to be adjusted so that it was closer to the tab that pushes it. The disconnect lever still has to be pulled down firmly to engage this switch. When the interlocks are cleared and the contactor is closed, resetting the alarms should make the white "POWER SUPPLY READY" light illuminate on the Halmar control room panel.

In order to test the power supply before the arc heater was ready, some alternative resistive load had to be provided. Of course, a megawatt capacity resistor is not exactly a common off-the-shelf item, but a water barrel resistor can be made by simply placing two electrodes into a container of water. A water barrel resistor was designed, consisting of two long, narrow plates of aluminum scrap fastened to a Lucite and wooden frame (Fig. 2.7). A fifty-gallon trash barrel was borrowed to complete the load resistor.

Figure 2.7 Water Barrel Resistor

On June 7, 1995, the power supply was finally successfully operated with a water barrel resistor. At this juncture, the main effort turned to getting the arc heater ready to connect to the power supply.

There were a couple of important tasks to complete before attempting to operate the power supply with the arc heater. First of all, as discussed in Chapter 2.2, interlocks needed to be developed to protect the arc heater from damage due to a gas or water flow interruption resulting from a system failure or operator error. Secondly, the arc ignition system had to be made operational. An ignition system is necessary because the spacing between the electrodes of the arc heater (0.02 inches) often requires more than the DC voltage output of the power supply to ionize the nitrogen flowing though this gap. Accordingly, Thermal Dynamics installed a welding-type arc igniter, containing two 5000 Volt transformers in series in order to put a 10,000 V ripple on top of the DC power supply voltage (Fig. 2.8). This same arc ignition system was donated to UTA along with the arc heater. Unfortunately, this arc initiation device had hidden defects. First of all, the spark gap, which acts as a high voltage switch, was improperly connected. Once the spark gap connection was corrected, the ignition circuit could then produce a 10,000 V ripple. However, there was still a much more serious underlying problem. The circuit contains capacitors and a large choke coil that is supposed to block the 10,000 Volt ripple from going back into the power supply. Although the coil had no visibly apparent damage, it actually had shorted windings. When the igniter was engaged, the 10,000 V ripple went back into the power supply with very little attenuation. This level of high frequency voltage was intense enough to affect portions

of the power supply control circuitry that had no actual physical connection with the high power lines. Apparently, the affected circuits merely had to be close enough for the

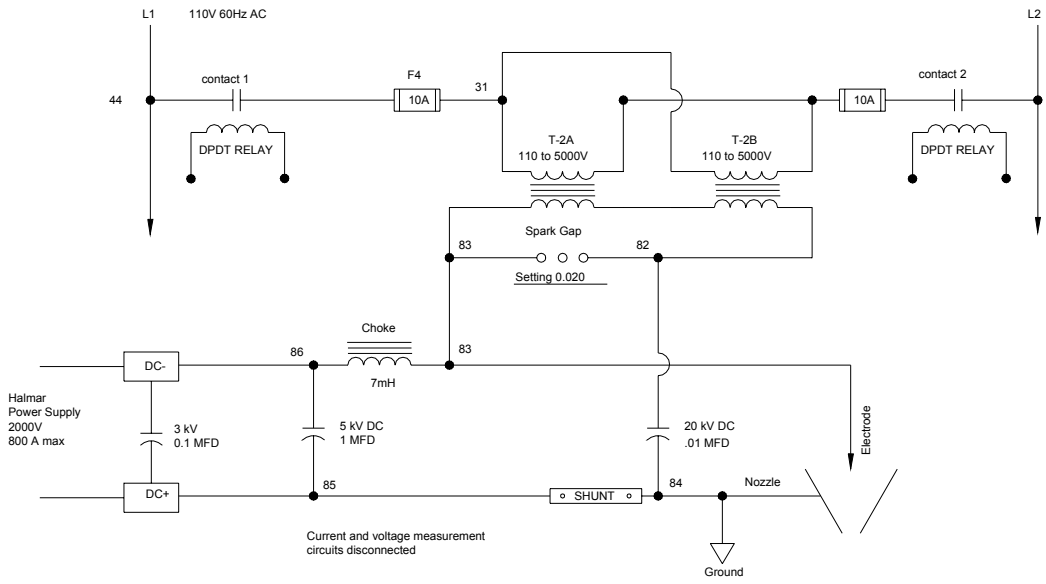

Figure 2.8 Thermal Dynamics Arc Ignition System Diagram

ripple to jump over to them or perhaps magnetically influence them. Unfortunately, some of the power supply control circuits were directly connected to this flyback voltage, which had the electrically equivalent effect of a jackhammer. The main control board, called the plasma interface board, has two inputs from the high power lines, one indicating current and the other indicating voltage. The current feedback signal is from a calibrated shunt, which will yield a proportional voltage drop with the amount of current flowing though it. For example, a current of 800 A yields a 100 mV signal from the shunt to the plasma interface board. The voltage feedback signal comes from a

series of step-down resistors connected to the power supply output terminals. For this measurement, the maximum open circuit voltage of the power supply, 2380 V DC, corresponds to a 1.5 V feedback signal to the plasma interface board. The first hint that the ignition flyback was damaging the power supply controls, came when the control panel meters began giving obviously false readings, such as 800 A when the contactor was not even closed. Through phone calls with a Halmar engineer, it was determined that the isolation amplifiers on the plasma interface board had failed. These isolation amplifiers were replaced, and the attempts to run the arc heater were resumed. The panel meters started displaying faulty readings again, but this time, new isolation amplifiers did not resolve the problem. The plasma interface board was sent to the factory where it was found to be damaged beyond repair. Unfortunately there was little choice but to purchase a replacement plasma interface board for about $5,000. At this point, the ignition system choke coil came under suspicion. After a newly acquired inductance meter gave a low value for the choke coil, the coil was taken to Nova Magnetics to be evaluated. Nova Magnetics confirmed that the choke coil was shorted, and accordingly replaced the windings around the original iron core. To prepare the facility for resumed attempts at operation, the choke coil was reinstalled and the replacement plasma interface board was connected and calibrated.

In an effort to further improve the filtering of the flyback voltage, the capacitors in the igniter box were changed to have greater capacitance and a new capacitor was installed between the terminals of the power supply. At about this time period, the Electrical Engineering Department provided very helpful advice regarding safety and

problems with the ignition system. In accordance with this advice, a 14' long solid copper rod was driven into the soil under the floor beneath the arc heater to provide a robust, low inductance ground for the arc heater. In addition, a grounding stick, for discharging any remaining static charge on the power terminals (so they may be safely handled) was also attached to this ground rod. In studying both the arc heater and power supply electrical plans, Dr. Nunnally, of the Electrical Engineering Department, discovered that the polarity of the power supply output was wrong for the F-5000 arc heater. Evidently, the F-5000 differs from most industrial plasma torches, in that it has the anode grounded rather than the cathode. This important detail was overlooked by Halmar during the design process, so it was necessary to make a field modification to the power supply to correct its polarity. The polarity was changed by switching the high power wire connections rather than reconfiguring the SCR's. This involved relocating the current measurement shunt from its original location, which had one end bolted to the bridge and the other bolted to the negative terminal, to an entirely different location. Drawings were submitted to Robicon for a new shunt mounting, and they made the copper pieces and supplied the standoffs.

In July 1996, an attempt was made to run the arc heater that resulted in a brief electrical fire in the igniter unit. It appeared that a crack in the old insulation of one of the wires going to the spark gap allowed an arc to form between the wire and a metal noise suppression enclosure surrounding the spark gap unit. The original spark gap and the 5000V transformers were destroyed and the choke coil windings were again shorted.

A new spark gap and transformers were installed along with the rewound choke coil to repair the ignition system.

With the ignition system repaired and the arc heater electrodes properly adjusted, the power supply was finally successfully used to fire the arc heater in October 1996. A brief period of shakedown testing of the facility continued into November. The shakedown testing was then suspended to correct a flow restriction problem with the nitrogen injection system. When testing resumed, the high flow, high power part of the arc heater's operating envelope was explored. As the gas injection flow rate was increased, it became much more difficult to get the arc started with the ignition system. Sometimes the igniter would have to be engaged for several seconds, and a few times the arc heater completely failed to start. During this time period the power supply started making an unusual grinding noise. At the suggestion of a Robicon engineer, an oscilloscope was attached to the current and voltage feedback wires connected to the plasma interface board in order to observe the quality of the DC output. The power supply was to be operated with the water barrel resistor as a load and the oscilloscope trace was to be described over the phone to the engineer. When the power supply was turned-on, high current appeared on the feedback wires and immediately scorched the control boards to complete failure. The underlying cause of the destruction was that the oscilloscope probes were grounded to the wall socket rather than being at a floating potential. This error created the potential difference that brought the intense current into the electronic control boards. Not only was the plasma interface

board (functionally) destroyed, but the two FR6-I SCR triggering boards were destroyed as well (but the oscilloscope was not damaged).

Eventually the controls were replaced and factory technicians were contracted to provide the field service to make the power supply operational again. The downtime of the facility was used to implement an alternative arc ignition technique involving argon injection instead of a high voltage ripple. The argon arc initiation technique has been so successful, that the prior ignition system is no longer of any utility and should eventually be physically removed from the facility.

The power supply functioned well for a long series of probe development test runs. However, given the previous wrenching experiences, the facility was operated sparingly. Test runs were strictly reserved for situations when conditions seemed right for obtaining good data.

In August 2003, the power supply failed in a similar fashion to the accident in 1997. The failure occurred one second into the first arc heater test run using methane as the injected gas. When the controls failed, the power supply probably went into an uncontrolled current ramp-up that was arrested when an SCR fuse opened, triggering a shutdown. Robicon has attributed this failure to a malfunction on the plasma interface board.

This issue of the recurring failures of the power supply controls needs to be addressed before facility operations resume. One approach would be to retrofit some kind of optical isolation devices into the voltage and current feedback lines. Another suggestion is to insert fast-blow fuses into the feedback wires. These fuses would need

to have an interlock switch that would shutdown the power supply (like the SCR fuses have) to prevent an uncontrolled current ramp-up. A non-technical solution may be to negotiate a maintenance contract with Robicon that would require them to fix such failures, free-of-charge, under a warranty arrangement.

2.4 Vacuum System

A vacuum exhaust system considerably broadens the possible applications of a supersonic wind tunnel. Large pressure ratios can be obtained to operate hypersonic nozzles without having to pressurize the driving gas to extreme pressures. In addition, high altitude conditions may also be simulated.

At the start of development work described herein, the vacuum vessels were already installed, but there was still much to be done to make the vacuum system complete and operational. The vacuum system's vessels consist of a test cabin and a 4.25 m^3 vacuum tank connected by two constant area diffuser sections (see Fig. 2.6). The test cabin and the short diffuser are completely inside the Aerodynamics Research Center (ARC) in the Aeropropulsion Lab together with the arc heater. The longer diffuser section passes from the inside though a panel in the outside wall to the vacuum tank, which is outside between the power supply and cooling water tank. The test cabin was designed to be a free jet test section, rather than a solid or perforated walled test section. When it was designed, it was anticipated that a high expansion ratio nozzle would be fitted to the arc heater to form a roughly 11-in diameter free jet within the test cabin.

To help recover pressure from the highly expanded free jet, the exit of the test cabin features an inlet lip to capture the jet and promote the formation of a shock train in the constant area diffuser. Although the test cabin is designed to accommodate a high expansion ratio nozzle, making or modifying a nozzle for this purpose has not been pursued. The three optical ports on the test cabin are situated to observe a model in the free jet midway between the entrance and exit. Unfortunately, this placement does not work well for the experiments performed thus far with the facility. The primary interest has been to observe the flow emerging from the arc heater's low expansion nozzle.

During the early stage of this project, making a small auxiliary test cabin with optical ports having a direct view of the nozzle exit was seriously considered. This configuration would have made it possible to use shadowgraph or schlieren techniques to study the flow in the vicinity of the nozzle exit. Moreover, laser flow diagnostics could also be contemplated with this type of test cabin. At the time, the estimate of $5000 to fabricate an auxiliary test section seemed as though it would consume too much of the research budget.

One problem encountered during the shakedown tests was that firing the arc heater into the room filled it with noxious gases and displaced the oxygen in the room. At the time, this safety issue was partly addressed by allowing the room's air handler enough time to make a few "air changes" before allowing anyone in the room. An "air change" is the time period for the whole room volume to flow through the ventilation system. Typically, buildings are designed to make air changes every eight minutes and with approximately 10% of the air flow coming from the outside. Accordingly, for the

shakedown testing, everyone was kept out of the room for at least 20 minutes after a run. In addition to allowing time for air changes, the suction side of a rented manhole blower was temporarily fitted to the hatch opening of the vacuum tank to help exhaust noxious gases. The roof vents were also opened to allow more fresh air to enter the room. However, this makeshift approach did contribute to the most significant safety incident with the facility. After a test run, in which the arc failed to form, a student entered the room to adjust a valve without waiting twenty minutes. There were no noxious gases in the room, but the nitrogen discharged into the room diluted its oxygen content to the point that he almost fainted before getting out of the room.

This safety problem was one factor that prompted a naïve request for a dedicated room ventilation system. The other factor was the plan to eventually inject hydrogen into the arc heater, which called for a way to prevent hydrogen from accumulating in the room in case of leakage or some other accidental discharge. With a high rate of air exchange with the outside, experiments could have been continued with the arc heater firing into the room air. Unfortunately, the ventilation system proposed to the physical plant was too expensive (approximately $30,000). Eventually, the reason for the high cost was revealed: the consulting engineer had prepared a “bulletproof” design. Not only was there to be a high rate of airflow, but also the flow was going to be kept laminar, so that the noxious gases would not mix with the incoming fresh air. So the proposed system not only had large blowers, but also very sizable ductwork. Having explored this possible shortcut for going directly to more advanced experiments, the facility was prepared for the arc heater to discharge exclusively into the vacuum vessels.

Although the vessels are probably massive enough to withstand a brief arc heater firing, a generous amount of water-cooling was provided to them. Predicting where the heat transfer might be locally intense could be difficult, especially for a variety of operating points and experimental configurations. Moreover, it is preferable to provide a possibly excessive amount of cooling rather than risking the integrity of expensive pressure vessels.

The process of soldering copper cooling tubes to the outside of the test cabin and short diffuser took several months. Much of that time was spent developing a workable soldering technique to join the copper tube to the steel vessels. Copper may be readily soldered to brass or copper, but soldering to steel requires special preparation. First of all, the scale must be sanded or ground off the steel to reveal a shiny surface. This exposed surface then has to be tinned with acid core solder within minutes of having uncovered it. To tin the surface, a propane torch was used to heat the surface and, once the solder melted, the solder would be spread by scraping the surface with the tip of a large common screwdriver. The additional abrasion of the screwdriver tip considerably enhances the adherence of the solder to the steel. Normally, one 1in. by 6 in. exposed strip would be tinned at a time. Once a tinned path for a tube to attach to was completed, a portion of a tube at the midpoint of the tinned path would be soldered into place, using wire or a hose clamp to hold the tube. After attaching the tube in the middle, the temporary clamp was usually removed, and the soldering proceeded, working away from the initial joint. This method allows the unattached portions of the tube to thermally expand without restraint. If instead, one first attached the ends of the

tube, and then worked towards the middle, the tube could buckle from the thermal stress. The big screwdriver also proved to be very useful for pressing the copper tube against the vessel surface while the solder solidified. Since it has a simple shape to work with, the short diffuser section was chosen as the first vessel to have tubes attached. When the time came to attach tubes to the more complicated test cabin, most of the technical difficulties of the soldering process had been overcome. The tube lengths on the test cabin are roughly the same, so that the water flow rates would be about the same for all the tubes.

For the vessels located outside, a more crude approach to cooling was used: simply running water over the external surfaces. To supply the water, a spray manifold, made of PVC tubes and fittings, was attached to a small pump, which received water from a modified trash barrel. The water falling off the bottoms of the vessels drops into gutters to return back to the water barrel. Not surprisingly, the gutters catch most, but not all of the water, so it was necessary to install float valves in the barrel to provide make-up water. The external cooling apparatus functions adequately, but there is plenty of room for improvement, especially in regard to the splattering water causing maintenance problems. The cooling system for the vacuum vessels is actually not totally finished. The portion of the long diffuser that is within the room still lacks cooling tubes. The interim solution for this deficiency has been to drape a couple of wet towels over this part of the diffuser, in preparation for a test run.

To couple the arc heater to the test cabin, it was necessary to design an adapter bulkhead. The design was straightforward, but it took some searching to find a machine

shop capable of fabricating large diameter flanges and disks. Uniflex was contracted to make the bulkhead for $750. The quality of the machine work was excellent and the bulkhead has since worked flawlessly. It was painted with high temperature silver paint (withstands up to 1000 $^{\circ}$F) and insulated on the inside face with a thin layer of Refrasil refractory fabric. Although water-cooling for this bulkhead is not provided, no evidence of heat damage has been seen.

During the hurried initial purchasing of facility components in 1989, two large mechanical vacuum pumps were obtained to maintain a vacuum during a test run. However, it was subsequently discovered that the vacuum pumps could only produce the required mass flow rate with the inlet gas being close to atmospheric pressure. The flow rate figure given in the pump specifications applies to "free air" delivery rather than the flow rate for vacuum inlet conditions. As Figure 2.9 from the pump manual shows, the flow rate drops precipitously with decreasing inlet pressure. Under realistic conditions, the two pumps working in parallel would only be able to sustain a mass flow of 0.0008 kg/s whereas the minimum discharge of the arc heater is roughly 0.06 kg/s. To remedy the shortfall in the capabilities of the mechanical vacuum pumps, a compressed air-driven ejector pump has been incorporated into the facility to provide a sustained vacuum while the arc heater is firing. An ejector pump is a fairly common suction device used for pressure-vacuum wind tunnels and rocket test facilities. For this application of an ejector, a large primary mass flow exits from a supersonic nozzle and entrains a small secondary mass flow, creating suction. From the preliminary analysis, it was determined that it was possible to get adequate performance with a single stage

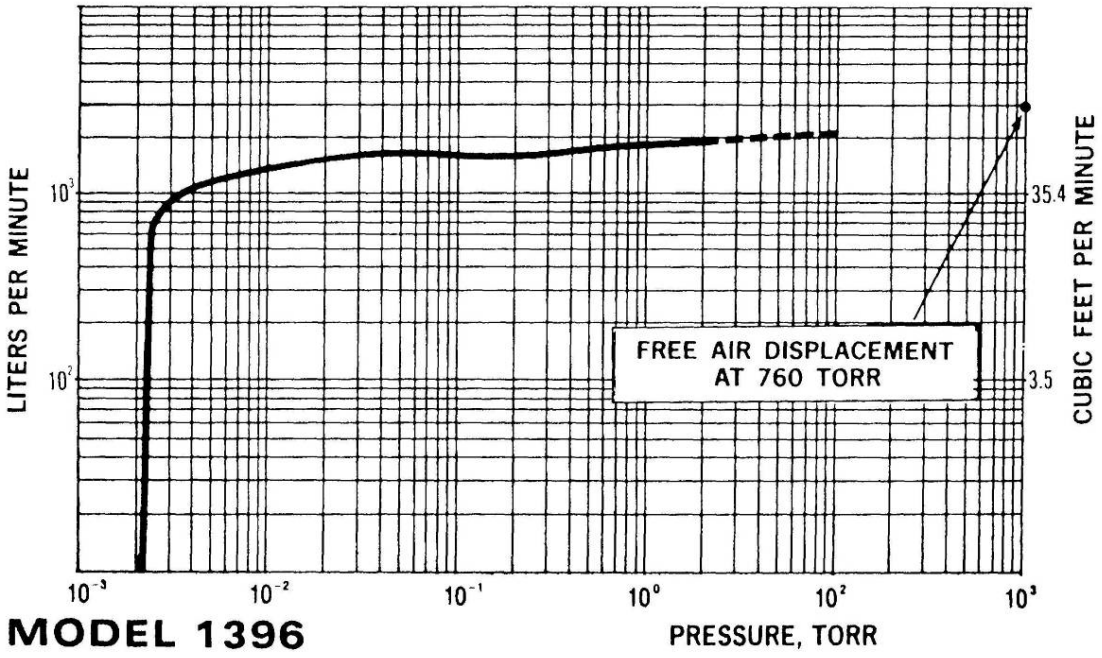

Figure 2.9 Mechanical Vacuum Pump Operating Curve

ejector pump rather than with a multiple stage pump. This finding was very fortuitous since for a multi-stage ejector pump, the required driving mass flow rate increases by roughly an order of magnitude for each stage. The sensitivity of the ejector pump performance to the vacuum vessel gas temperature was also investigated. The results of the analysis revealed a substantial decrease in the attainable pressure ratio as the vacuum inlet temperature increases. This finding is a key motive for providing cooling to the vacuum vessels.

A group of undergraduate students also participated in the design of the ejector pump, which primarily involved running an analysis program, designing a conical nozzle and making a fiberglass subsonic diffuser. This author's contribution was primarily in designing the air injection system to drive the ejector pump and,

secondarily, specifying that the ejector was to be constructed from standard pipe fittings to minimize the expense.

The required air mass flow rate of 1 to 2 kg/s could not be delivered by the existing regulator that supplied the ARC's high-pressure air distribution lines. Therefore, a much larger regulator had to be selected and purchased. In addition, a higher capacity air filter had to be acquired as well, and connected in parallel with the existing filter (Fig. 2.10 and 2.11). The Grove 302G regulator does have integral setscrew needle valves to set the dome pressure, but these proved to be very difficult to use. For this reason, a hand-loaded regulator was purchased and installed to set the dome pressure of the Grove regulator. This hand-loaded regulator, pressure gauges and

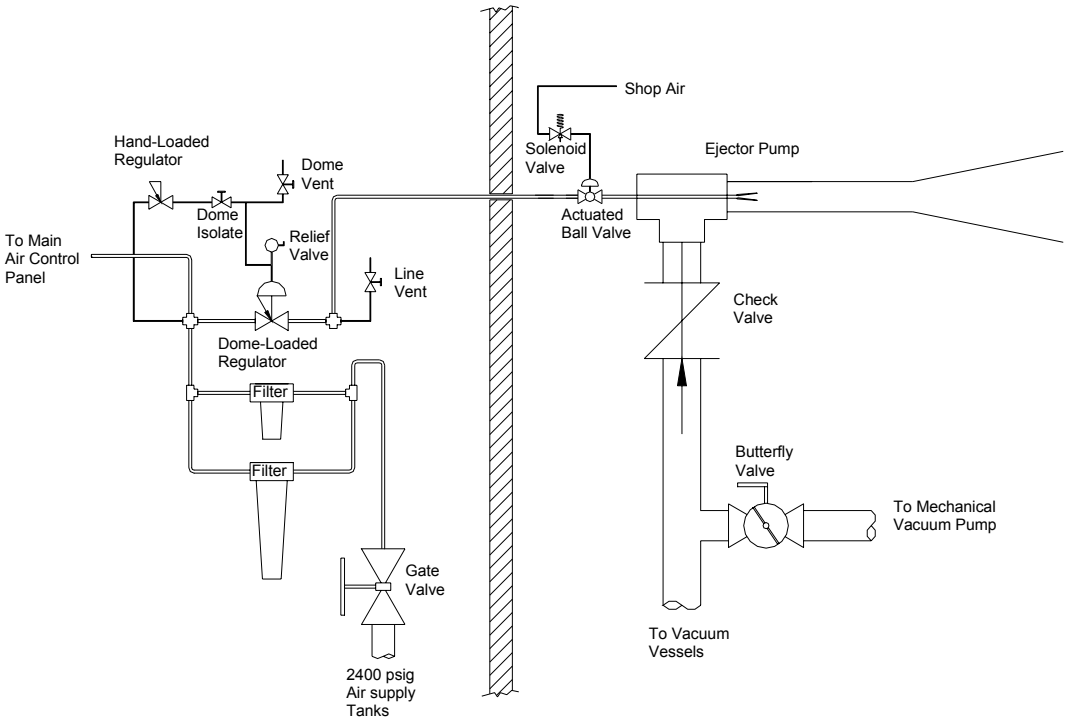

Figure 2.10 Ejector Pump System Schematic

vent valves were mounted on a small panel on the wall rather than being incorporated into the ARC's main air control board (Fig. 2.11). A relief valve set with a cracking

pressure of less than 1000 psig is connected to the dome to limit the discharge pressure of the regulator. However, exceeding 1000 psig will only blow out the seals of the actuated ball valve (located just upstream of the supersonic nozzle), and not cause any other damage. The rest of the plumbing downstream of the regulator is rated for the full system pressure.

Figure 2.11 Air Injection System for Ejector Pump

The ejector pump resulting from the undergraduate collaboration consisted of an assembly of 4” stainless pipe and fittings with a 1” O.D. tube injection tube nested inside. After this design work was completed, a conical attachment surface was designed in order to enhance the performance and adjustability of the ejector pump (Fig.

2.13). For clarity, this vacuum flow inlet device was usually referred to as an "annular wedge" although this is probably not the precisely correct geometrical term. This annular wedge was installed so that its position relative to the injection nozzle could be adjusted from the outside.

When the ejector pump was first tested after being installed it did not function properly regardless of the driving pressure or where the annular wedge was positioned. The ejector pump could only achieve a mild vacuum of 4.3 psia at best during "blank-off" tests (vacuum vessels sealed with no flow from the arc heater). To understand why

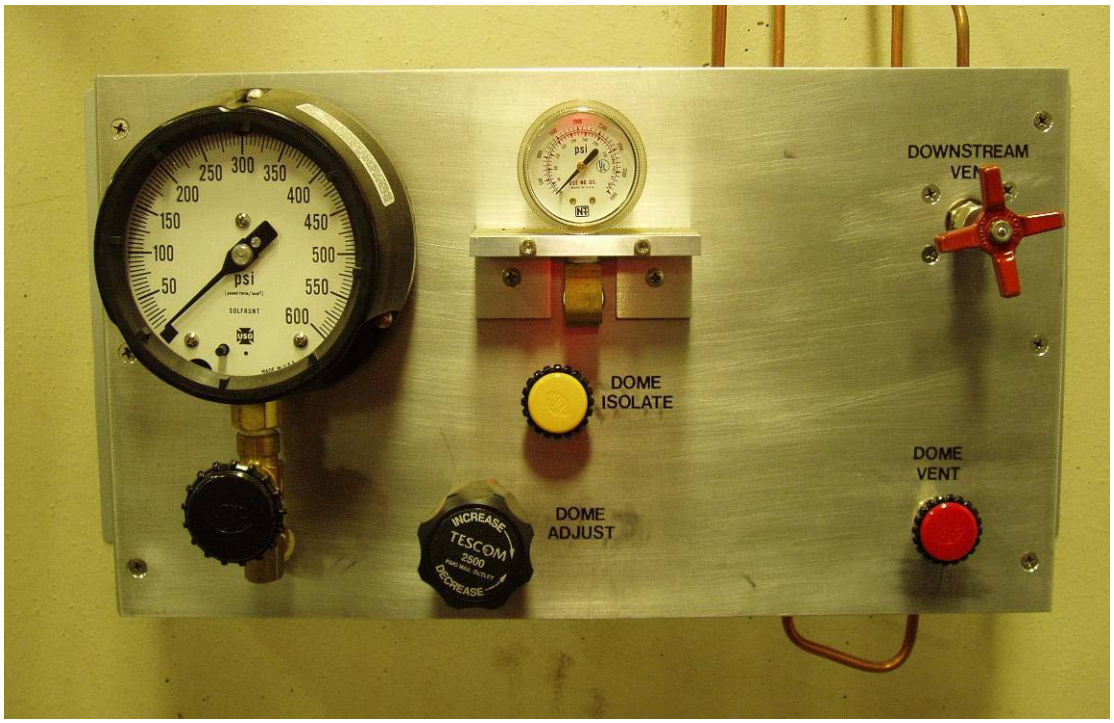

Figure 2.12 Ejector Pump Control Panel

the ejector pump was not performing as well as predicted by the analysis program, Ref. 13 was re-examined. When the area ratios (A_d/A^*, the duct area to nozzle throat area

and A_{ne}/A^*, the nozzle exit area to the nozzle throat area) of the existing pump were compared with the test data in the report, it was noted that the ratios were not in the range of the given experimentally proven geometries. To better match this range, the 4" pipe nipple was removed, and a reducing bushing and 3" pipe nipple were installed in its place. When the ejector pump was retested, it immediately achieved much lower

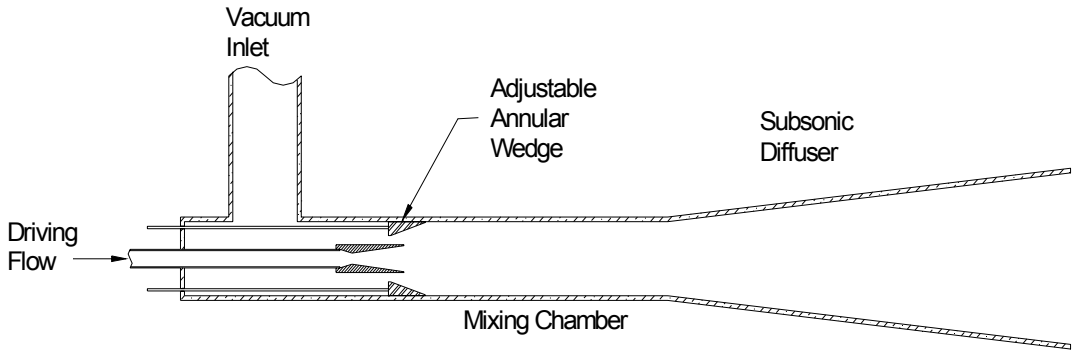

Figure 2.13 Initial Configuration of Ejector Pump

vacuum pressures. The minimum "blank-off" pressure improved to 0.65 psia. Apparently, the supersonic jet was not able to attach to the inside surface of the 4" pipe giving a mixed flow regime pattern as shown in Figure 2.14 excerpted from Ref 13. Installing a 3" pipe allowed the supersonic jet to attach to the inside of the pipe and form a shock train.

After achieving this level of rudimentary effectiveness, the development work on the ejector pump was not continued due to more pressing research priorities. As it presently stands, the ejector pump lacks a subsonic diffuser and an annular wedge that are compatible with the 3" pipe mixing section (Fig. 2.15). Accordingly, there is some

unfinished work that needs to be done to optimize the ejector performance. It is anticipated that this additional development could be accomplished in a fairly

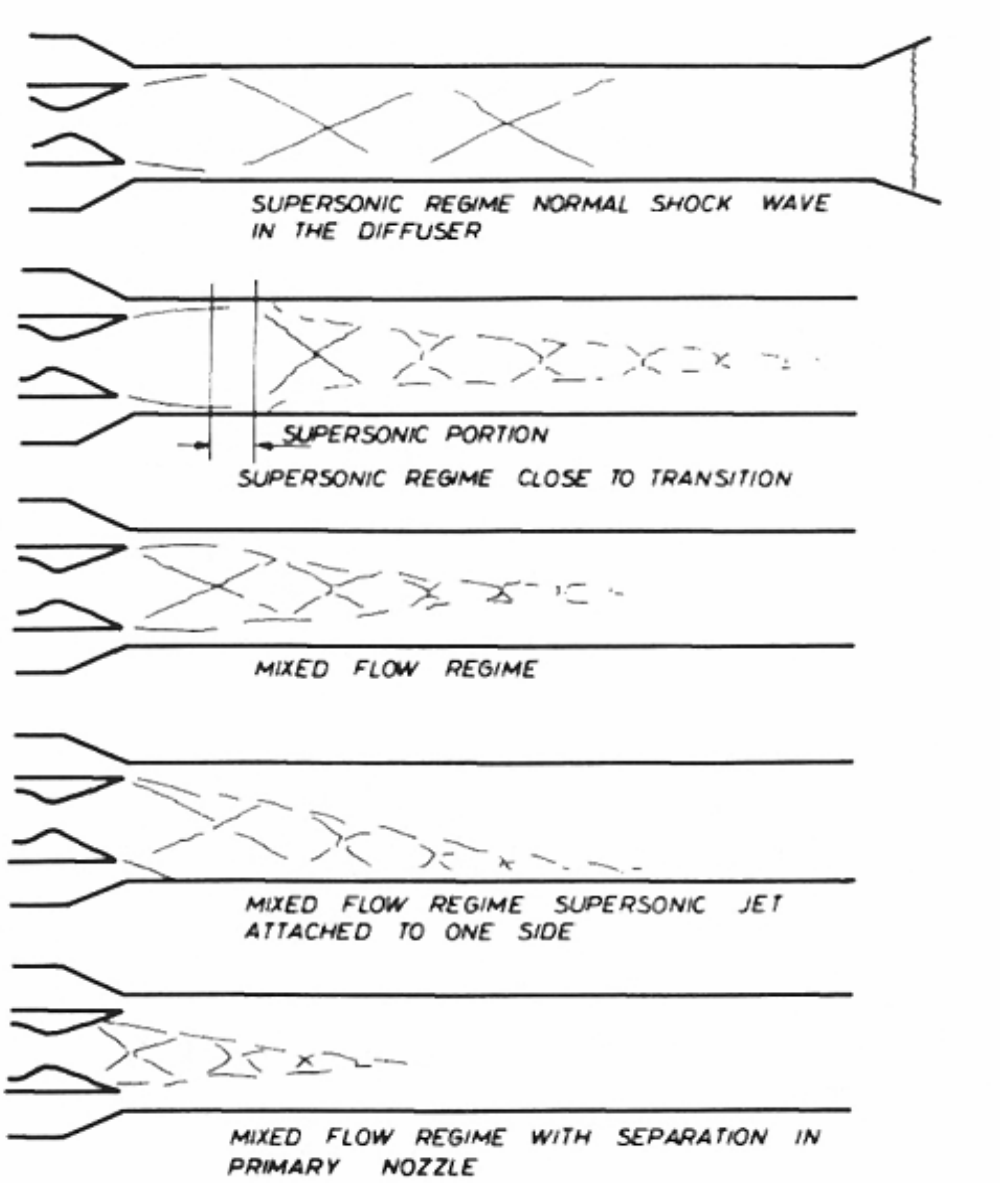

Figure 2.14 Flow Patterns in a Supersonic Ejector

straightforward and inexpensive fashion. Although the ejector pump has been successfully operated with the arc heater running, its operating envelope is largely

unexplored. During much of the time since the ejector pump was installed, the arc heater power supply and/or the Clark CM6 compressor have been inoperable and awaiting repair. There is sufficient compressed air storage (roughly 700 kg) to drive the ejector pump for several minutes.

Due to the inherent and intense roar produced by a supersonic jet stream, a silencer was made in an effort to minimize the noise produced by the ejector pump (Fig 2.16). This silencer is basically an inexpensive wooden duct containing acoustical foam baffles with narrow airflow passages among them. In retrospect, there are a couple of

Figure 2.15 Ejector Pump Installation

shortcomings with the silencer due to its wooden structure. First of all, the silencer has not weathered well; a metal structure would have been more durable and aesthetic. Secondly, the wood might catch fire if arc-heated flow enters it without sufficient cooling.

During the fuel reformation research, a bypass duct was installed along the silencer to circumvent this hazard. There is not a danger of fire when the ejector pump is operating because the arc-heated gas is mixed with a cool mass flow of air that is ten times greater. The acoustical foam is fire resistant. When a sample of the foam was subjected to a propane torch flame, the fire would spontaneously extinguish once the torch was removed.

Figure 2.16 Ejector Pump Silencer

For a time, the mechanical vacuum pumps were considered to be of little value to the facility because for a free-jet wind tunnel, the starting and running pressure ratios are fairly close. However, considering that the ejector pump can discharge air faster

than the 1250 hp Clark compressor can pump, it is much more convenient and energy efficient to use the mechanical vacuum pump to provide the initial vacuum than to use the ejector pump. The Sargent-Welch vacuum pump is driven by a 7.5 hp motor and only needs a few minutes to pump the vessels down to a tenth of an atmosphere.

Regretfully, the vacuum pumps were almost totally neglected and only partially sheltered for most of the time period since they were installed near the vacuum tank. It was not until the MSE-TA funding was awarded that any effort was made to refurbish, and connect vacuum plumbing to, the mechanical vacuum pump. The pump that had been sitting outside unused for over a decade, unfortunately, had rusted surfaces inside the rotor case and could not be rebuilt on site successfully. Luckily, the same model vacuum pump had been removed from the hypersonic shock tunnel and was sitting in storage. This particular pump had been replaced with one of the two original arc heater facility vacuum pumps, due to it splattering out large quantities of oil. A serviceman at a vacuum pump service shop kindly diagnosed the malfunction over the phone: the vacuum pump needed a clean, new exhaust filter. Installing this pump from storage and running it with the arc heater facility proved to be thankfully easy. Because of the compressor facility being out of service, having the mechanical vacuum pump operational proved to be critical to conducting the fuel pyrolysis investigation. At about this time, a 4-in. check valve was installed in the vacuum line just upstream of the ejector pump. This valve prevents outside air from entering the vacuum vessels through the ejector pump when it is not being driven. Although it has not been tested, the check valve should allow the mechanical pump to provide the initial vacuum prior to a test run

with the ejector being engaged only slightly before the arc heater is fired. The check valve will open once the vessel pressure exceeds the suction pressure of the ejector, which is expected to provide a fairly seamless transition.

2.5 Nitrogen Injection System

The nitrogen injection system was the most complete portion of the facility prior to 1994 (Fig 2.17). The main components of the system were a compressed air-driven gas compressor, a high flow dome-loaded regulator, a critical flow nozzle, and a

Figure 2.17 Nitrogen Injection System

donated 1-ft^3 storage vessel. It appears that many of the fittings and tubing from HiP (High Pressure Equipment Company) were selected on the basis of the pressure rating of the storage vessel (15,000 psi) rather than the rated output of the Haskel compressor (5,000 psi). Some of the plumbing is actually rated for 40,000 psi. The gas injection board is controlled remotely by energizing solenoid valves. One solenoid valve directly provides compressed air to drive the Haskel gas booster pump, whereas another supplies compressed air to actuate the main injection valve.

When the injection system was used for the shakedown test runs it was discovered that a flow rate of more than 0.08 kg/s could not be sustained for the entire run (Fig 2.18). The arc heater voltage and power would correspondingly drop as well

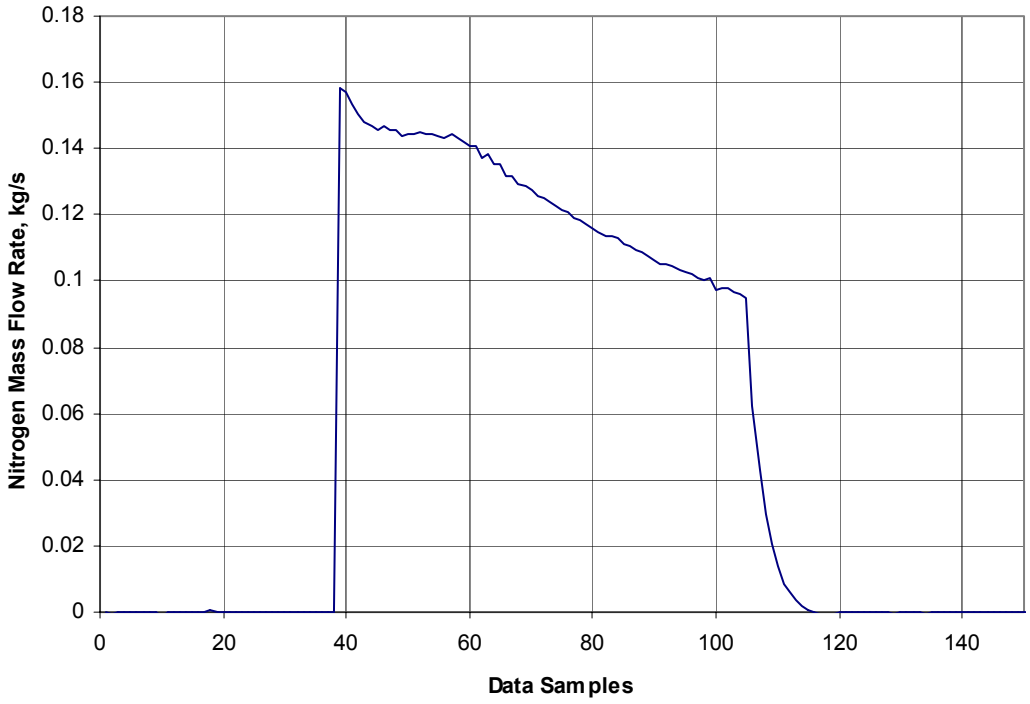

Figure 2.18 Unsteady Gas Injection Due to Flow Restrictions

during a test run. Consequently, some of the more flow-restricting fittings had to be replaced. First of all, the adapter plug on the end of the storage vessel was replaced with a plug with a larger orifice. The replacement plug was machined on-site out of steel hex stock because of the difficulty in finding a compatible off-the-shelf plug. However, this measure alone did not solve the problem. In addition, it was necessary to replace a manual HiP needle valve with a Hoke ball valve in the gas line leading from the tank to the gas board. The final step in eliminating flow restrictions was removing an air-actuated isolation valve, that was located just upstream of the regulator. A length of tubing was installed in place of this valve. Once this modification was complete, there was no further difficulty in injecting gas at the full capacity of the regulator.

The next major injection system modification came in response to problems associated with the arc ignition process. With the suspicion that the ignition system was the culprit in the power supply malfunction, more modifications were made to enable the facility to operate reliably over the entire range of output voltages. Fortunately, this author consulted with a retired expert, John Poole, who had performed much of the engineering on Thermal Dynamics' arc heaters and had progressed to make more advanced arc heaters of his own design. John Poole offered two important suggestions to remedy the ignition problems. First of all, start the arc heater on a minimal flow rate of gas for ignition and then increase the flow. Secondly, introduce argon into the gas flow. He explained that argon has a lower ionization potential than nitrogen (requiring only about one-third as much voltage as nitrogen) and the ions also tend to persist longer. Unfortunately, the existing nitrogen injection system did not include any

provision for flow rate adjustment from the control room. Even in the unlikely event that it could be done quickly enough, attempting to adjust the regulator in the same room as the running arc heater was considered too dangerous. Furthermore, the experiments planned for the arc heater, simulating hydrogen–air combustion products expanding over a single expansion ramp, conflicted with running the arc heater on pure argon or an argon-rich gas mixture.

The approach eventually adopted was to modify the injection system to first inject a low flow rate of argon and then automatically transition to pure nitrogen after the arc is established. An argon injection system consisting of a storage bottle, regulator and remote-actuated valve, was connected by a pipe tee to the existing nitrogen injection system (Fig. 2.19). This arrangement allows the starting (argon) and running (nitrogen) injection pressures to be set independently. The gas controls were altered so

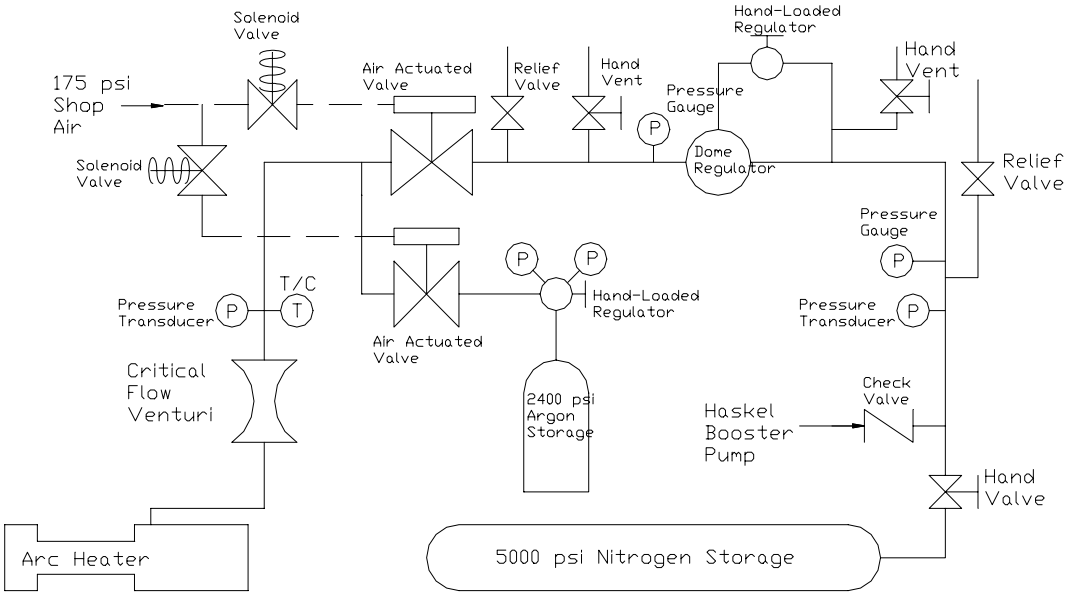

Figure 2.19 Injection System Modified to Start with Argon

that the argon could be injected by manually engaging a switch in the control room. Nitrogen injection was modified to begin automatically when the power supply current meter signal indicates that there is at least a 200-amp arc within the arc heater. This automatic function is performed by a comparator circuit, which monitors the current meter signal and engages a relay to bring on the nitrogen flow. The argon flow is turned off, once the nitrogen valve is fully open, by a lever mounted on the valve actuator that contacts a normally closed switch installed in series with the manual switch in the control room. This approach of overlapping the argon and nitrogen injection flows avoids any interruption in the gas flow to the arc heater.

Previously, the nitrogen injection system was capable of providing for only approximately 30 seconds of operation at a midrange mass flow rate of 0.12 kg/s. Blowing the original 1-ft^3 storage tank down from 5000 to 1000 psi provided about 4 kg of nitrogen for a test run. A modification to this system has been incorporated that increases the run time, and makes the output mass flow much more steady by decreasing the variation of temperature and pressure of the gas, as it is blown down from its initial storage pressure. During the prior shakedown testing, the gas mass flow was observed to occasionally rise by as much as 7% due to these variations (Fig. 2.20). Figure 2.21 shows the decrease in gas temperature during a test run. (The intermittent noise blips on the plot are due to the data sampling going in and out of phase with noise from an unknown source.) The extra mass flow stretches the arc farther, which increases the operating voltage (and power) (Fig. 2.22).

As the tank is blown down, the contents drop in temperature according to the polytropic relationship:

$$\frac{T_{initial}}{T_{final}} = \left(\frac{P_{initial}}{P_{final}} \right)^{(n-1)/n}$$

For an adiabatic process, n=1.4 and for an isothermal process n=1.0. However, the actual blowdown process does not correspond well to either of these idealizations, so Ref. 14 recommends assuming n=1.2 (Fig. 2.23).

To implement the modification, three 1.76 ft^3 bottles packed with strips of metal were connected to the system (Fig 2.24). Originally, the nitrogen system was supplied by a manifold of six gas bottles placed in the room beside the control board. To make room for the packed bottles, these supply bottles were relocated to the outside wall of

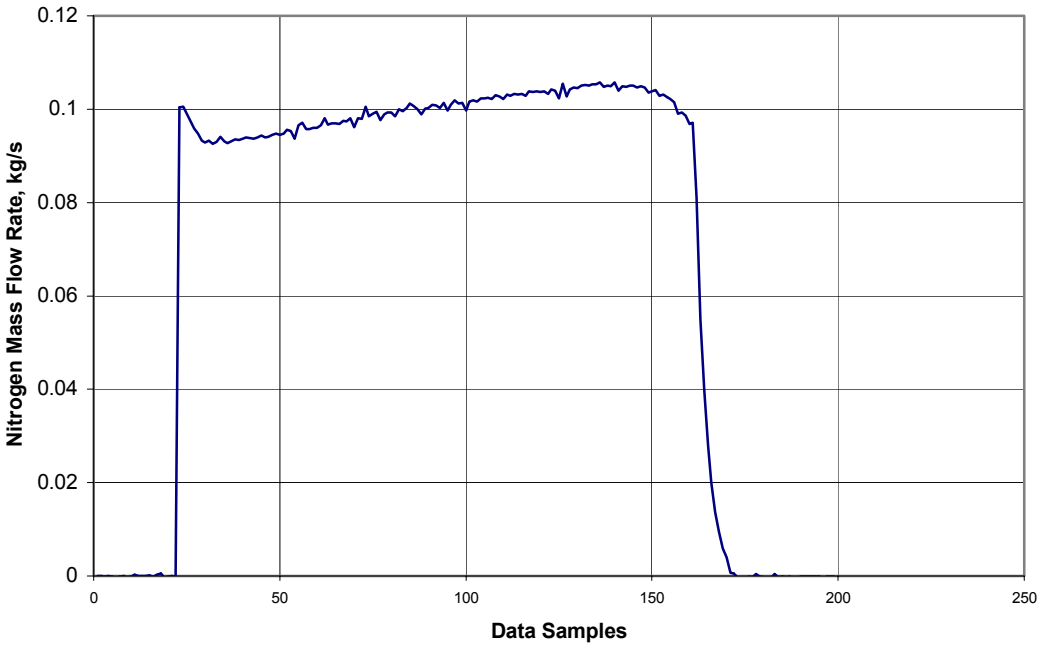

Figure 2.20 Unsteady Mass Flow During Blowdown

the east side of the building. This outside location is far more convenient for exchanging empty bottles for full bottles from the delivery truck. During operation, the

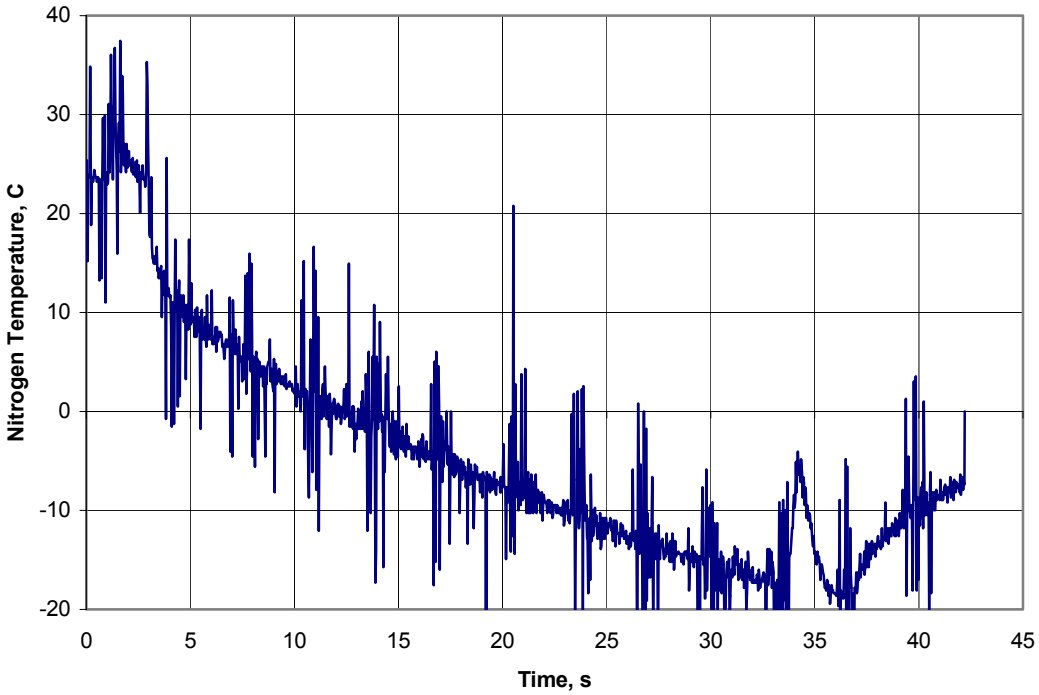

Figure 2.21 Gas Temperature Drop During Blowdown

large mass (140 kg) of metal packing transfers heat to the much smaller mass of injected gas to minimize the effect of expansion cooling (Fig. 2.24). In addition, the initial storage pressure was lowered from 5000 psi to 2400 psi, which not only narrows the range of inlet pressure that the regulator must respond to, it also reduces the ratio of initial to final gas temperatures by about 40%, according to the polytropic relationship. This upgrade makes 20 kg of nitrogen available for injection, increasing the run time to 130 seconds at 0.15 kg/s. With additional packed bottles, the run time could be increased for high mass flow rates to as much as 200 seconds, where cooling water system limitations come into play. Neglecting the heat exchange between the primary

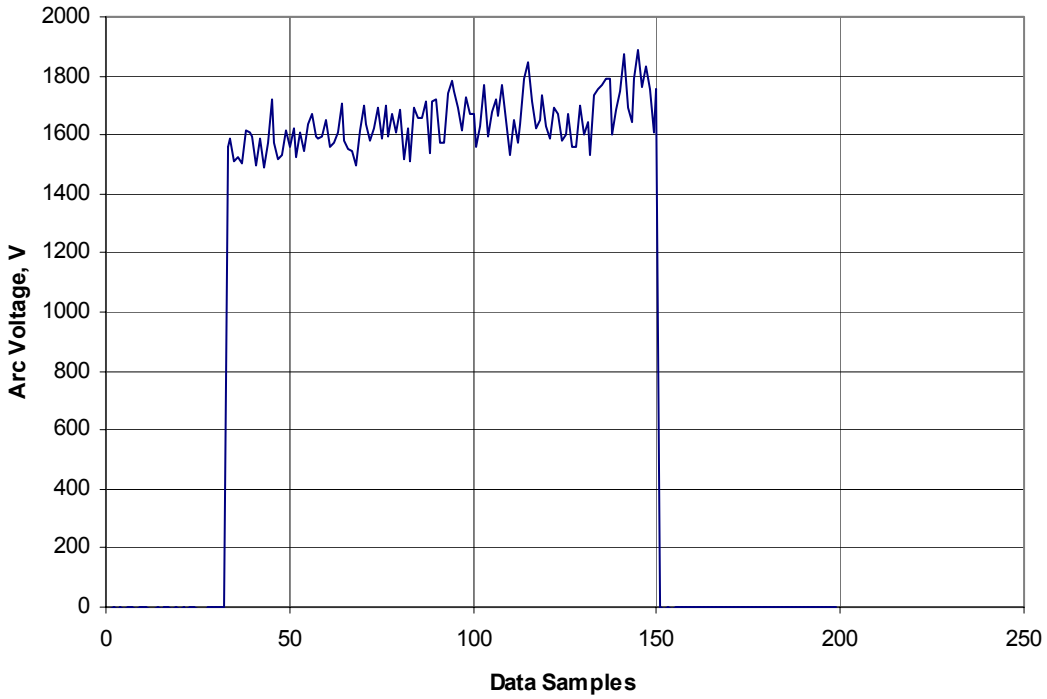

Figure 2.22 Effect of Gas Mass Flow on Arc Voltage

and cooling tower loops, it would take approximately this long to boil the normal amount of water in the primary loop with the arc heater running at maximum power. The cooling tower loop was reportedly not designed to keep-up with the instantaneous rate of heat transfer from the arc heater to the primary cooling water loop. Test runs with the modified injection system have yielded very well regulated mass flows. A full blow-down from 2400 to 800 psi is predicted to exhibit a mass flow increase of less than 2%. If tighter mass flow control is required, then a test run could simply be shortened so that only a partial blow-down is required.

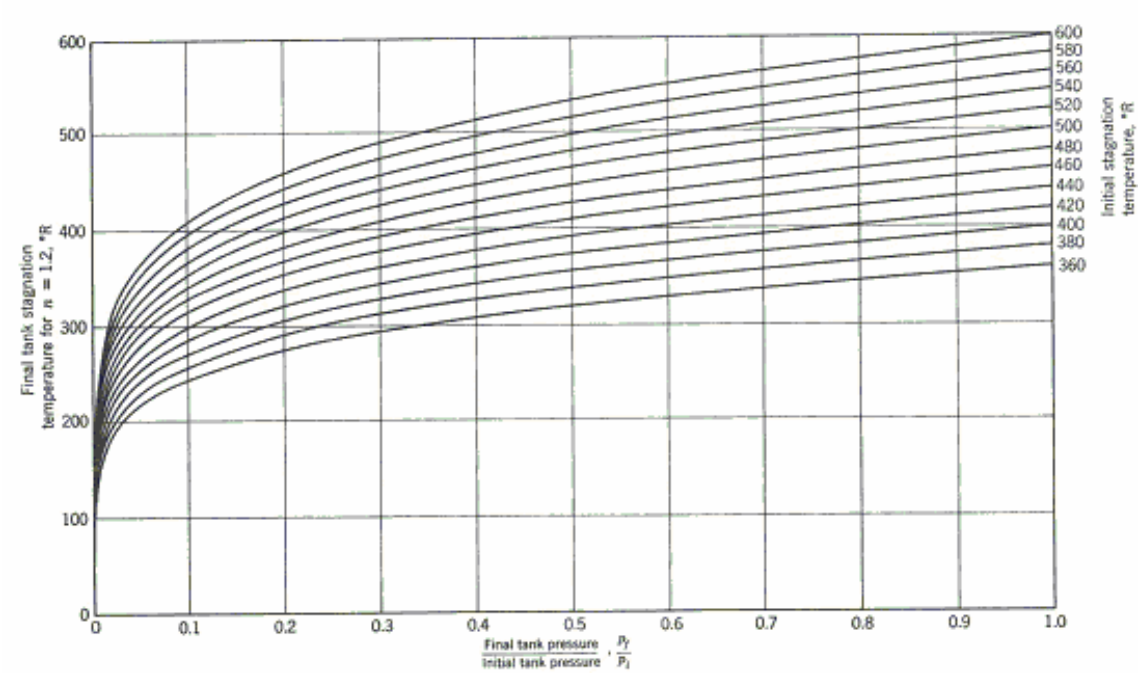

Figure 2.23 Final Temperatures in a Storage Tank Assuming n=1.2

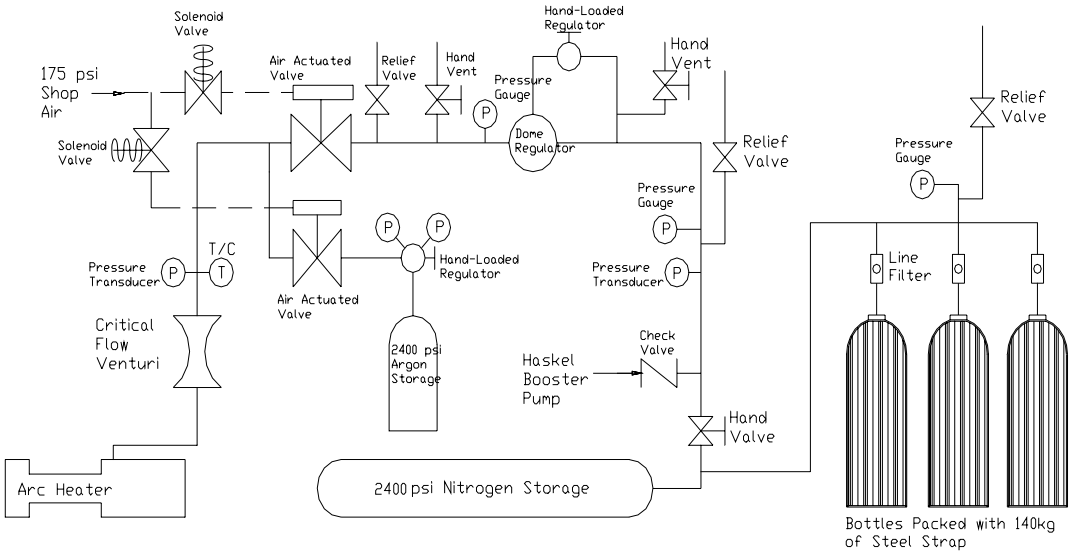

Figure 2.24 Gas Storage Upgrade

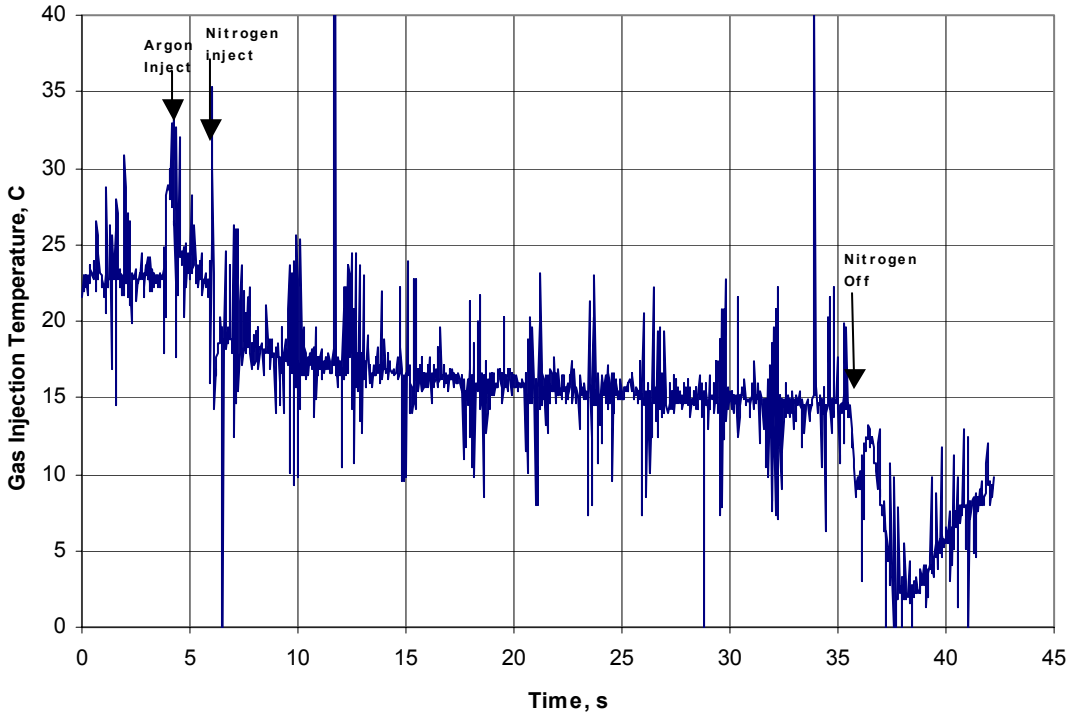

Figure 2.25 Reduced Temperature Drop after Installation of Packed Bottles

2.6 Secondary Gas Injection Systems

Prior difficulty with mass flow regulation with the nitrogen injection system was a major influence on the design of the fuel gas injection system. What good is it to have a long duration test run capability if the conditions during the run are unsteady? Reducing the pressure change within the storage reservoir during a blowdown significantly reduces the variation in outlet gas temperature. An additional practical consideration was providing enough gas storage for a two-day supply at a high test run frequency, which sometimes reached the level of ten runs per day during the prior shakedown testing of the arc heater. For these reasons, a four-bottle gas storage configuration was initially chosen.

Unfortunately, using multiple hydrogen bottles brings forth a much more stringent set of National Fire Prevention Association (NFPA) codes than those that apply to just a single bottle of 300 standard ft^3 or less capacity. In short, a single bottle can be put practically anywhere a welder might need to work, but more than one must go into a specialized storage space. The NFPA codes call for a storage space with strong walls and a light roof.

Experiments conducted at the ARC on detonations demonstrated that it is difficult to make a hydrogen-air mixture at atmospheric pressure actually detonate. This is not to say that a deflagrative explosion could not occur under these conditions, but the pressure generated from such an explosion would be considerably less than a detonation. Due to the proximity of an apartment building and a daycare to the ARC, the UTA Environmental Health and Safety Department seemed to be concerned to the

extent that only a detonation-proof building would allay their objections. For this reason, an internal pressure of 300 psi was chosen as the design criterion for the building, corresponding to 130% of the full detonation pressure of hydrogen.

A rectangular building was initially envisioned, but the bending stress predictions for this structure vividly illustrated why pressure vessels are almost universally round in cross-section. Accordingly, the storage building design proceeded using ASME pressure vessel codes as a guide. The structure of the building consists of two steel cylindrical half shells joined together by a hinge (Fig 2.26 and Fig. 2.27). One of the half shells is welded to the floor grate while the other may be swung open to permit easy access to the inside of the building. The latch mechanism is designed to withstand the large stresses from bending that would result from holding the half-shells together during an explosion. A dozen pieces of rectangular steel tube were welded together to provide sufficient resistance to bending. The purpose of the chain is to hold the latch in engagement to the shell ledges rather than allowing the latch to be pushed outward by an explosion, out of contact with the ledges. A four bar linkage with a handle is used to lift the latch away from the shell ledges to open the building. The commercial steel structure is predicted to yield at 900 psi of internal pressure giving a safety factor of about three. The roof is made of four sheet metal blow-away panels with four small screws (#4-40) holding each panel in place. In the event of an explosion, the screw heads are expected to tear through the light gauge mounting brackets. The panels are tethered together by a steel cable so that they may blow-off upward, but are constrained to stay around the vent stack.

The building was designed to exploit natural draft ventilation. Lighter-than-air gases, leaked inside the building, will have a strong tendency to be directed right up the stack.

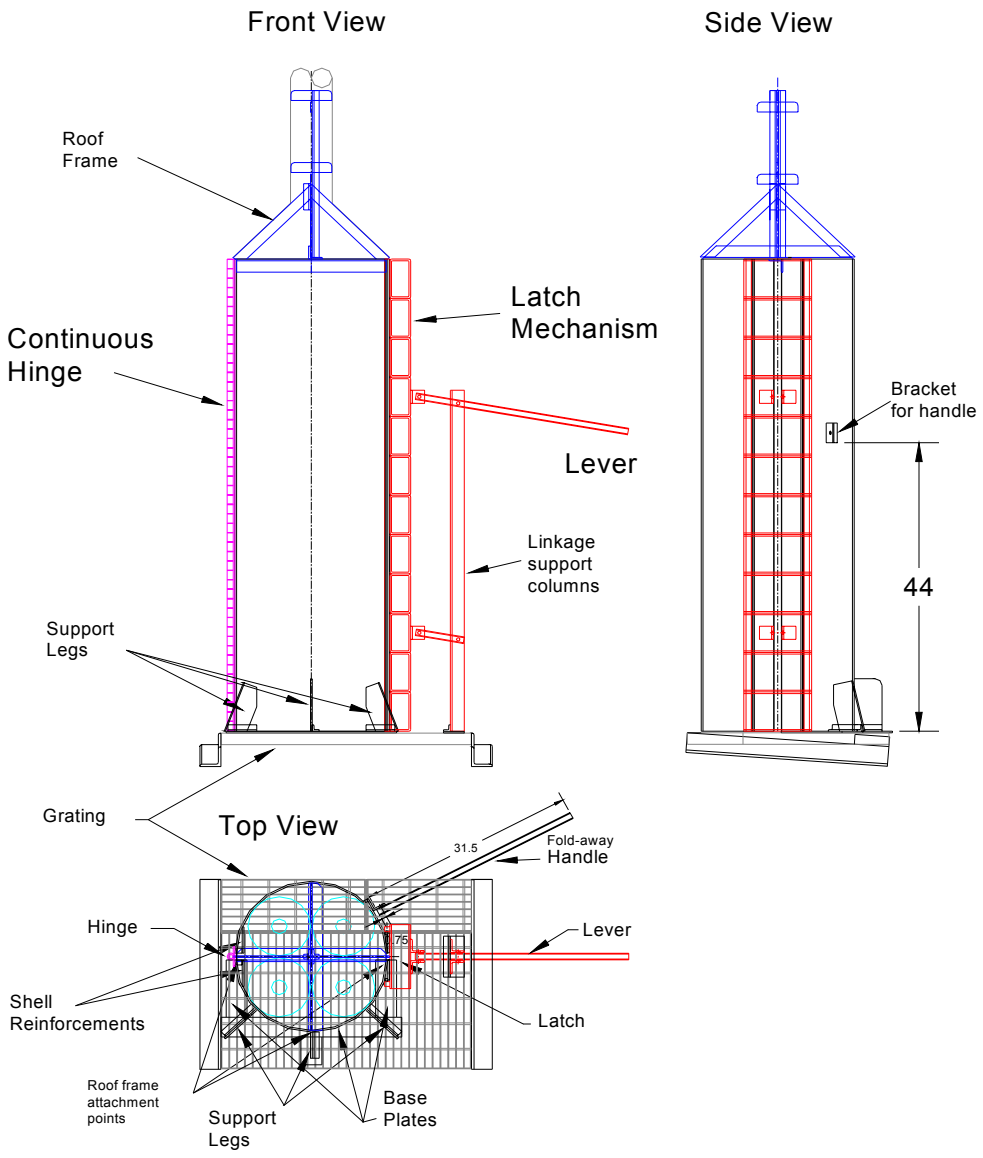

Figure 2.26 Fuel Storage Building Design

The air may enter underneath the building through the bottom grating. The top of the stack is located above the roof of the ARC. The upper half of the stack is painted black

Figure 2.27 Fuel Storage Building

to help induce a convective draft up the stack. To address the potential hazard of lightning striking the fuel storage building, the vent stack is connected to the ARC's lightning rod bus cable.

Because a forced exhaust system for the arc heater room was not in the offing, some alternative means of addressing fugitive fuel gas leaks was required. The approach used was to enclose the supply and actuation lines within a transparent hose (Fig. 2.28). This enclosing hose was in turn, connected to a hose going to a vent stack mounted outside, above the laboratory roof. The remotely actuated fuel supply valve is mounted on the outside wall facing east near the vacuum tank. The compressed air used to actuate this supply valve is conducted in a plastic hose fastened onto the metal fuel line. If the fuel line catches fire, the plastic actuation line will melt and release the pressure in the actuator that holds the fuel supply valve open. Hydrogen fires are usually not visible.

An oxygen injection system was designed, but not assembled. The necessary valves, fittings, and tubing have been purchased and are in storage. All of these parts have been cleaned for oxygen service at the factory and are labeled as such. An expanded metal cabinet was built and installed on the east wall of the ARC for storing the oxygen bottles. A new cleaned-for-oxygen-service regulator will need to be purchased, because the original was scavenged for another part of the facility.

If and when this oxygen system is assembled, the installer must be cognizant of the inherent danger of fire that a high-pressure oxygen system poses. Basic fire prevention involves removing at least one of the three causal elements of a fire: fuel,

oxidizer, and an ignition source. These elements cannot be totally separated in an oxygen system. In an oxygen atmosphere, just about anything that is not already oxidized is a fuel. This is why the plumbing has to be clean; oil or debris would basically act as kindling. Metals will burn in oxygen if they are ignited. The potential ignition mechanism for an oxygen system is adiabatic compression. The primary hazardous scenario is a sudden valve closure causing the flowing oxygen to compress to the point that it gets hot enough to ignite the metal plumbing. The higher the system pressure is, the greater potential there is for ignition by adiabatic compression.

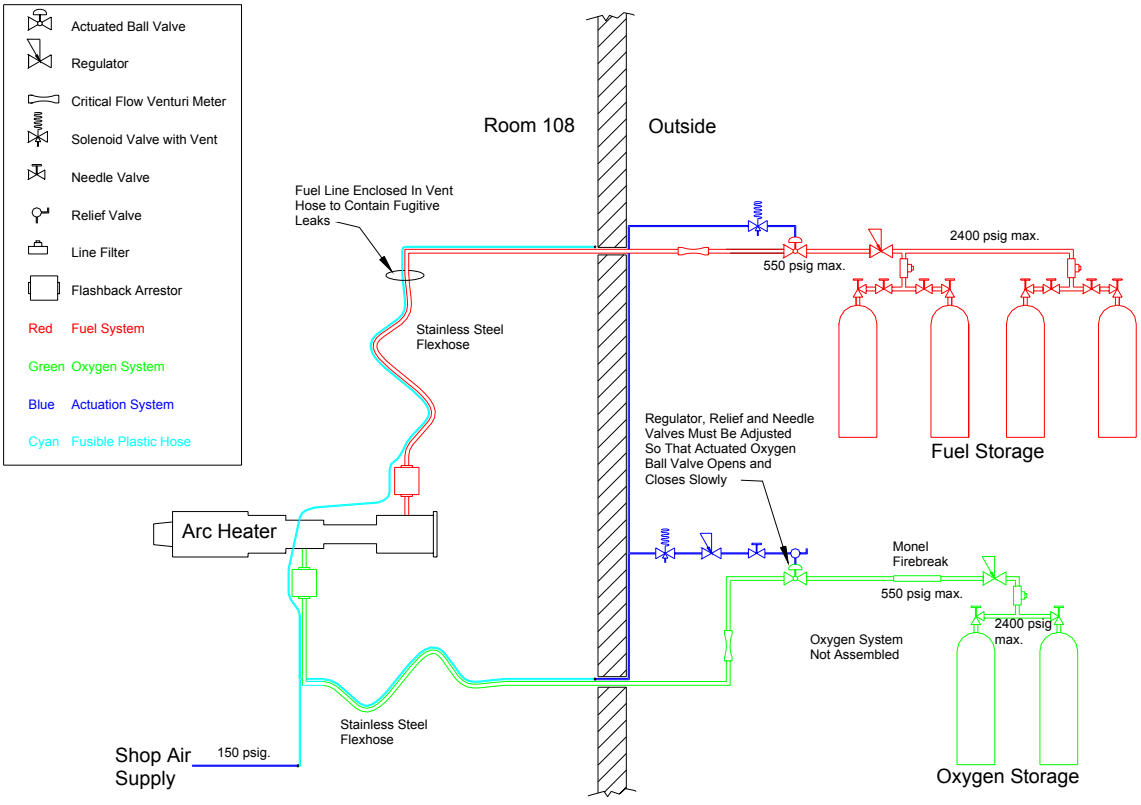

Figure 2.28 Fuel and Oxygen System Design

2.7 Injection Segment

The plenum chamber of the arc heater was to be modified in order to inject hydrogen into a nitrogen-oxygen mixture for the simulation of the chemical and gas dynamic state of the flow exiting a scramjet combustor. Although this specialized injection segment was machined years ago, it has never been installed and tested (Fig. 2.29 and Fig. 2.30). The reason that it has not been tried is that the probe system was not completely ready to evaluate the effect of the injection segment on the arc heater flow quality. A test run with the injection segment installed would have only served to demonstrate or refute the survivability of the segment. In addition, the fuel gas injection

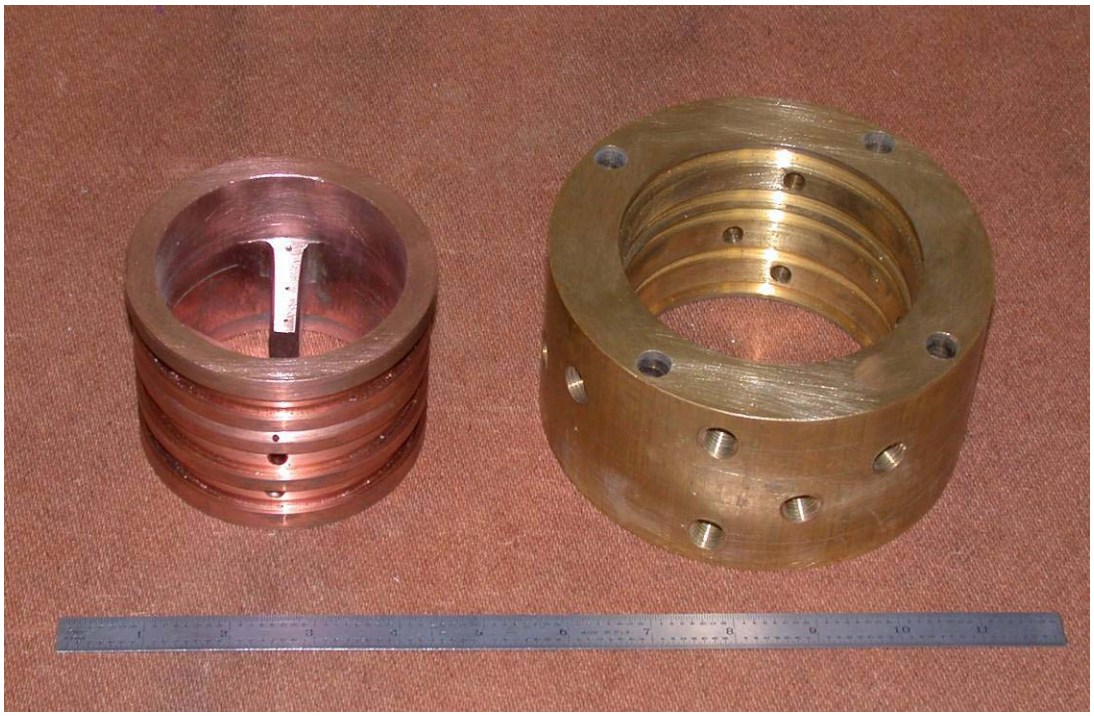

Figure 2.29 Injection Segment and Cooling Water Housing

system was not completed until after the fuel reformation research was begun.

The unusual feature of the injection segment is the presence of injection struts that protrude into the flow. The secondary gas flow is discharged through small holes in the leading edges of the struts. The rationale of the protruding struts was to introduce

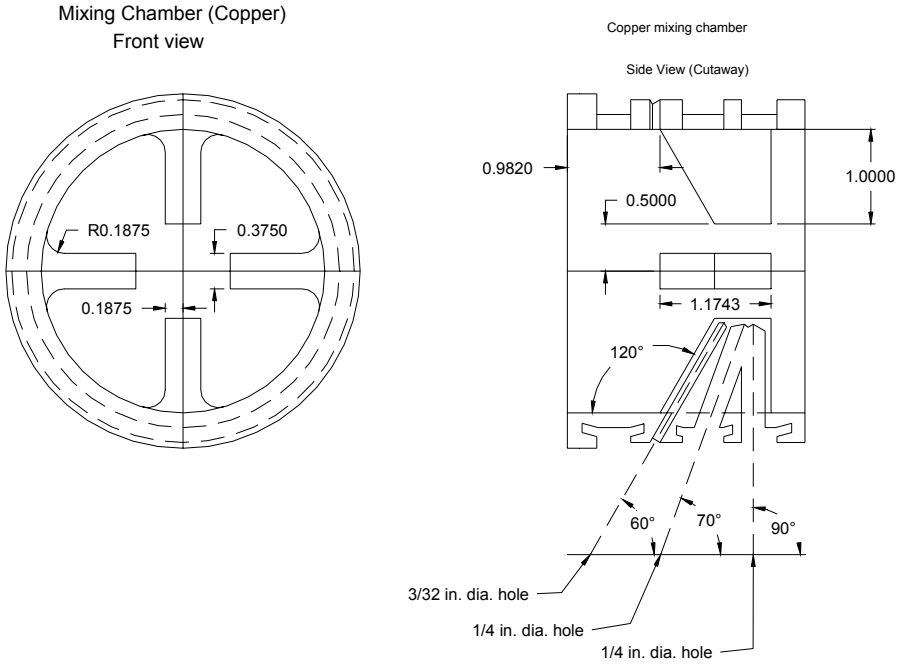

Figure 2.30 Injection Segment Design

more hydrogen into the core of the flow and also to enhance mixing through the formation of trailing vortices. During a conversation at a conference, a European Space Agency researcher complained that cold gas injected radially from the wall into the plenum chamber of their arc heater did not mix readily with the primary arc-heated gas.

If this approach eventually proves to be unworkable, there is a more conventional injection segment on hand from AEDC that has injection holes flush with the inside surface (Fig. 2.31).

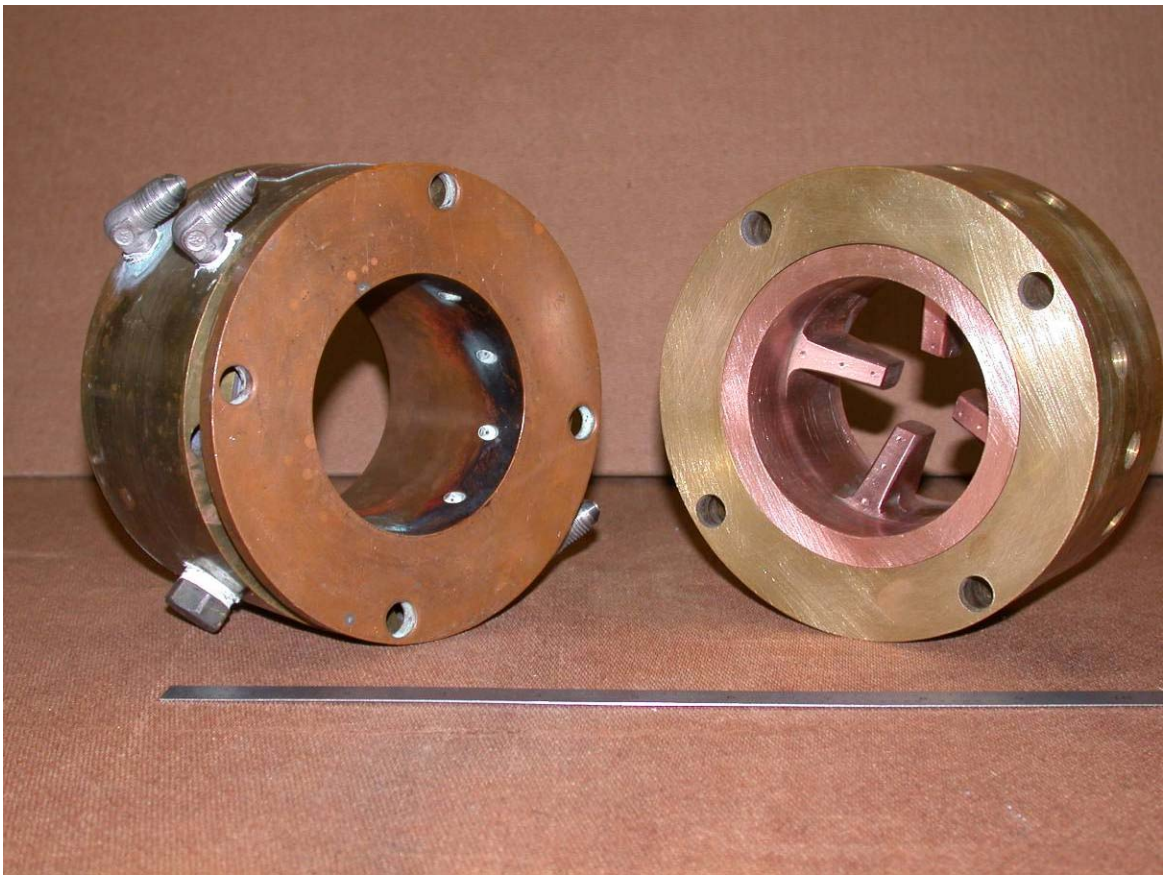

Figure 2.31 Plenum Chamber Gas Injection Segments

2.8 Flow Diagnostic Probes

Because of the high temperature of the flow exiting an arc heater, making diagnostic measurements in the flow is extremely challenging. For the F-5000 running on nitrogen, the bulk temperature ranges from 3000 to 5000 K at the nozzle exit. Moreover, it is not unusual for an arc heater to have a very peaked temperature and enthalpy distribution across the exit plane, with the peak temperature typically amounting to about twice the bulk-averaged temperature (Fig. 2.32 from Ref. 15). Some non-metallic heat shield materials such as reinforced carbon-carbon can withstand arc-heated flow without cooling to some degree, but generally not at full intensity or indefinitely. In fact, historically, the main application of arc-heated wind tunnels has

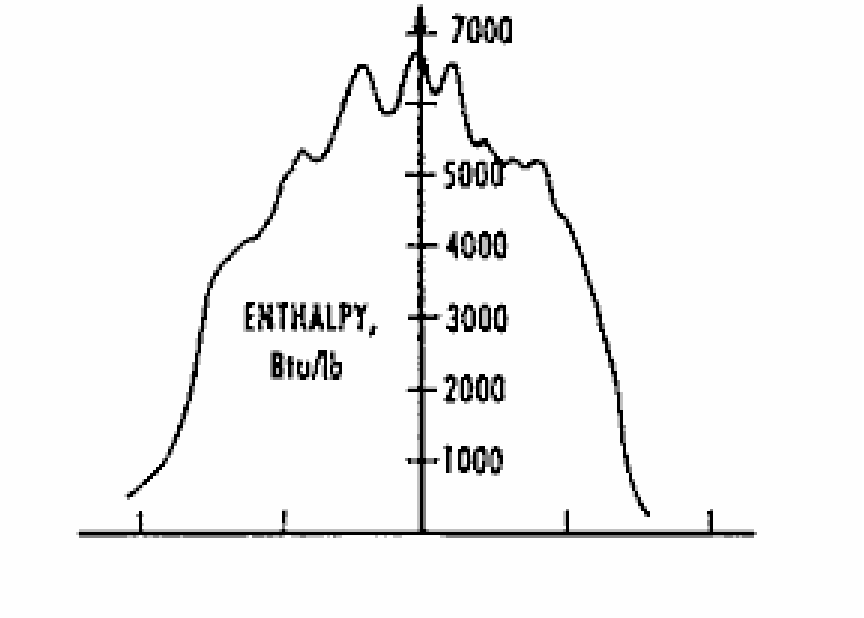

Figure 2.32 Typical Peaked Enthalpy Profile at Nozzle Exit

been to test such materials to failure. A number of different metallic probes have been developed for plasma flow surveys. Some uncooled probes, such as a null-point calorimeter, which consists of a copper slug with a thermocouple attached to the back, must be quickly swept though the flow in order for it not to melt. Except for an ablative probe, probes that linger in the flow are generally made of copper and are water-cooled.

The Greyrad probe design (Ref. 16) is actually one of the simpler designs of water-cooled probes (Fig. 2.33). The probe is used to make a calorimetric measurement

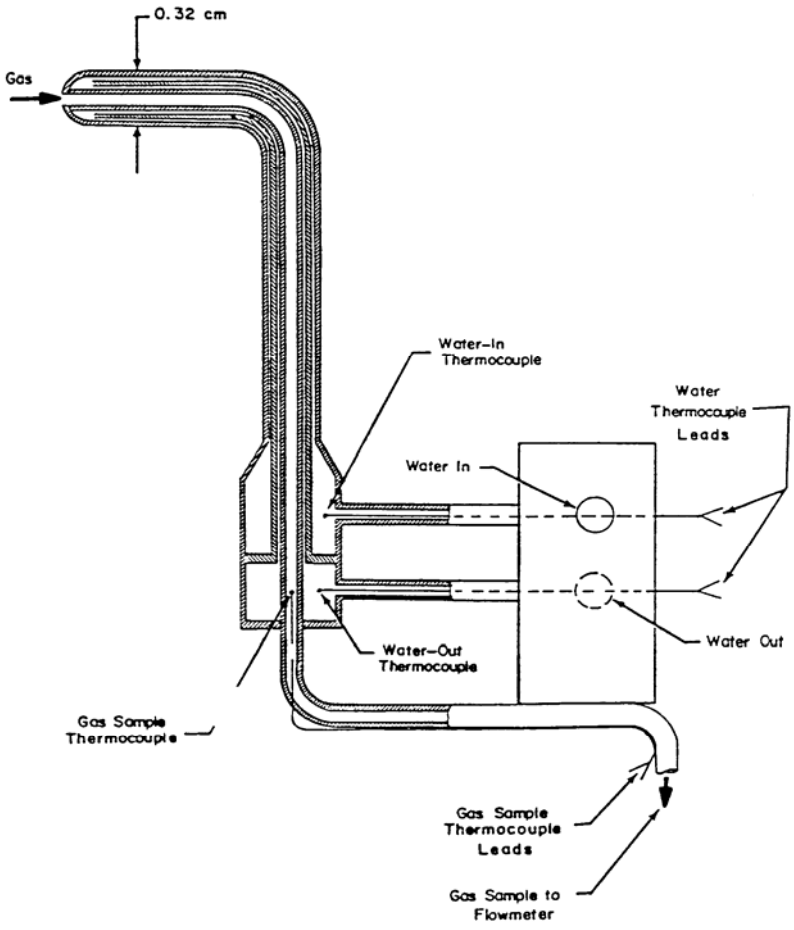

Figure 2.33 Greyrad Calorimetric Total Enthalpy Probe

of the total enthalpy of the flow. The enthalpy probe consists of nested tubes that direct the cooling water to impinge on the inside of the probe tip just opposite the external stagnation point. Thermocouples are placed in the cooling water supply and return lines, as well as the gas tube outlet. Flow meters are used to measure water and gas mass flow. In order to determine the total enthalpy at the probe tip, two successive energy balances are performed on the probe. The first energy balance measurements take place with no flow through the inner gas tube, so that the external heat flux on the probe may be determined. For the second balance, gas is allowed to flow through the probe, exchanging heat with the water flow in the process. The total enthalpy at the probe tip may then be calculated from the known quantities of external heat flux, the entering and leaving water temperatures, the water and gas mass flow rates, and leaving gas temperature.

$$\dot{m}_{gas}(h_{inlet_{gas}} - h_{outlet_{gas}}) = \left\{\dot{m}_{water} C_{p_{water}} \Delta T_{water}\right\}_{gas\ flowing} - \left\{\dot{m}_{water} C_{p_{water}} \Delta T_{water}\right\}_{no\ gas\ flow}$$

This equation may be solved for the unknown, $h_{inlet_{gas}}$.

After researching other probe designs, the Greyrad design was adopted. A strong motivating factor was that it appeared to be feasible to fabricate one on campus, rather than having to purchase a commercial probe for thousands of dollars. In addition, the probe was also useful for measuring ram pressure and collecting gas samples which is more convenient than needing additional probes for these other measurements.

The first probe eventually proved to be ineffective. The probe stayed intact in the arc-heated flow, but lacked the sensitivity to make useful enthalpy measurements.

The faulty probe design was chiefly due to not realizing that there were papers describing the details of the Greyrad probe. It was mistakenly thought that the design was originally classified, and thereby not discussed in the contemporary literature. The first attempt at making a probe was based almost solely on a single schematic drawing from a US Air Force report on the LORHO program. The page with the schematic was stamped “unclassified”, which was interpreted to mean that the probe design had been secret for a time and subsequently declassified. The crucial issue that was overlooked was that the probe surface area immersed in the hot plume should be minimized in order to provide adequate sensitivity. The main factor in determining the geometric design of the first probe was the layout of the existing test section vessel (Fig. 2.34). To reach the exit plane of the nozzle from the traverse mechanism, the probe had to extend several inches downward and forward. Moreover, the probe tip had to be long because of the length of the vessel neck to the front flange. These two factors contributed to the first probe having an excessive amount of external surface exposed to the plasma-heated flow.

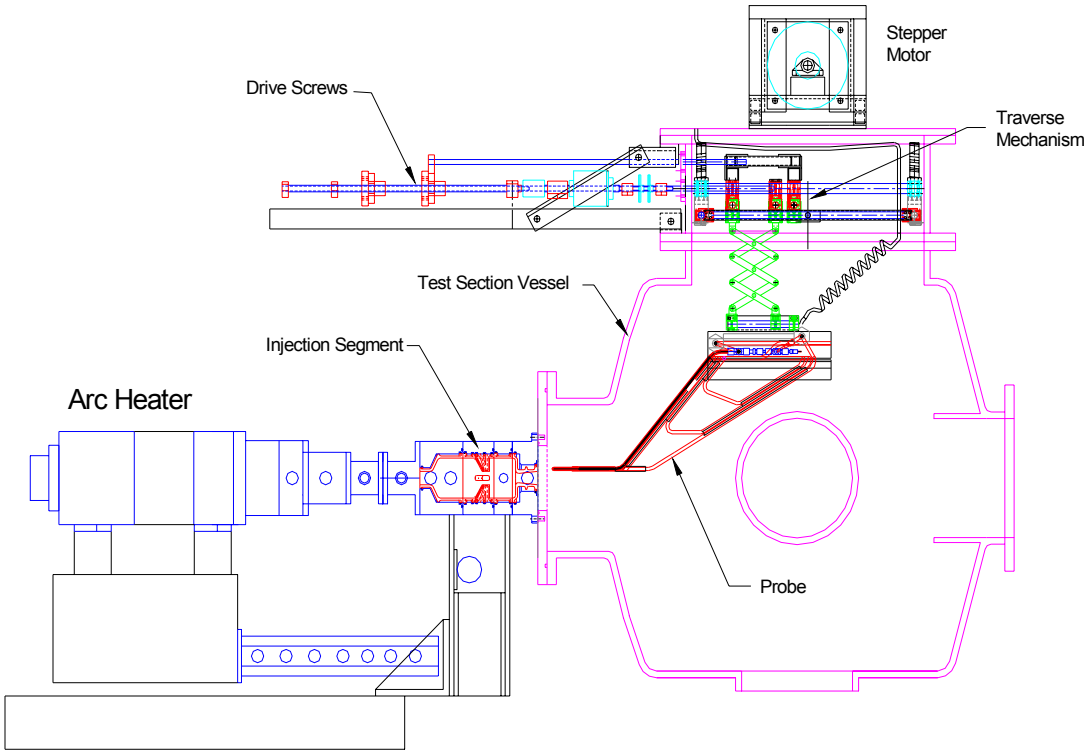

Figure 2.34 Set-Up with Long-Necked Test Cabin

The first probe also featured an elaborate structural framework of copper tubes and joining blocks to support the leading nested tube against the force of the arc heater stream (Fig. 2.35). The design philosophy at the time was to have nothing except water-cooled copper within several inches of the plume. Accordingly, all the thermocouples were installed at the top of the probe, which was protected by heat shields. Nanmac ribbon junction thermocouples were selected because they offered very fast response and were much less delicate than equivalently fast, bead junction thermocouples. Flat ribbon junctions have much more surface area per unit mass than the common spherical bead junction. These Nanmac ribbon junction thermocouples typically have response times of less than 30 milliseconds (under conditions not specified by the manufacturer). The type E thermocouples used to measure the temperature difference in the cooling water were factory installed into flow-through compression fitting housings. The

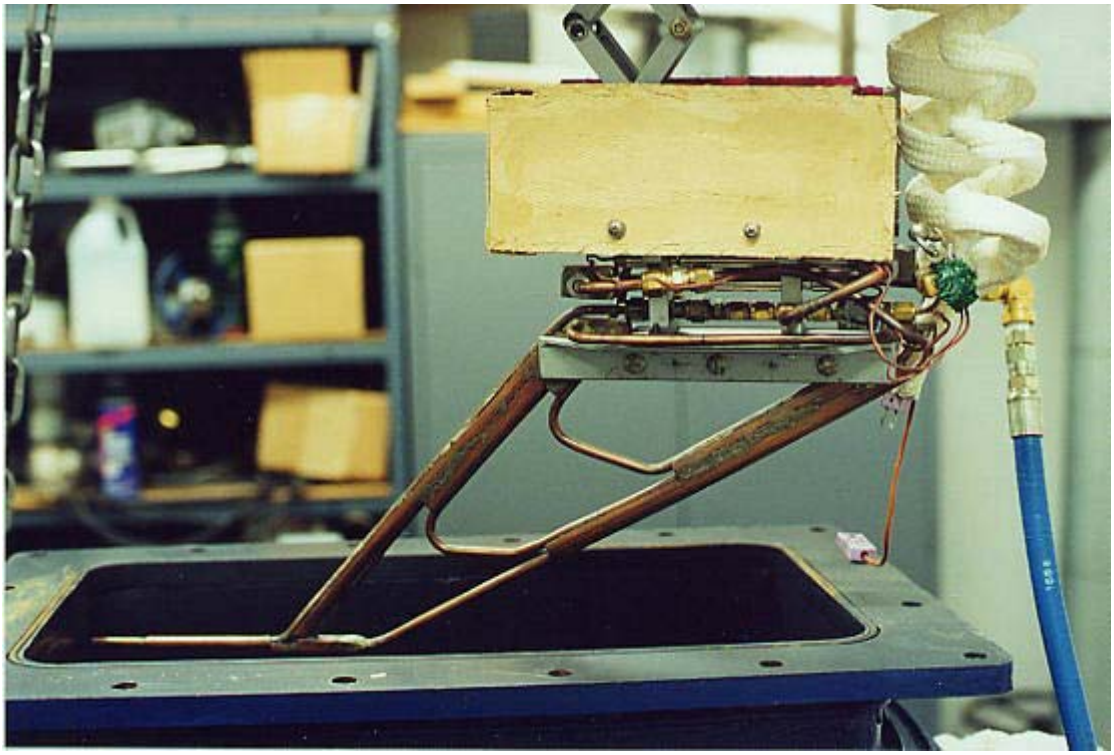

Figure 2.35 First Generation Probe Being Lowered into Test Cabin

leaving gas temperature thermocouple was also a type E ribbon junction thermocouple. This thermocouple has a conventional configuration of an exposed junction at the end of a stainless steel sheath. The junction end of this thermocouple was inserted into a compression tee, in a position that allowed the gas flow to impinge upon it.

The fabrication of the first probe proved to be very difficult and required considerable study and practice of silver alloy brazing techniques. The probe assembly proved to be a formidable heat sink; it had to be heavily insulated with alumina silica fabric in order for a single propane torch to gradually heat it up to a brazing temperature of 1200° F. The large number of brazed tube joints was particularly troublesome. Weeks were spent in an effort to fix all the pinhole leaks at the tube joints. The high thermal conductivity of copper and silver did not allow the hand torch heating to be

localized at a single joint. For this reason, fixing a leak in one joint often created a leak in an adjacent joint. To achieve the tube nesting for the first probe, brazed joints were avoided by using compression fittings instead. However, putting the compression tees in this configuration does not make disassembly possible once the ferules are swaged into the tubes.

Once the probe was finally ready, it was connected to the main cooling water system. It was then discovered that sufficient water flow through the probe could not be obtained with the 300-psi supply pressure. As a rule of thumb, the water velocity should be on the order of 50 feet per second inside the nested tubes to achieve a sufficiently high rate of convective heat transfer. To remedy this problem, a twin-piston pressure washer pump, capable of producing 1000-psi was purchased. The belt-driven pump was then mounted on a 4-inch I-beam along with a 1.5 HP motor (Fig. 2.36). The pressure washer pump discharges 2.2 gallons per minute at 1725 rpm, so to obtain 1.0 gallon per minute, pulleys were installed to make the pump shaft rotate at half the motor speed. To obtain this flow rate of 1.0 gallons/minute through the probe, a supply pressure of 800-psi was required.

Figure 2.36 High-Pressure Twin-Piston Pump

The first operational test with the first probe was a sweep though the plume several inches from the exit plane of the nozzle. Damage occurred in an unexpected location, the back of the probe assembly where it connects to the traverse mechanism. The thermocouple wires were burned and the Teflon gas tube and a thermocouple connector melted. The location of the damage appeared to have been shaded from direct thermal radiation from the plume, so the damage probably was caused by hot, recirculating airflow driven by the arc heater jet. The plastic thermocouple connectors were replaced with ceramic connectors and the burned wires were replaced with thickly insulated wires. As a further step, more heat shielding was added to the back of the probe base.

Once the probe testing resumed, the next difficulty encountered was electromagnetic noise corrupting the signals. The source of this noise was eventually traced to the cable connecting the traverse system stepper motor to its driver. Adding another layer of shielding to this cable fixed the problem.

Traversing probe measurements were tried first. The probe would be moved a tenth of an inch and stopped. Then the stepper motor driver's output (motion busy) would cycle the gas tube solenoid valve after a delay from a timer circuit. The probe system seemed to be working well in regard to the motion and the valve cycling, but the thermocouple measurements were not showing a step change when the gas tube valve was open.

After this disappointment, a less ambitious probe measurement routine was tried: measurement of a single point on the nozzle centerline, with the solenoid valve manually engaged rather than automatically. This would give the probe plenty of time to make a good measurement. After a couple of test runs conducted in this manner, it was evident that there was not a discernable change in the probe water ΔT when the gas tube valve was opened (Fig. 2.37). The heat flux from the internal gas flow was just too tiny relative to the external heat flux on the probe. In Figure 2.36, no increment in the ΔT signal is seen when the gas tube valve is opened, but in reviewing the video footage of the test run, a leak appeared on the probe during the last few seconds of the run. A vapor stream covered part of the probe, and this change in the external heat flux can be seen on the ΔT plot.

The developers of the Greyrad Probe define the probe sensitivity σ as

$$\sigma \equiv \frac{\left[\left(\Delta T_{water}\right)_{gas\ flow} - \left(\Delta T_{water}\right)_{no\ gas\ flow}\right]}{\left(\Delta T_{water}\right)_{gas\ flow}}$$

For their probes, they achieved sensitivities ranging from 0.1 to almost 0.17.

The design of the second total enthalpy probe began by examining if a larger diameter internal gas tube could be accommodated to allow more gas flow to increase the relative amount of heat flux from the gas flow to the cooling water. The diameters

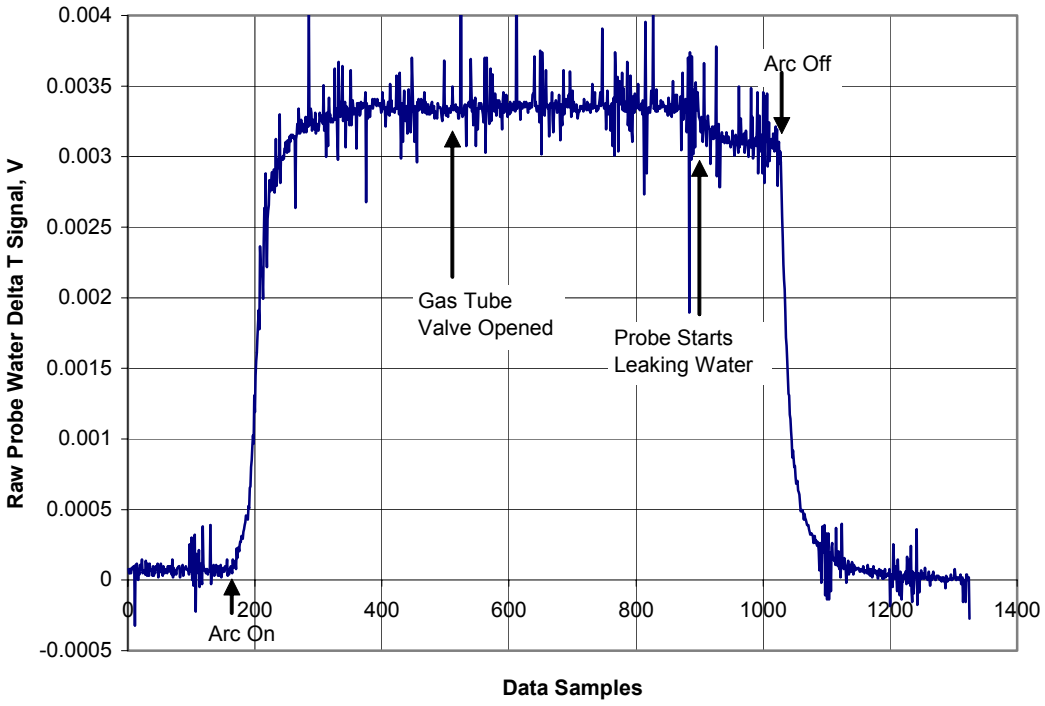

Figure 2.37 Insufficient Probe Sensitivity

of the nested tubes for the first probe were dictated by the sizes of available compression fittings. This resulted in a 1/16", 1/8", and 1/4" O.D. configuration, because there were no fittings available in between 1/16" and 1/8". Implementing the

nesting with brazed joints rather than compression fittings, allowed the flow areas inside the second probe to be tailored much better given the much wider choice of tube sizes. The new probe was designed with a 3/32", 5/32" and 1/4" O.D. combination of nested tubes. The inside of a 3/32" O.D. tube has almost four times the flow area of a 1/16" O.D. tube. The cooling water pressure loss in the first probe was extreme due to the long length of narrow cooling water passages. For the improved probe, the length of the nested tubes was minimized so that the cooling water pressure drop would not be as severe.

The fabrication process for the new probe was greatly improved over that used for the first probe. The technique of step brazing, using filler alloys with different melting points, was applied to making the new probe. The assembly procedure was carefully planned so that certain joints would be made with a higher melting temperature alloy so that the joint would not be disrupted when another joint was subsequently formed nearby with a lower temperature alloy. Three different brazing alloys were required to make the probe. The other technical improvement was attaching two hand propane torches together (so they could be held in one hand) to double the heat flux applied to the assembly. The brazing process works much better if the joint is quickly brought up to temperature rather than gradually.

Another departure from the first probe design was to have the support base come down much farther, so that the probe could be shorter and stiffer (Fig. 2.38). Thick-walled stainless steel tubes serve to provide cooling water and a gas outlet in addition to taking the structural loads. The thermocouples, that pass though the interiors of these tubes, are intended to stay with the base, rather than with the probe. Additional probes, material test coupon holders, or even models could be designed to fit onto this instrumented base. A new main heat shield was made to shade the instrumented base, and much of the traverse mechanism. The stem of the probe passes though a hole in the main shield.

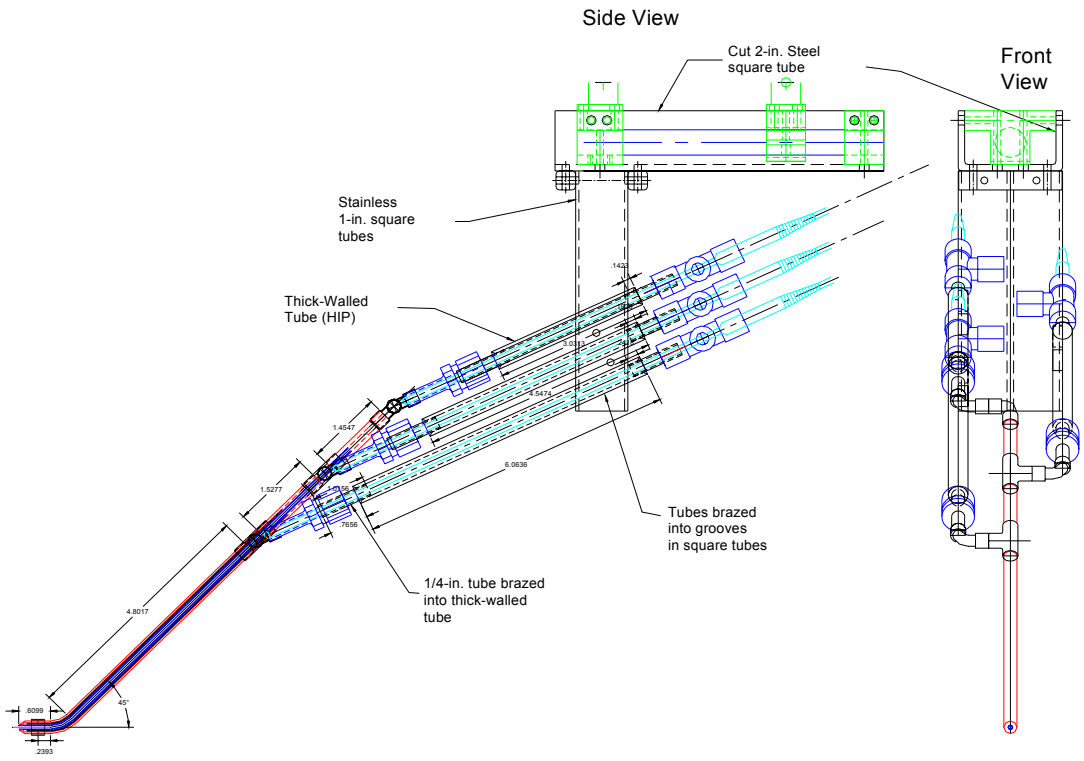

Figure 2.38 Second Probe Design with Mounting Base

Modifying the test cabin by shortening the neck to the front flange was essential for accommodating a probe with minimal surface area exposed to the hot plume. After ascertaining that shortening the neck would not weaken the vessel, most of the neck was sawed-off. A new flange was designed, machined and then welded in place onto the shortened neck. The shorter neck also allows much better access to the test cabin interior when reaching into it (Fig. 2.39).

The new flange has precise alignment marks machined into it that are used to position crossed threads across the opening to locate the centerpoint. This provides a reference point for positioning the probe tip and aligning the traverse system (Fig. 2.40).

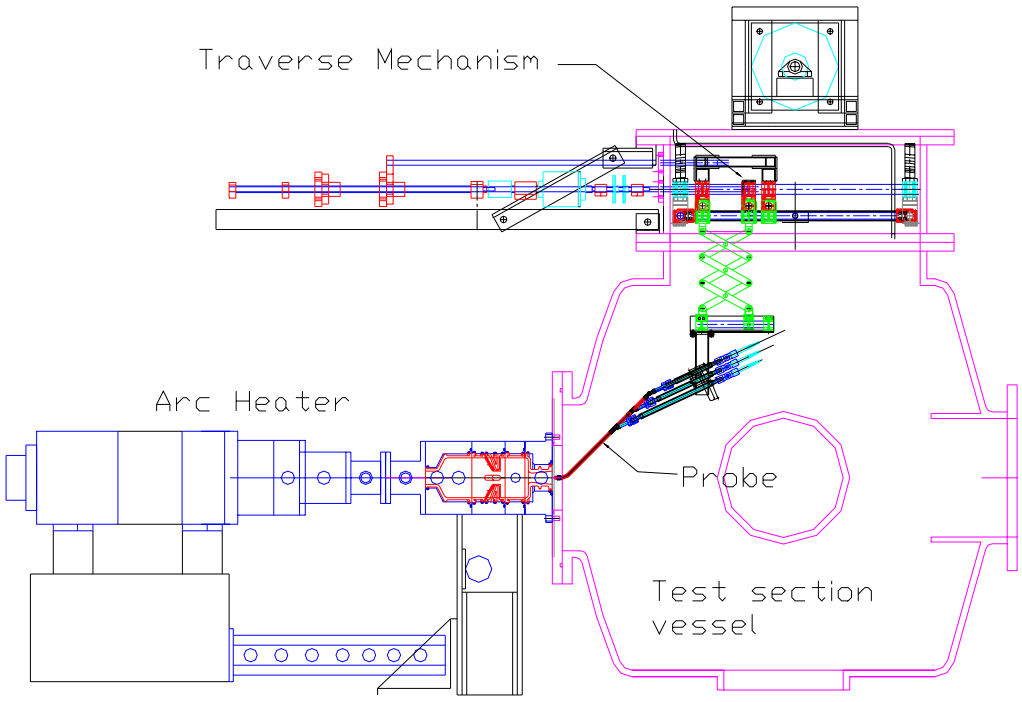

Figure 2.39 Second Probe Installed in Test Cabin with Shortened Neck

Calculations of the stress due to the moment of the estimated drag force on the probe predicted that the probe would probably bend, although this difficulty was not reported in the LORHO documentation. Indeed the probe did bend considerably during the first test run. The remedy was to reinforce the stem of the probe with a copper strip on the leading and trailing edges along with a split piece of 3/8" stainless tubing attached around the upper part of the probe stem (Fig 2.41). Although the bending was

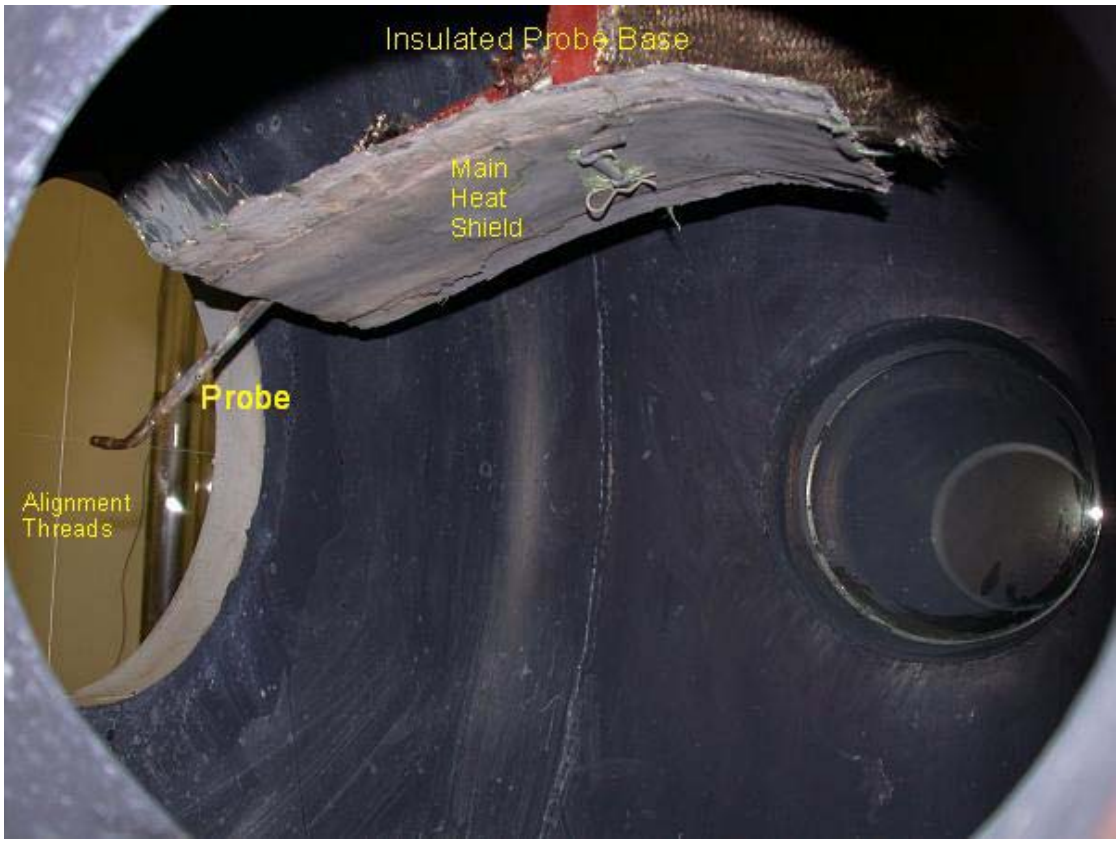

Figure 2.40 Probe Aligned with Crossed Threads

dramatically reduced by this modification, further test runs exhibited significant bending closer to the probe tip. One metallurgical characteristic of copper that

contributed to this difficulty is that it can only be hardened by cold-working. Furthermore, heating cooper will relieve the distortion in the metal grains imposed during cold-working, making the copper soft again. Accordingly, the probe could be bent quite easily by one's hands each time after being worked-on with the propane torch. The approach that finally solved the problem of the probe bending was to allow the probe to be bent by the flow stream during a test run and then manually bend it back afterwards. A few iterations of this procedure were sufficient to adequately stiffen the probe.

When the second probe was tested, it did prove to have acceptable sensitivity (Fig. 2.42). A series of test runs consistently indicated a sensitivity of about 0.1 (Fig. 2.43). Unfortunately, there was still one obstacle to measuring the total enthalpy: the lack of a good measurement of the leaving gas temperature. Much of the difficulty was

Figure 2.41 Probe with Stem Reinforcements

due to EMI on the thermocouple signal. Once the EMI was abated, the leaving gas temperature did not show much response to the opening of the gas tube valve. In order

to diagnose the problem with the gas temperature measurement, a test run was conducted with the probe tip centered on the nozzle exit and the gas tube open for the entire run duration (Fig. 2.44). A clean signal was obtained that shows a slow rise in temperature during the run. The response time of a temperature sensor in a gas flow would be expected to be much slower than the same sensor in a liquid flow, due to the great difference in the amount of mass flowing by. However, this particular thermocouple responded much faster than this to hot air from a heat gun being blown onto the ribbon junction. The problem is not the thermal lag in the thermocouple

Figure 2.42 Probe Immersed in Arc Heater Plume

junction itself but rather in the copper plumbing leading to the junction. There is a

sizable mass of copper for the gas flow to heat-up before an equilibrium temperature is reached. In contrast, the plumbing leading to the water temperature junctions comes into thermal equilibrium very rapidly due to the high velocity water flow. To greatly reduce the lag in the gas temperature measurement, the probe should be modified so that the gas flow thermocouple junction is located just opposite of the point at which the water flow exits the probe (Fig. 2.45). At this location the probe material will come into equilibrium quickly, and the remaining lag will only be due to heating the small mass of the thermocouple junction.

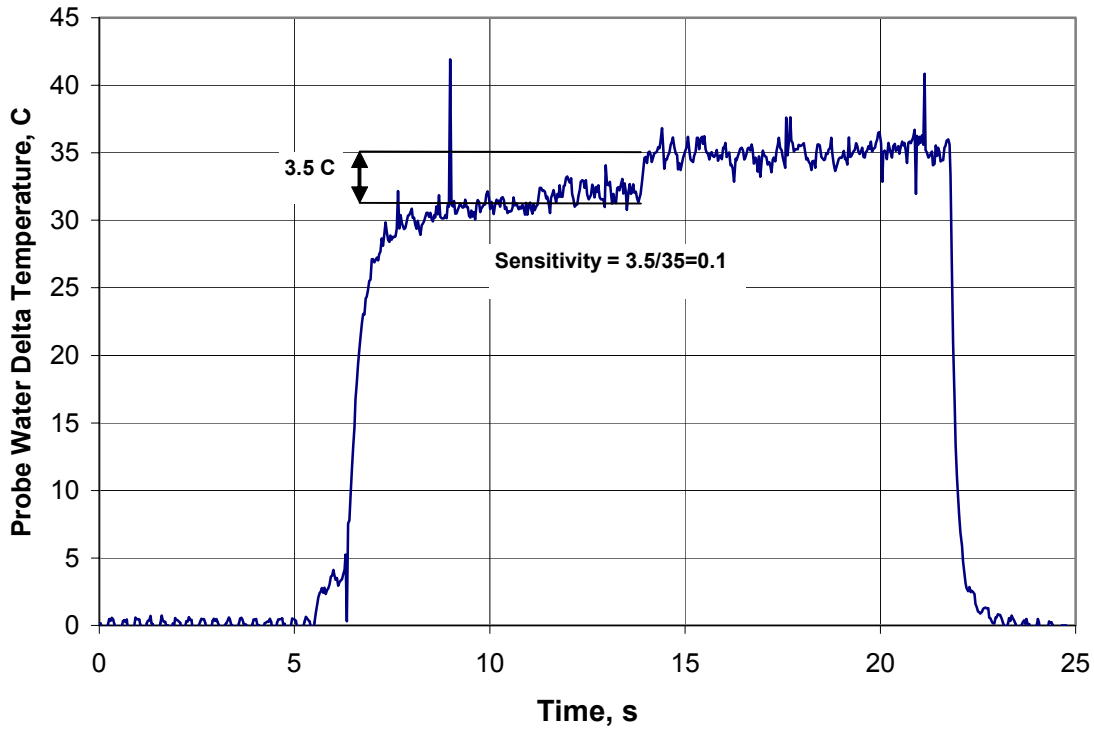

Figure 2.43 Sensitivity of Second Probe

Development of the probe measurement system was stopped with the beginning of the fuel reformation research, so this probe modification has not been made. Once

this is accomplished, it is expected that not only will single point total enthalpy measurements be possible, but also a whole series of point measurements will be attainable during a single test run. Probe sweeps of the nozzle exit have been conducted in this manner (Fig. 2.46), but they have lacked the leaving gas temperature measurements to determine a true total enthalpy profile. (Backlash in the traverse system caused the probe to be slightly off-center relative to the nozzle flow in Figure 2.46.)

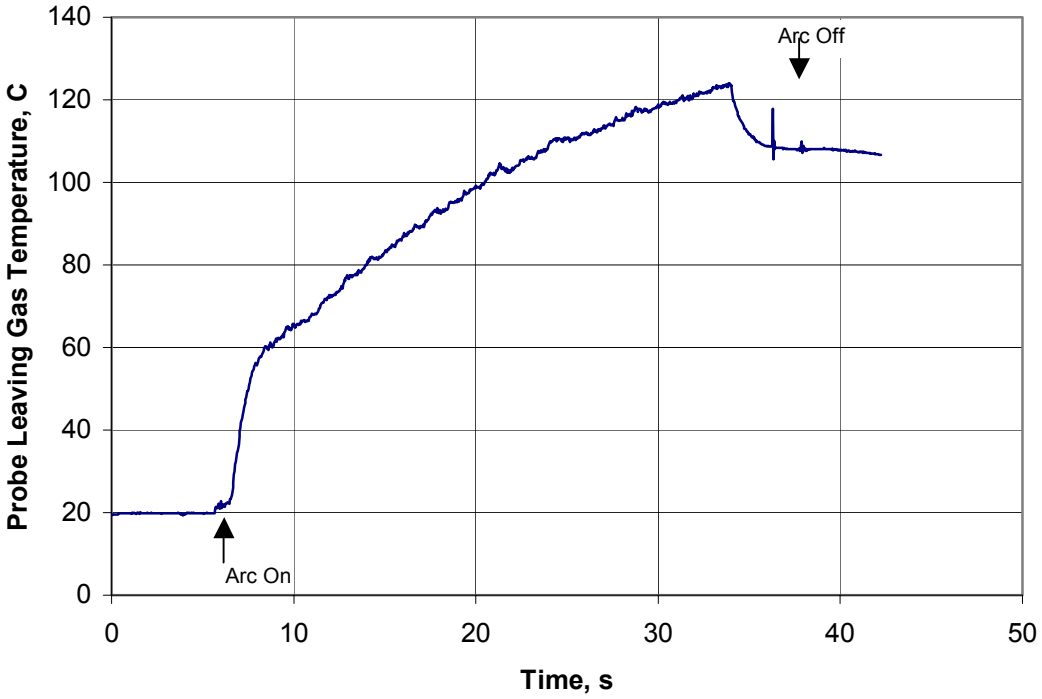

Figure 2.44 Lag in Probe Leaving Gas Temperature Measurement

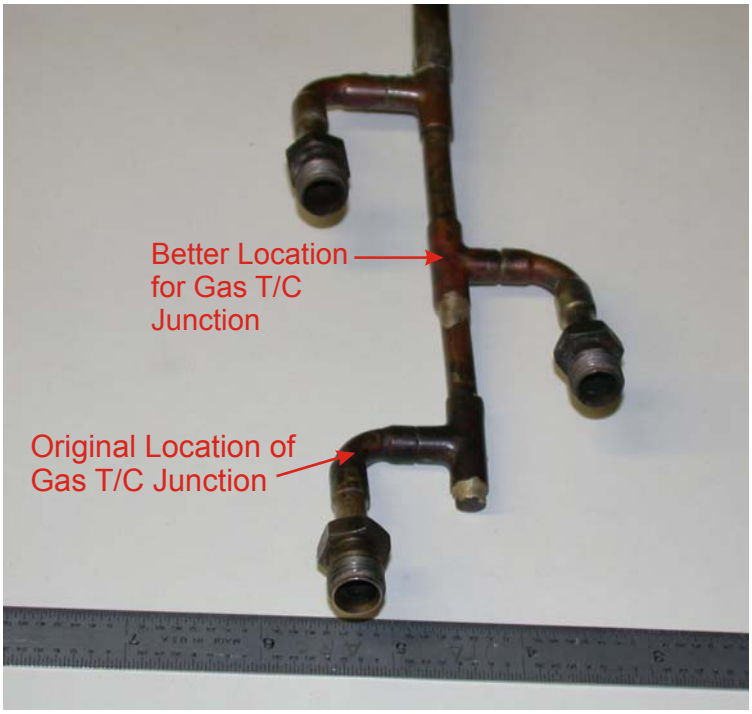

Figure 2.45 Modification to Address Lag in Gas Temperature Measurement

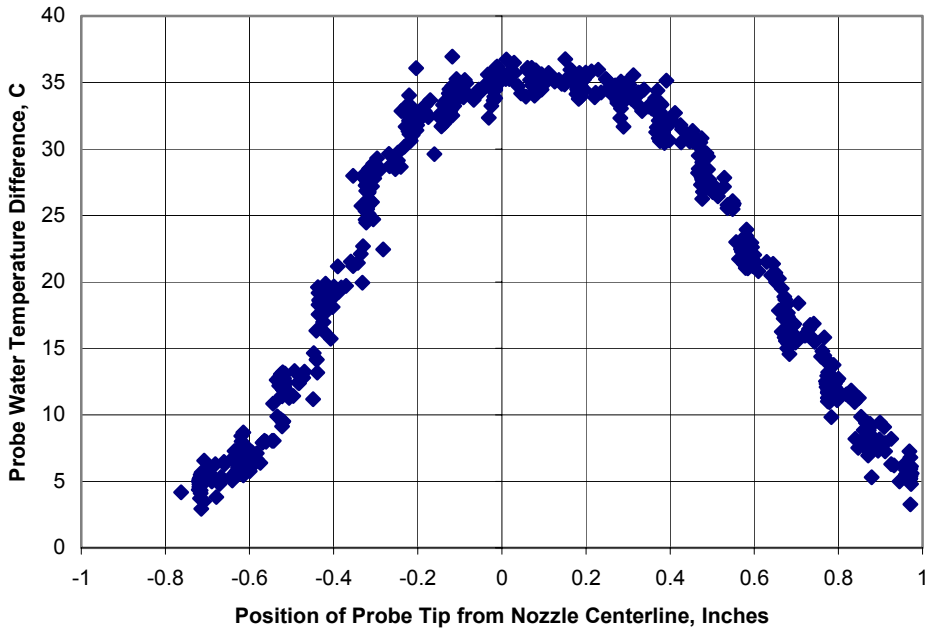

Figure 2.46 Heat Flux Distribution across Nozzle Exit

2.9 Probe Traverse System

One of the more crucial upgrades to the research capability of the facility has been the addition of a probe traverse system. This system allows probe surveys of the arc-heater flow to be performed, as well as providing the capability to insert a model or test article into the flow. The design of the traverse system was challenging because much of it would be exposed to heat and it would also have to allow a vacuum to be maintained in the facility vessels. The traverse mechanism is made up of more than 50 custom-designed parts, which required roughly 600 hours of machining time (Fig. 2.47 and 2.48).

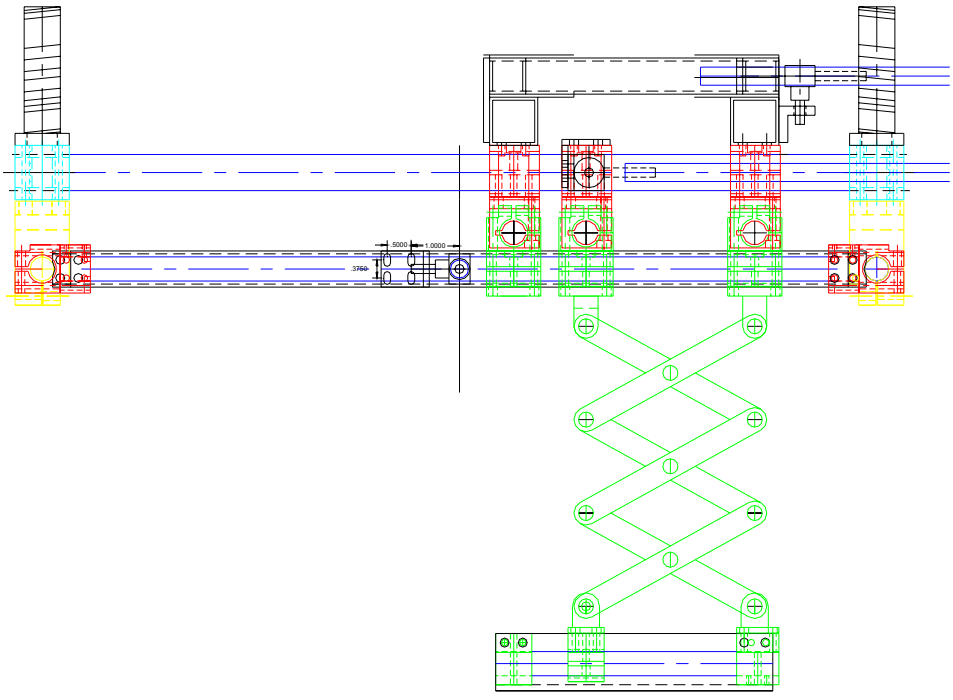

Figure 2.47 Side View of Traverse Mechanism

In retrospect, the traverse system design was overly ambitious. It may have been a better approach to first build a very rudimentary traverse mechanism, and then follow-up with a more advanced mechanism based on the lessons from the first. However, the choice was made to pursue a definitive design that would meet all the perceived requirements of SERN experiments and also have considerable versatility to support future research with the facility. In particular, having the capability to make a probe measurement in a new location every few seconds during a test run was aggressively pursued.

Initially, making the traverse system from commercially available linear motion assemblies was considered. However, these components almost universally contained aluminum or some other material that was not particularly tolerant to moderately high

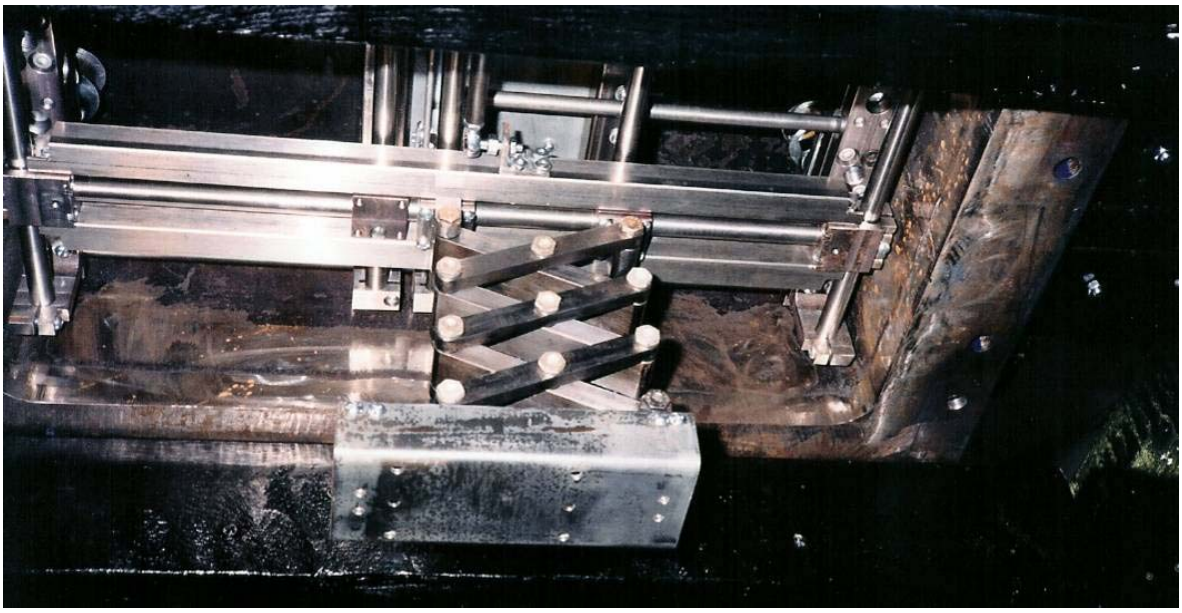

Figure 2.48 Traverse Mechanism without Heat Shields

temperatures. In addition, for the same level of strength, aluminum deflects considerably more than steel. The machined parts are made of low carbon 1214 steel, which was selected for its high degree of machinability. The original selection was 12L14, which contains lead to further enhance machinability, but Environmental Health and Safety recommended that the machinist wear a respirator while cutting it. It was judged that the gain in machinability was not worth the hassle of having to wear a respirator. If price and machinability were no object, a heat-resisting alloy, such as stainless steel, would have been a much better choice.

The most significant misjudgment in designing the traverse mechanism was due to a concern about small misalignments causing the mechanism to bind. Accordingly, the first design was revised to feature screw-fastened joints that would allow slight adjustments of the attitudes of all the shafts and bearings. In practice, it was found that such adjustments could rarely be made to the same degree of alignment precision that would have been present if the parts had been made without these joints. In other words, it is much easier to machine parts with a high degree of orthogonallity, than it is to subsequently adjust an assembly to be orthogonal. Eventually a procedure was devised for aligning the traverse mechanism, with the use of a surface table, a machinist square, vee blocks, and a dial gauge. This alignment procedure reliably minimizes the tendency of the mechanism to bind.

The mechanism can traverse a probe in all three Cartesian directions within a space 14.8-in. long by 7.5-in. wide by 11.9-in. deep. The probe motion is programmed into the stepper motor driver, via an RS-232 connection, and is then triggered to run

when an experiment begins. The traverse system is attached to an extension vessel that mounts on a rectangular opening on top of the test cabin vessel. The more heat-sensitive components of the system, the motor, drive screws, belts, and clutch brakes, are mounted outside the test cabin extension vessel (Fig. 2.49). The rest of the system,

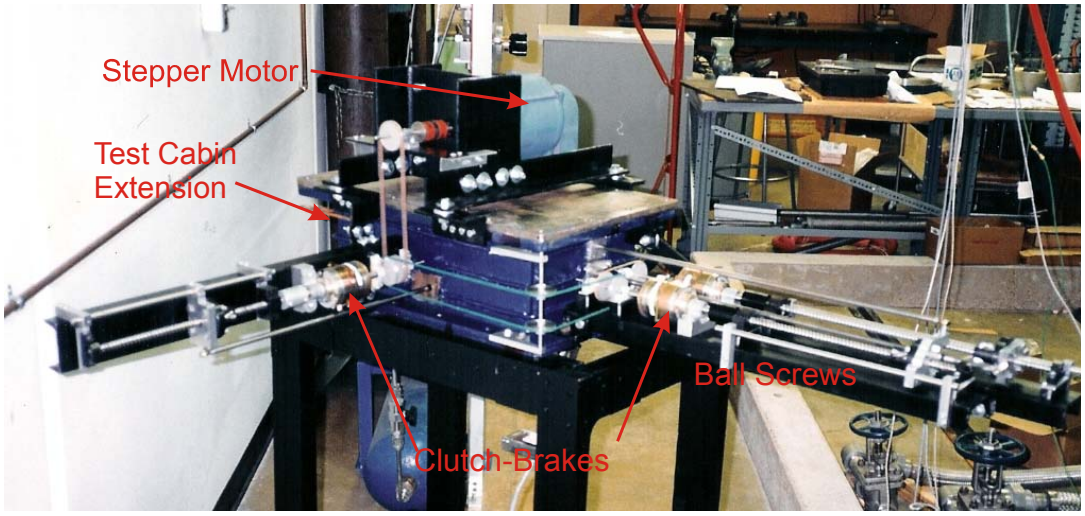

Figure 2.49 External Traverse System Components

inside the vessel, is designed to withstand at least 450 °F. Moreover, the mechanism inside is protected by heat shields, because direct water-cooling of the mechanism is impractical (Fig. 2.50). The elaborate heat shields are made of stainless steel sheets with a refractory fabric, such as Refrasil, sewn to the side facing the heat with nichrome wire. The fabric surface is then coated with a refractory cement to prevent the fabric from fraying away. In addition to the heat shields, jets of air spray onto the traverse mechanism through the top lid to help keep it cool during tests at atmospheric pressure. Moreover, the facility controls are interlocked so that either the ejector pump is operating or the cooling jets are engaged before the arc heater can be turned-on. Thus

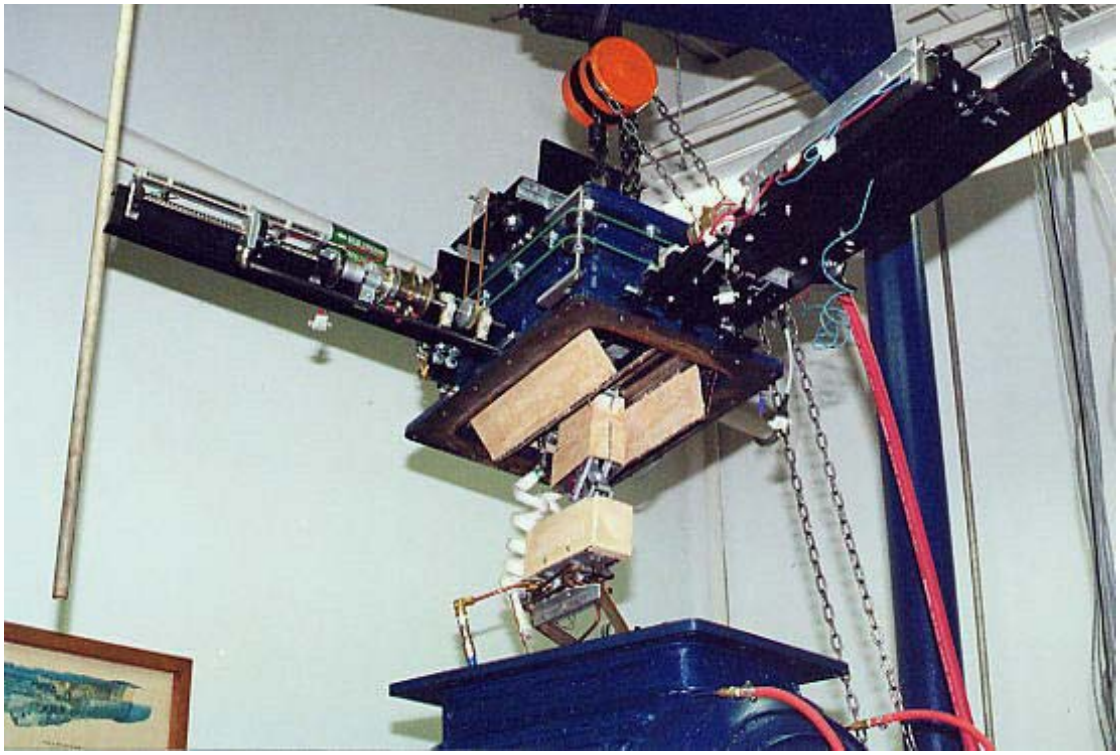

Figure 2.50 Traverse System Being Lowered onto Test Cabin

far, these measures have kept the traverse mechanism from being exposed to any more than 160 °C (Fig. 2.51). Pushrods from each drive screw pass though o-ring seals in the sides of the extension vessel to actuate the mechanism inside. To stay within budgetary constraints, a single stepper motor and driver were salvaged from a pitching airfoil apparatus, and multiplexed with electromagnetic clutch-brakes to drive three Cartesian axes of movement. This powerful stepper motor gives the system a rapid traverse capability (up to 25 inches/s), which allows uncooled probes such as a null point calorimeter to be used with the facility. The traverse mechanism was designed on the basis of minimizing deflection, which results in a structure with ample strength to insert models. A positional accuracy of ±0.03 inches has been demonstrated, which could be improved with further refinement. The linear resolution of the system, based on the

drive screw pitch and the number of steps per revolution of the drive motor, is 0.0025 inches. A precision linear potentiometer connected to the side-to-side axis gives an indication of probe position to the data acquisition system.

Apart from alignment difficulties, the most serious problem with the traverse system has been ceramic dust fouling the linear bearings. The bearings are made of a Teflon-lead composite with a steel backing that makes them much more compact than linear bearings with rolling elements. The source of the dust is the insulating materials

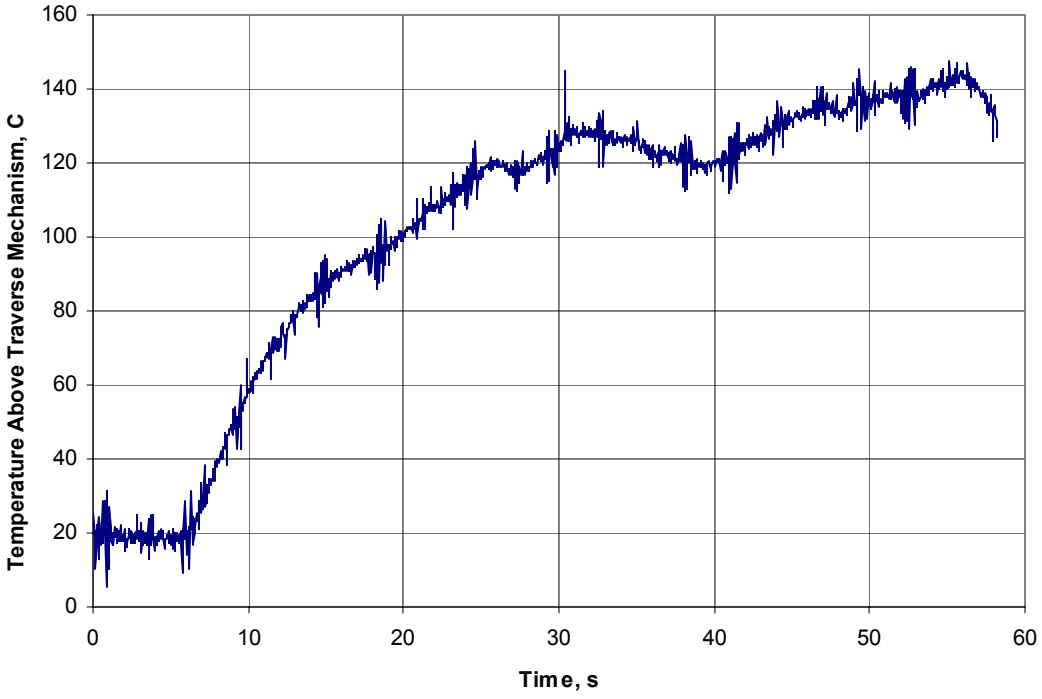

Figure 2.51 Temperature in the Vicinity of the Traverse Mechanism

used for the heat shields. The woven ceramic fiber products are particularly prone to fray in the gas currents induced by the arc heater jet. This problem is mitigated by coating the ceramic fiber textiles with silicone caulking or RTV. However, it is

recommended that flexible covers be installed over all the exposed shafts to better address this problem. If the bearings become badly fouled, then the mechanism has to be dismantled in order to replace them. The bearings are not expensive, but re-assembling and aligning the traverse system is quite an undertaking.

2.10 Data System

The test run data were acquired by an HP3852 data acquisition system. The data system has hardly been altered since Sarrat Boonjue set it up, so the interested reader may find the details in Ref 12. Commands for the HP3852 are transmitted though an HPIB (GPIB) interface from an HP Vectra computer that is equipped with a BASIC language processor card. The HP BASIC acquisition programs are very rudimentary. The HP3852 can record thermocouple data directly as temperatures with cold junction compensation, but the acquisition speed was unacceptably slow when it was used in this manner. To achieve an acceptably fast data rate (roughly thirty measurements per second on each channel), the acquisition programs only have the system record voltage values into a single vector without performing any data-reducing calculations. The vector of raw voltage values is transferred by floppy disk to another computer for reduction. At one point in the past, HPVEE, a graphical user interface data system control program, was tried, but it slowed the system down too much. However, there have been about four generations of computer CPU advancement since that time, so

HPVEE or LabView on a newer PC would likely work very well to control the HP3852. Though the data acquisition system is somewhat outdated, it probably has never been exploited to its full potential.

Electromagnetic noise has always presented a challenge in the effort to obtain quality data from the facility. Most of the success in mitigating this problem is the result of extensive application of shielding and good grounding practices. The worst source of noise, the 10,000 V arc ignition system, is no longer a factor since it is not used anymore. There is an unknown source of noise that is about 2 millivolts in magnitude and a few hundred hertz in frequency. The most successful approach against this noise has been to install active low-pass filters on the signal lines. Five Krohn-Hite filter-amplifiers were purchased for the most important signals. These eight-pole Butterworth filters have a cut-off frequency of twenty hertz and also amplify the signal by 100. On the probe water ΔT signal is an Omega OmniAmp III that amplifies the thermocouple signal 1000 times. Although it is referred to as a DC amplifier, it does function like a low pass filter due its lack of response to alternating or fluctuating voltage.

For the fuel reformation research, two isolation signal conditioners were purchased to protect the data acquisition system from the plasma torch power supply. One of them converts the torch voltage to a 0-10 V signal and the other takes the 0-50 mV output from the current measurement shunt and converts it to a 0-10 V signal.

The plasma torch system proved to be much noisier than the arc heater. The thermocouple and millivolt pressure transducer signals that had been fairly readable (with conditioning) during arc heater operations were totally obscured by the noise from

the plasma torch. Switching away from millivolt output transducers allowed data to finally be obtained for the plasma torch experiments. For the arc heater facility, it is recommended that the millivolt transducers be phased-out and replaced by current output, or high level voltage output transducers (such as 0-5V, 0-10V and 1-5V). In many cases, extant thermocouples installed in the facility could be replaced by RTD's and IC sensors (such as the Analog Devices AD592). Any new pressure transducer purchases should be for current output or high-level voltage output rather than 0-100 mV output.

CHAPTER 3

DESCRIPTION OF EXPERIMENTS

3.1 Arc Heater Pyrolysis Experiment

A primary reason that the fuel reformation research was awarded to UTA was the close similarity of the Thermal Dynamics F-5000 to a Linde arc heater. There are a few differences in the designs. The Linde arc heater has a coil to magnetically spin the arc termination spot, whereas the F-5000 relies strictly on swirling gas flow to stabilize the arc. The F-5000 has a plenum (sometimes referred to as stilling or settling) chamber, which the Linde arc heater lacks. A little-known fact about arc heaters is that they began as chemical processing devices that were much later adapted for use as high enthalpy wind tunnels.

Rather than trying to install the experiment completely in the test cabin, it was judged to be more practical to simply build small new vessels to insert between the arc heater and the test cabin. The main advantage was that it was easier to provide optical access to the flow emerging from the nozzle with the small vessels than within the test cabin. The two chamber vessels were made from 5” thick-walled pipe (schedule 160) with custom flanges welded onto them. A schematic is shown in Figure 3.1, and a photograph of the diagnostic chamber is shown in Figure 3.2. A water-cooled cold trap is located at the center of the diagnostic chamber for collection of the carbon particles.

This trap was designed with two removable sections, a hollow probe and a collection cup located at the base of the probe. These were to be removed after a test run for weighing the carbon deposit. Two viewing ports were located at the entrance to the chamber for observing the spectra emitted from the arc heater exhaust plume. A

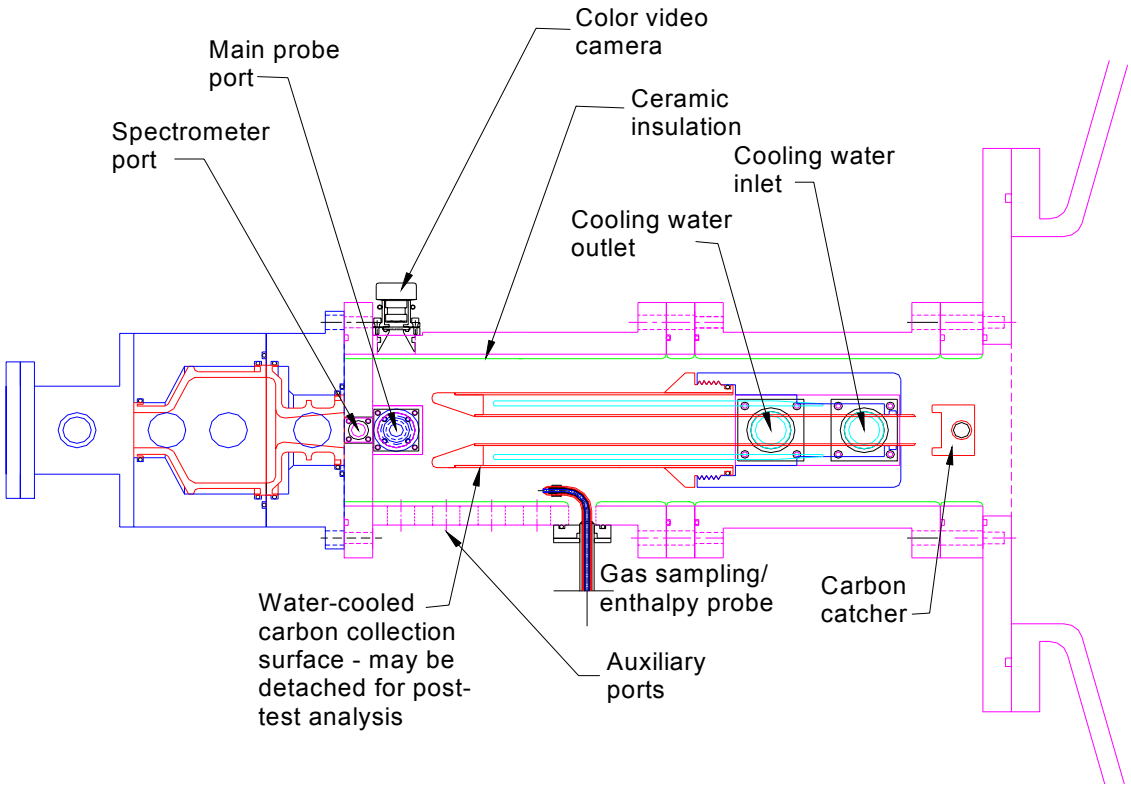

Figure 3.1 Diagnostic Chamber Set-Up

miniature video camera was also available for viewing the interior of the test section and arc chamber during actual runs.

Installing the gas injection system for the pyrolysis experiments principally involved following the existing plan for providing hydrogen for the SERN experiments with a few minor changes. To provide sufficient mass flow to the arc heater it was necessary to supply methane at full bottle pressure to the main nitrogen injection

system. For this reason, the bottle regulator and critical flow venturi were not installed, as they would have been otherwise. The mass flow would be measured with the larger critical flow venturi that serves the nitrogen injection system. High capacity flashback arrestors were borrowed from the Pulse Detonation Test Facility and installed (in parallel) just upstream of the arc heater. To provide a failsafe shutdown mechanism in case of a fuel line fire, a fusible plastic air actuation line was run along the fuel supply line from the arc heater all the way to where the fuel line enters the room from outside.

Additional cooling water pipe and fittings were installed in order to move the

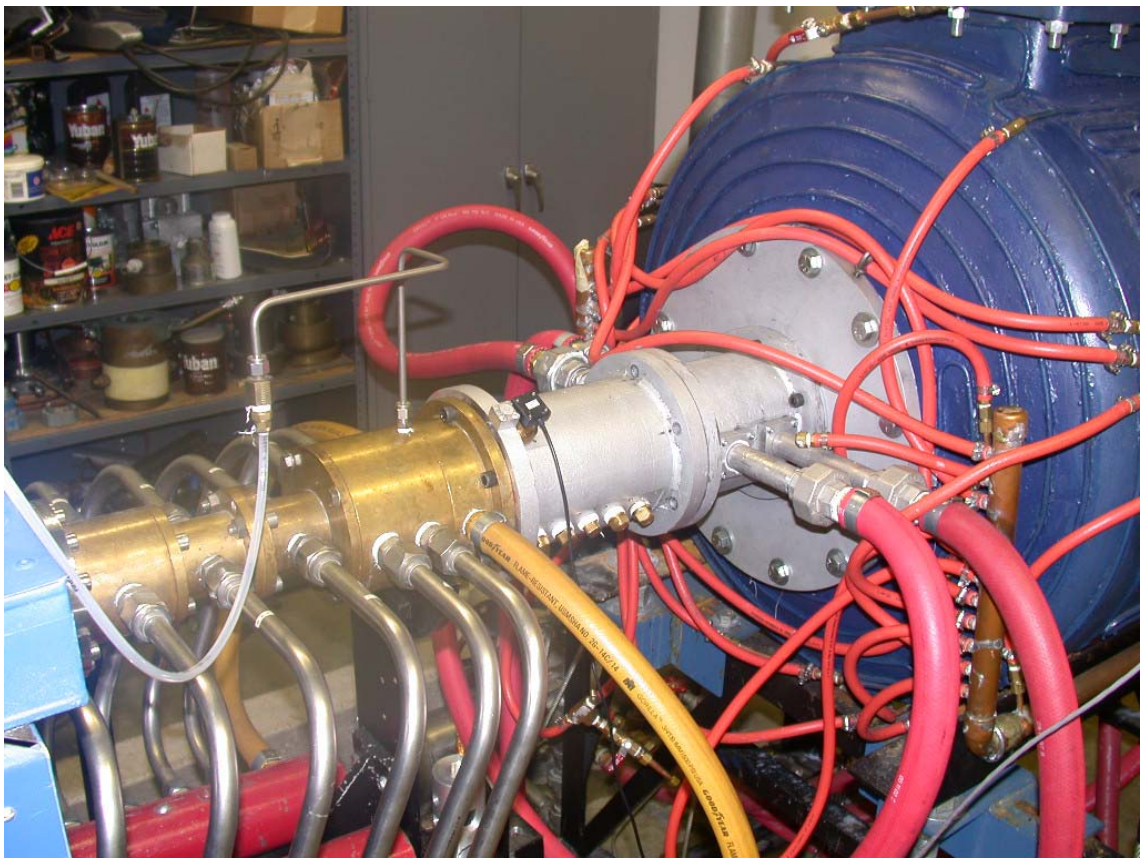

Figure 3.2 Assembled Test Apparatus

arc heater farther away from the existing test section to allow insertion of the new diagnostic chamber. Furthermore, cooling lines were run from the arc heater cooling water manifolds to the carbon trap within the diagnostic chamber.

In addition to the normal arc heater instrumentation (described in Ref. 17) for determination of arc heater total pressure and enthalpy, an Ocean Optics USB2000 fiber optic spectrophotometer was used to examine the emission spectra from the gas species (Fig. 3.3). This instrument has a bandwidth of 350 to 1000 nm, spanning the visible to near infrared spectrum.

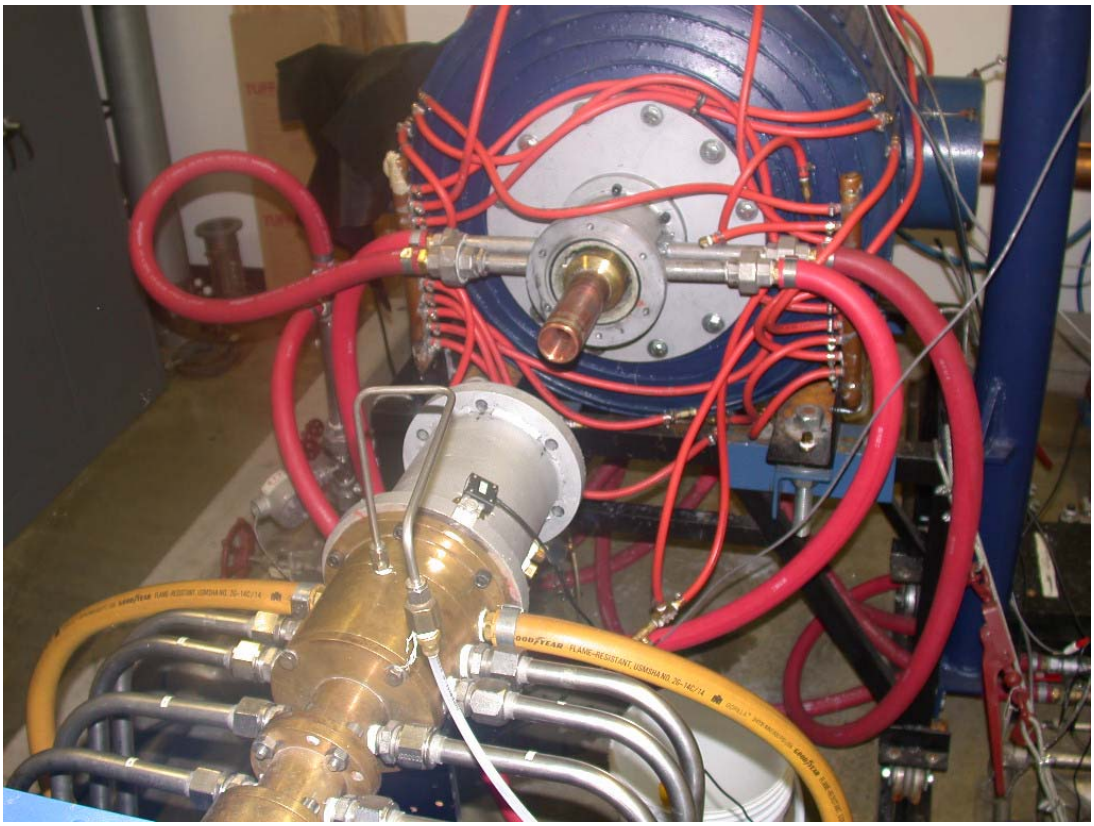

Figure 3.3 Diagnostic Chamber Separated to Reveal Carbon Trap

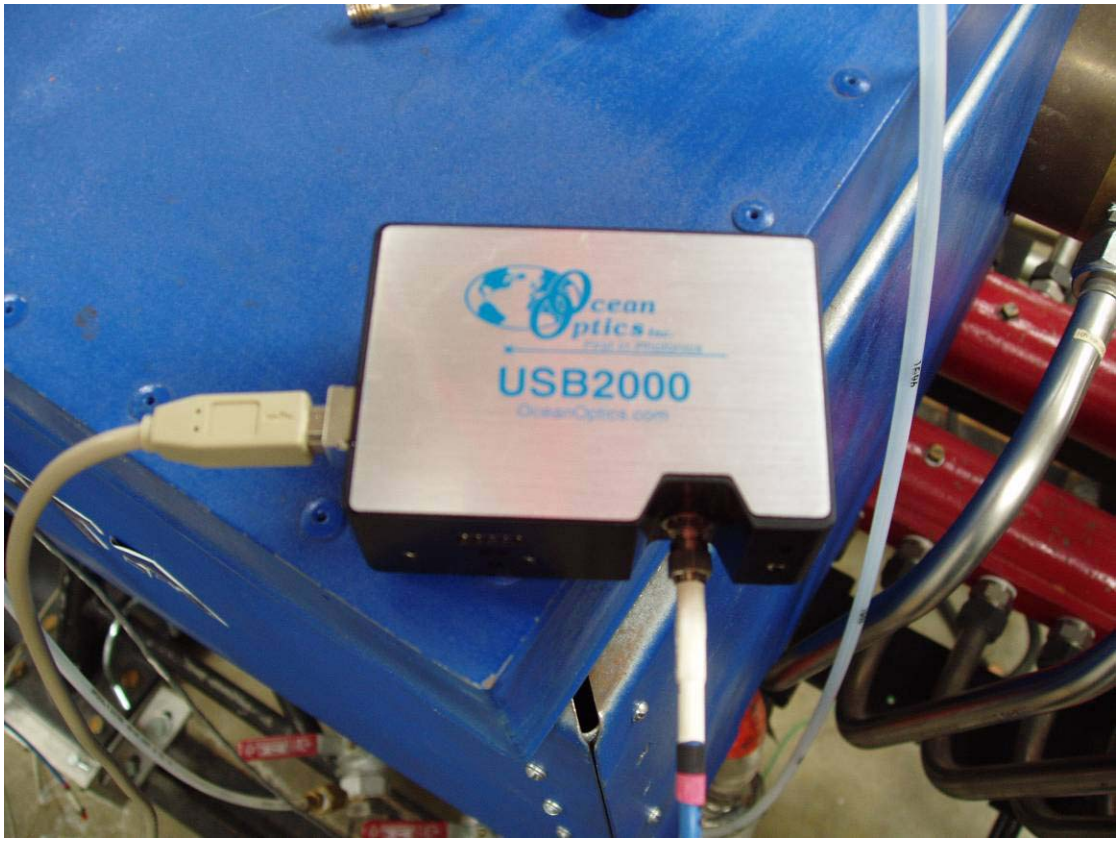

Figure 3.4 Ocean Optics USB2000 Spectrophotometer

The experimental test program commenced with shakedown testing of the arc heater with methane. However, a failure occurred in the DC power supply after only one second of operation during the first test run. The nominal conditions for the first test run were I = 500 A, $\dot{m}$ =0.11 kg/s, h_t = 4500 kJ/kg, and p_t = 3.5 atm, although the run duration was too short to obtain sufficient data for determining actual arc heater bulk enthalpy and pressure. The spectrometer was not installed for this test run; however, as shown in Figure 3.5, the carbon cold trap was totally covered with a very fine carbon

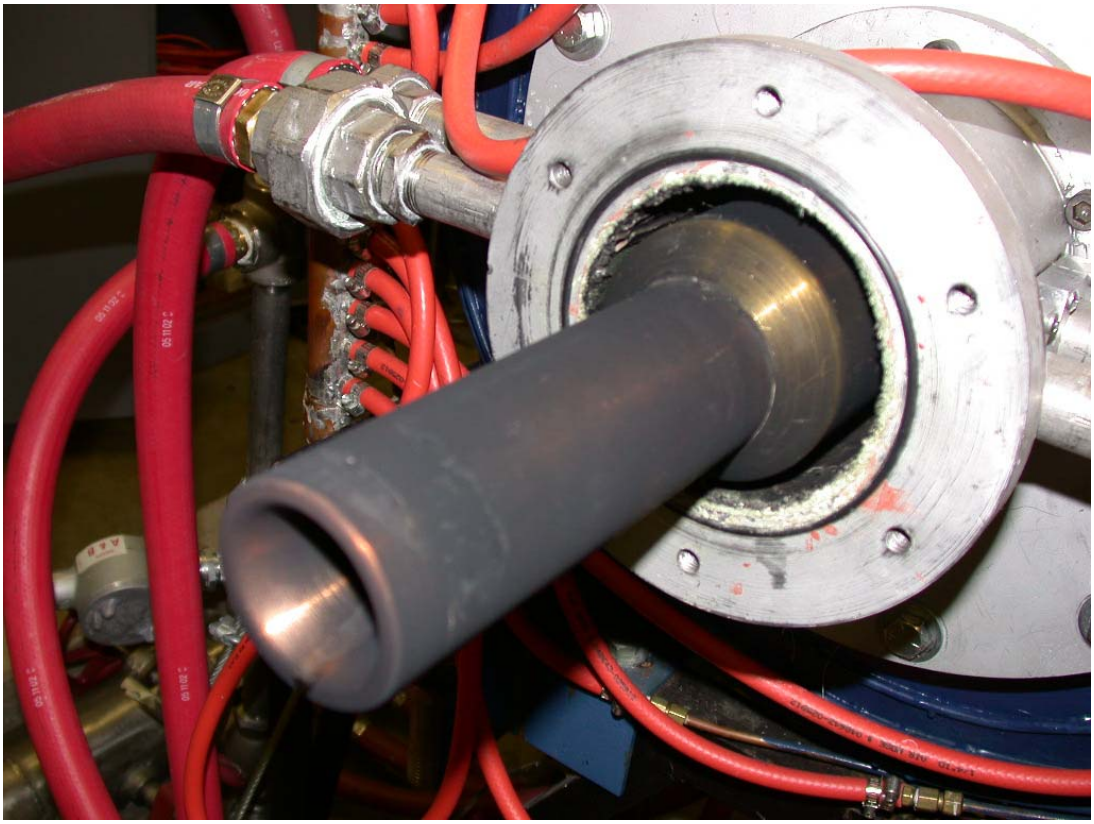

Figure 3.5 Cold Trap Covered with Carbon after Test Run

powder deposit, clearly indicating that methane pyrolysis had occurred. The brief arc heater test coated all of the surfaces downstream of the plenum chamber with a thin layer of carbon, indicating that hydrogen was liberated from methane molecules. Although the arc heater electrodes are cold surfaces, a post-test inspection with a borescope revealed no carbon build-up upstream of the plenum chamber. This finding may have important implications since other methods of fuel reforming tend to create a carbon build-up, which progressively restricts the flow.

3.2 Plasma Torch Pyrolysis Experiments

Because the damage to the Robicon arc heater power supply was too expensive to have repaired in the short term, the hydrocarbon pyrolysis experiments were continued using a modified industrial plasma-cutting torch. The modified Hypertherm Powermax 600 unit (Fig. 3.6) has only about 1/300th the electrical power of the arc

Figure 3.6 Hypertherm Powermax 600

heater facility, but it was expected that the physical and chemical phenomena occurring within the small torch were potentially similar to a larger scale case. The Hypertherm torch unit is nominally rated at 5.6 kW, with an operating voltage of 50-320 V, a variable current output of 20-40 A, and a supply flow rate of approximately 6 scfm. The modifications to the Hypertherm torch were made to address potential safety problems.

Unlike the arc heater, the small cutting torch is cooled by gas flow rather than water flow. Only a portion of the gas flow going into the torch head (model PAC123T) actually goes in close proximity to the arc. Most of the gas flow is used for cooling and confining the cutting jet. A surprising aspect to the Hypertherm torch head is that some of the gas flows back into the plastic handle. This presents no problem if one is using air or nitrogen that the torch is designed to use, but is a considerable fire hazard if a fuel gas is substituted. Therefore, it was necessary to remove the handle and enclose the back portion of the torch head so that the combustible gas could be contained and vented outside (Fig. 3.7). As an additional precaution, the torch head enclosure also had a continuous flow of argon going into it. The gas control plumbing was taken out of the plasma torch power supply as an additional safety measure. To prevent the pyrolysis products from burning, the plasma torch was discharged into an evacuated test cabin. This practice was followed for this entire study.

Just prior to MSE-TA's contract deadline, a few pyrolysis experiments were performed with the Hypertherm torch. The emission spectra of the pilot jet of the torch running with a methane feedstock did imply the presence of hydrogen; however, it was difficult with our limited background to surmise much else from the spectral data. From these initial experiments, the strongest evidence for hydrogen liberation actually came from the associated production of free carbon from the brief arc heater run.

The pilot jet mode of the Hypertherm unit is a feature of the torch that allows it to operate without transferring the arc to a work piece, which is particularly helpful when cutting expanded-metal. However, the unit will only deliver 12 A in this mode

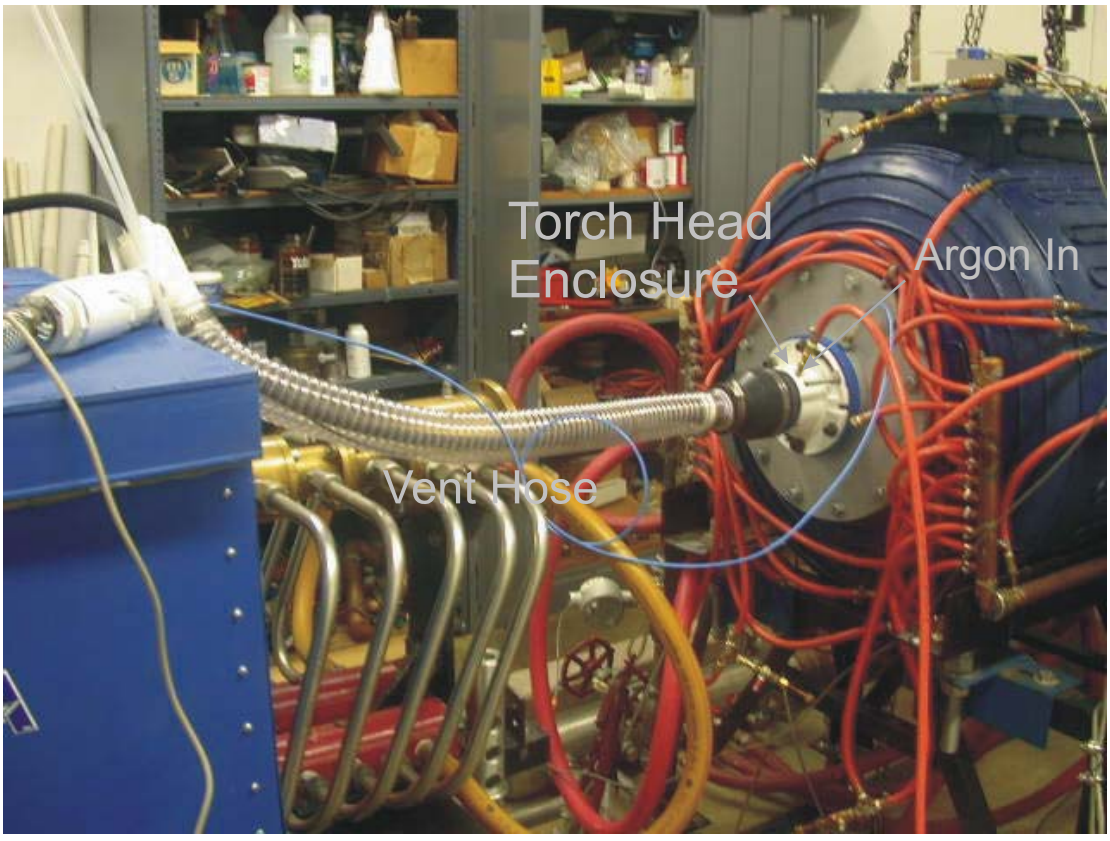

Figure 3.7 Plasma Torch Installation

until the jet contacts a conductive workpiece, which allows the arc to transfer to it. Once the arc is transferred, the power supply will deliver the current selected on the dial, from 20 to 40 A. Therefore, to utilize the full power of the Hypertherm unit, it was necessary to make an anode for the arc to transfer to. The design of this anode component was heavily influenced by prior experience in fabricating water-cooled calorimetric total enthalpy probes for the arc-heated wind tunnel (Fig. 3.8). Accordingly, the anode cooling water jacket has the same water passage configuration as a Greyrad probe. The other aspects of the anode design were motivated by a desire to avoid any further modification of the Hypertherm torch head.

The insulator portion of the torch head has a threaded end for attaching a bypass flow-directing shell around the torch nozzle. A brass adapter piece was made to screw onto this thread and to also block the bypass flow around the nozzle. The copper anode block attaches to the adapter with four non-conductive (PEEK) screws. A gasket seals between the anode block and the adapter piece and also electrically isolates these parts from each other. The face of the anode is situated 0.0313 inch from the tip of the nozzle and features a countersunk flow orifice. The 0.0625 in. diameter anode orifice is considerably larger than the 0.038 in. diameter of the nozzle orifice. Past the anode orifice, the flow area abruptly increases to the inside of a ¼-in. copper gas tube. At this location, four ports were installed to permit pressure measurements, observation of the emission spectra, and the injection of a secondary gas flow. The anode section was instrumented with temperature transducers for making calorimetric measurements in the same manner as a Greyrad probe. The entering and leaving water temperatures were

measured along with the leaving gas temperature. A turbine flow meter was used to measure the cooling water flow. Accounting for the gas mass flow was complicated by the design of the Hypertherm torch head, which diverts most of the gas flow for purposes other than being arc-heated. According to Hypertherm, the air flow is 50 scfh though the nozzle orifice, 160 scfh around the outside of the nozzle, and 150 scfh

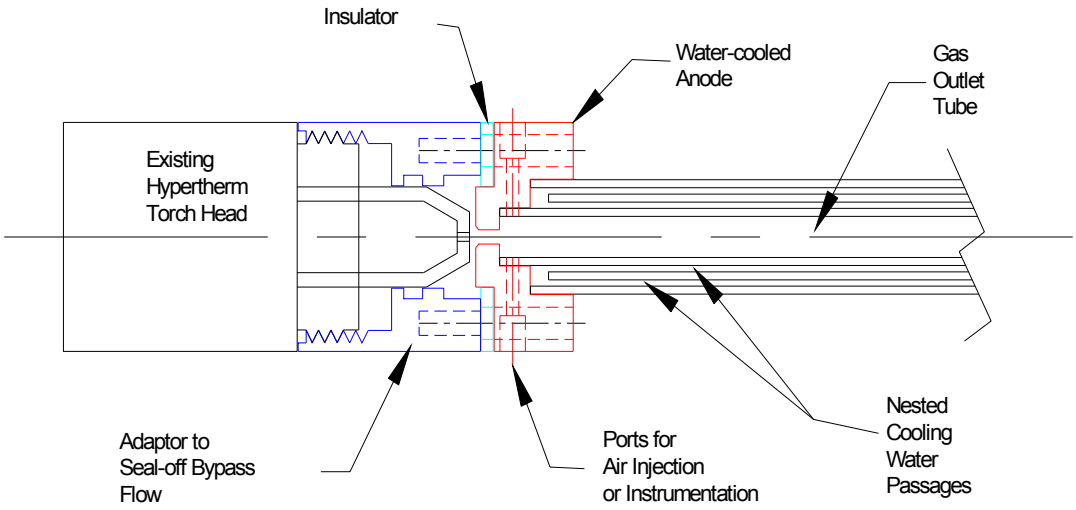

Figure 3.8 Plasma Torch Attached to Water-Cooled Anode

flowing out the back of the torch head for an operating point of 40A. There are no data available for other operating conditions which will give somewhat different proportioning of the flow rates, but it is clear that only about 15% of the gas flows in proximity to the arc. The gas flow exiting the back of the torch head fulfills two functions. First of all, the flow cools the cathode by flowing through a spiral groove on the back of the electrode. Secondly, the pressure and drag from the gas flowing through the groove is actually utilized to move the cathode tip from being in contact with the inside nozzle surface (in order to initiate the arc) to a proper gap for maintaining a stable arc. When the gas flow is stopped, the cathode tip is pushed forward by a spring

to rest against the inside nozzle surface. For this reason, it seemed that blocking all the gas flows except the nozzle flow from the torch head would have caused it to not function properly. Moreover, altering the way the arc initiates probably would necessitate some rather time-consuming modification to the power supply controls. The approach that was taken was to try to determine the relevant mass flow at the gas tube exit rather than at a gas inlet. Of the large variety of methods for measuring the mass flow of a gas, most (if not all) require knowledge of the gas properties, which further requires knowledge of the chemical composition of the gas. This issue was not considered a critical obstacle since determining the outlet gas composition was a main objective of this investigation. One advantage to using the small-scale torch is that the entire outlet flow can be readily diverted into a portable sample container.

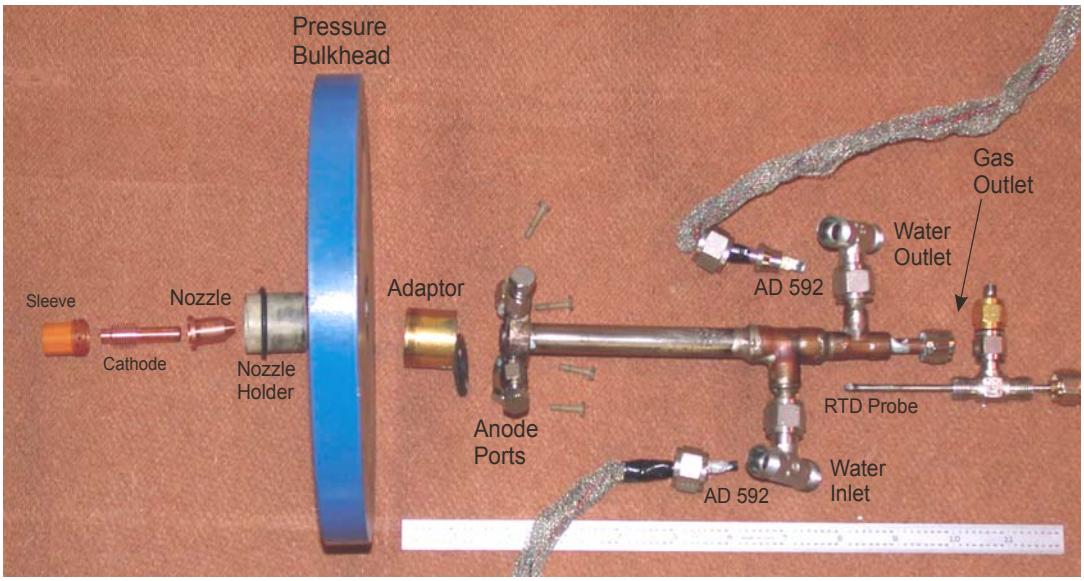

Figure 3.9 Disassembled Arc Pyrolysis Apparatus

Once the anode was completed, the first trial runs were conducted using nitrogen gas. After resolving minor problems with the apparatus operating on nitrogen, runs with methane were attempted. For these beginning experiments, the arc would flash on momentarily, but not sustain when methane was supplied to the torch at the same pressure (120 psig) as the earlier nitrogen tests. At first, the problem was mistakenly attributed to a pressure switch on the Hypertherm power unit turning-off the power right after the gas started flowing. Eventually, the difficulty was discovered to have a more fundamental cause: the endothermic pyrolysis reaction was extracting energy to the extent that no part of the flow was hot enough to have sufficient ions and free electrons to support an arc. The solution was to reduce the supply pressure so that there would be less mass flow relative to the electrical power input. In addition, lowering the gas density also makes it easier to ionize. For the supply pressure range of 40 to 60 psig, the torch was able to maintain an arc when fed with methane. However, the torch voltage fluctuated considerably during all the pyrolysis test runs in contrast to the nitrogen runs, which displayed very steady arc voltages. This arc instability is consistent with the experience of other researchers (Ref. 18 and Ref. 7) who have directly arc-heated hydrocarbons in plasma torches. Some of the voltage instability may be due to the transient formation and destruction of carbon deposits on the surfaces of the electrodes, which would cause fluctuations in the arc length. Generally, the voltage during a test run would trend downward, which is consistent with a progressive shortening of the arc. If transient carbon deposits are the actual mechanism creating the instability, then a larger, higher voltage torch would be expected to run more smoothly

due to the length of the arc being much greater relative to the size of the carbon deposit formations. Because of the variation in the instantaneous voltage, the voltage values cited for each test run are averages taken over the duration of the run. The torch power supply generally managed to maintain a constant current during the experiments.

It was evident from the initial test runs that the anode assembly was probably going to have a fairly short lifespan due to erosion from the arc. Because fabricating an anode assembly is a substantial investment in effort, the test runs were conducted in a cautious manner and pace. Test run time was limited to less than ten seconds to minimize damage to the apparatus. In particular, the orifice of the uncooled nozzle would tend to distort under prolonged heating, directing the flow out of line with the anode orifice and gouging the anode face. Unfortunately, this restriction precluded operating the torch long enough to achieve completely steady test run conditions.

Having settled the problem with sustaining the arc, the outlet flow was routed to a solenoid valve, which would divert the flow to a sample bag when energized. When not energized, the valve allowed the flow to dump into the evacuated test vessel. A 5-micron filter was installed upstream of the solenoid valve to remove any carbon particles from the flow before it was dumped or sent to the sample bag. Foil sample bags were used to contain the samples rather than typical Tedlar bags, which are permeable to hydrogen. The SKC foil bags were certified to hold hydrogen for at least five days; however, in practice they seemed to retain a consistent mixture for months.

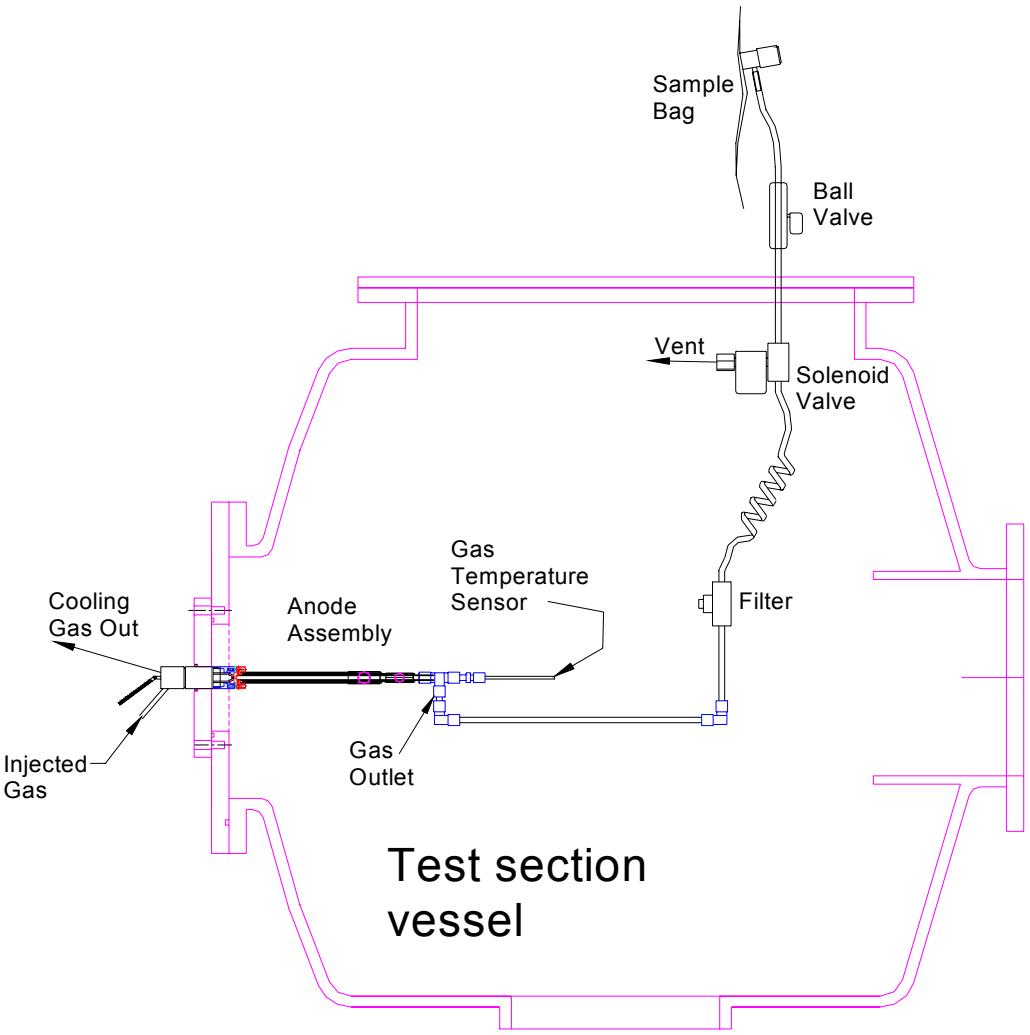

Figure 3.10 Gas Sampling Configuration

The pyrolysis apparatus was usually dismantled after every test run for the purpose of extracting the carbon and inspecting for damage. The most effective means of extracting the carbon was by lightly pounding inside the gas tube against the anode block with an 1/8" diameter metal rod. Tube brushes were also used to extract carbon. The extracted carbon generally consisted of chunks and flakes rather than the fine

powder obtained from the arc heater run. Typically, about 90% (based solely on visual estimates) of the carbon, deposited in the gas tube of the anode assembly. It was hoped that the carbon could be precisely weighed in order to determine the mass and mole rates from the test runs. However, it was very difficult to get all of the carbon onto the scale because the airflow in the room tended to disperse it and some would also get onto skin and clothes. Furthermore, one could not be completely sure that all of the extracted

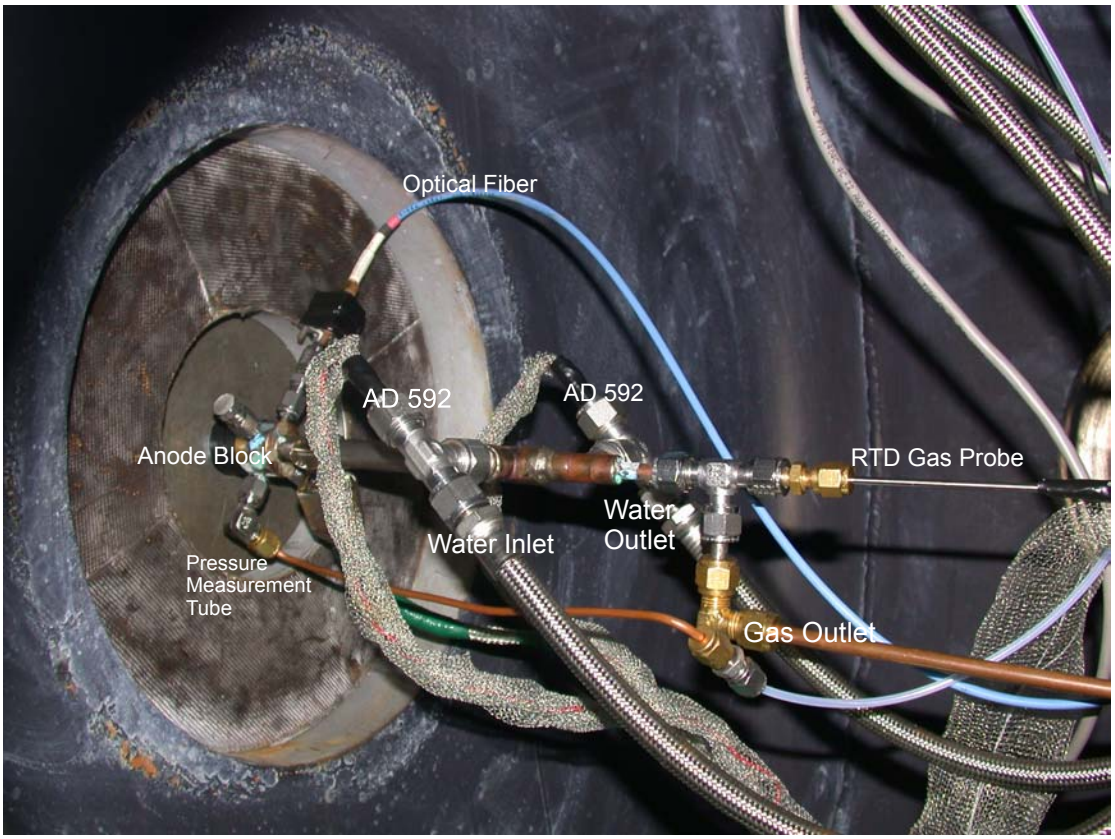

Figure 3.11 Apparatus Installed Inside Test Cabin

carbon came from just from the preceding test run.

The electromagnetic noise produced by the Hypertherm power supply and torch (Fig. 3.12) was a persistent difficulty in regard to making pressure and temperature

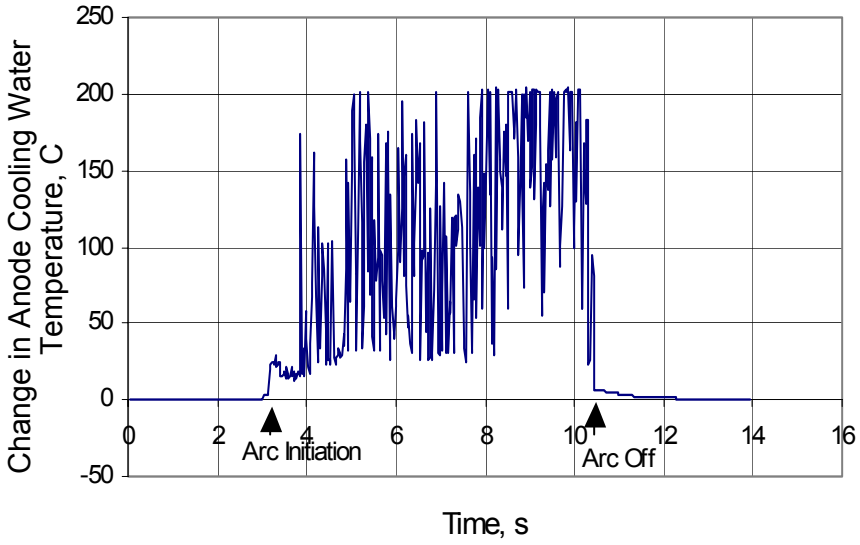

Figure 3.12 Thermocouple Signal Obscured by EMI

measurements). The severity of this interference was not anticipated since thermocouple and millivolt-output pressure transducers had been successfully used on the much more powerful arc heater facility (albeit, after a great deal of effort involving shielding, amplification and active filtering). Moreover, the Hypertherm unit was selected specifically because it does not rely on a very noisy high voltage, high frequency circuit to initiate the arc. This potential source of trouble was vividly appreciated since the arc heater facility originally had a 10,000V high frequency igniter that was so damaging to integrated circuitry that it was abandoned in favor of a different arc initiation technique. Purchasing voltage output pressure transducers allowed readable signals to be acquired; however, there was not such an immediate solution to cleaning-up the thermocouple signals beyond the measures of shielding, amplification and filtering that were installed from the outset.

Accordingly, alternative temperature transducers, RTD's and Analog Devices AD592 temperature-sensing integrated circuits, were tried. The AD592 transmits a current signal that is proportional to the temperature (273μA corresponds to 273K). Current signals are inherently much less susceptible to EMI than low millivolt range voltage signals, such as from a thermocouple. The main concern in using these alternative temperature transducers was achieving a sufficiently fast response time. For this reason, instead of purchasing an off-the-shelf RTD probe with an enclosed element, probes were handmade having exposed elements (Fig. 3.13).

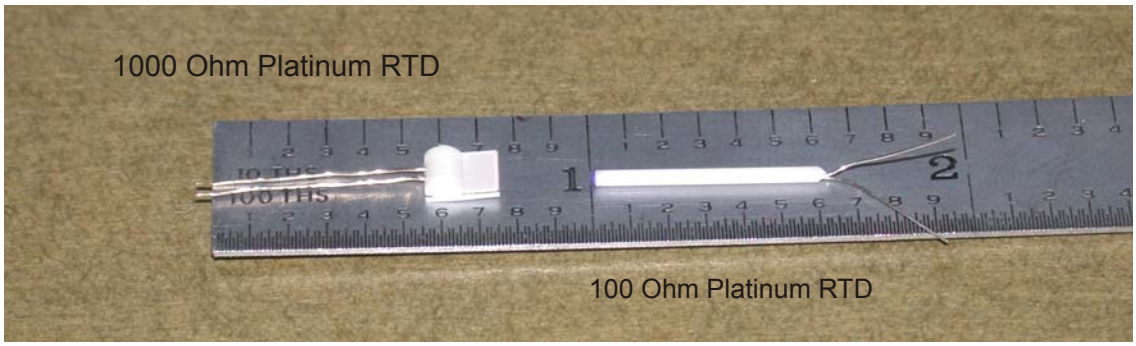

Figure 3.13 RTD Elements

In order to improve the response time of the AD592's most of the plastic case around the integrated circuit was removed with a hand file. The AD592's are potentially slightly more accurate than a platinum RTD, less expensive ($10) and also require less signal conditioning. However, the AD592 is limited to less than 105 °C, so the chips were used for the cooling water flow and the RTD was used for the gas tube flow. A circuit based on an Analog Devices ADT70 integrated circuit chip was used to condition the signal from the RTD. The ADT70 was designed specifically for this application of RTD signal conditioning.

Having been replaced by AD592's, the type T thermocouples originally installed on the anode to measure the rise in water temperature, were relocated outside the test cabin to where the water lines pass through the top lid. Due to being farther away from the torch, and having the shielding augmented by a ½" thick steel test cabin lid, the thermocouples produced a ΔT signal that was no longer obscured by noise (Fig. 3.14). The response of the sheathed thermocouples was slightly faster than the trimmed-

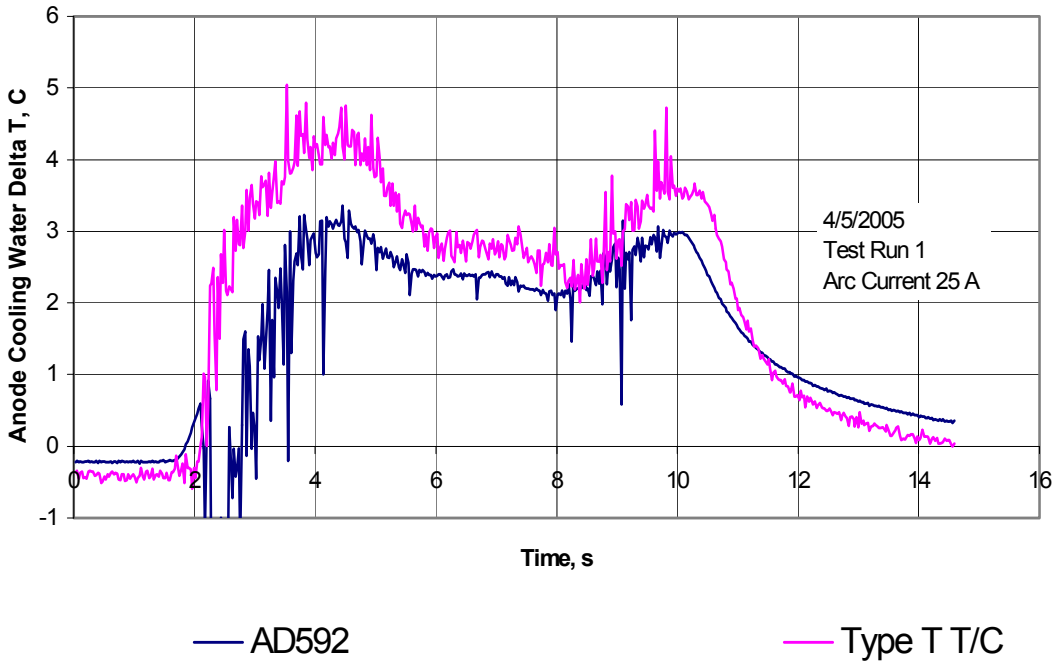

Figure 3.14 Response of Temperature Sensors

down AD592's, but both kinds of transducers were quick enough to show some thermal response to voltage fluctuations (Fig. 3.15).

Initially an RTD gas probe was made with a 100-Ohm cylindrical wire-wound element. This probe was used for a few test runs until the element wires broke at the

element base, which resulted from not achieving a secure mounting to the stainless steel tube. A replacement probe was made with a 1000-Ohm thin-film RTD element. This probe performed better in accuracy and responsiveness (Fig. 3.16). The lag observed in Figure 3.16 is due to the time it takes for the anode apparatus to adjust to a temperature change. In calibration tests, the RTD probe responded in less than one second when placed in the steam above a container of boiling water. The only disadvantage involved with this probe was that the anode assembly gas tube had to be reamed to provide clearance for the square element.

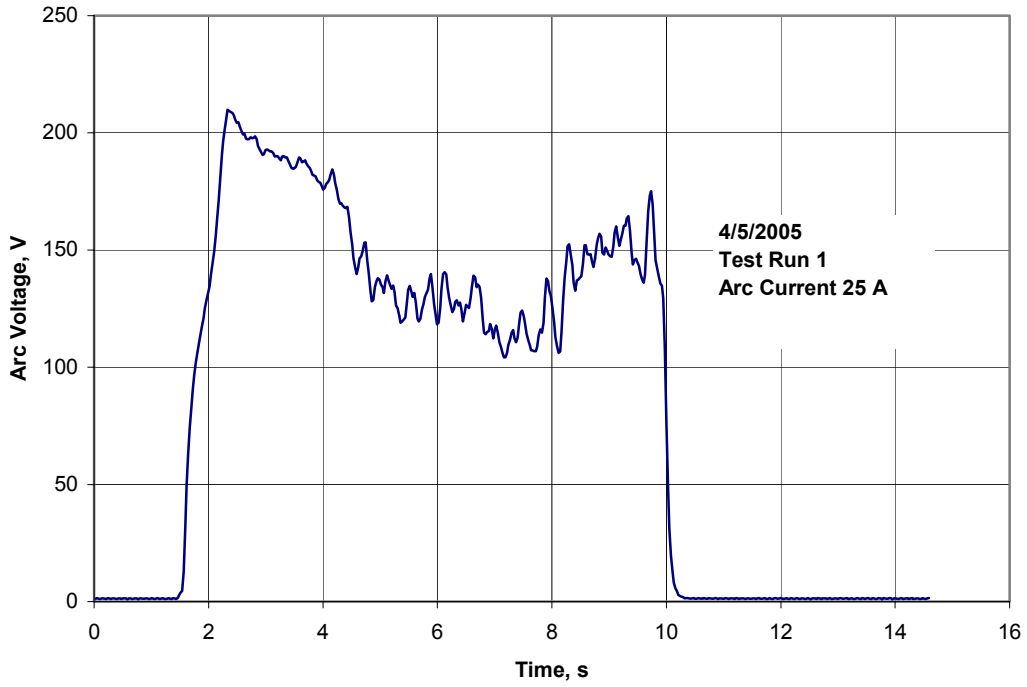

Figure 3.15 Voltage Fluctuation

Temperature-indicating lacquers were purchased along with the RTD elements as a backup approach to determining the gas temperature if the RTD's failed to work.

These lacquers permanently change color within milliseconds of being exposed to temperatures above a given threshold. The lacquers were effective in confirming the temperature measurements of the RTD's and also in providing a means to determine what temperatures different parts of the apparatus were being exposed to.

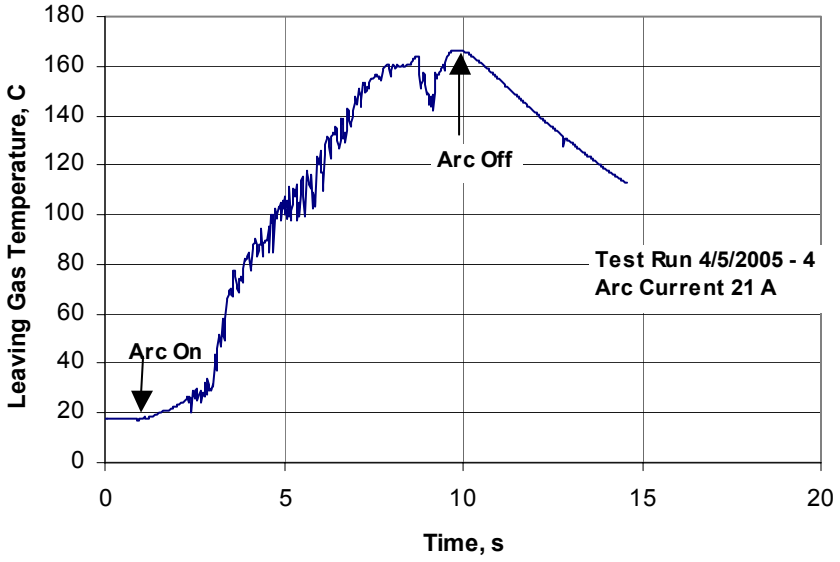

Figure 3.16 RTD Measurement of Leaving Gas Temperature

Various attempts were made in getting some indication of the bulk temperature near the arc in the interest of knowing the reaction conditions. The first approach attempted was to use an eroding coaxial thermocouple to measure the temperature just downstream of the anode constriction. There was speculation that this direct measurement technique might be feasible with a hydrocarbon feedstock due to the endothermic pyrolysis reaction lowering the gas temperature to around 1700 K, much less than what would be obtained from arc-heating nitrogen or air. Unfortunately, in order to sustain an arc in a hydrocarbon gas, the temperature apparently has to be at a

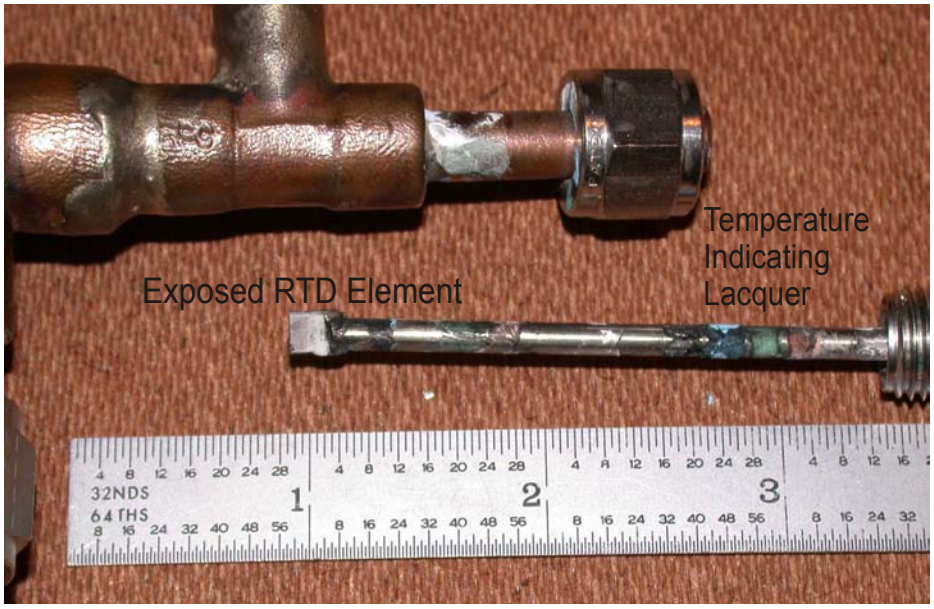

Figure 3.17 RTD Probe with Exposed Element

level comparable to arc-heated nitrogen. The thermocouple did indeed erode when placed close to the anode block. It lost about ½" of material off the end, but did not produce a usable signal during the test run. The only indication of the temperature at this location was that it was well above the melting temperature of stainless steel. The gas temperature sensors were kept 6.25" downstream from the anode block for subsequent test runs, which is the point where the water exits the cooling water jacket.

Another approach used to try to glean the reaction temperature was by examining the emitted light with a spectrophotometer. This involved attempting to determine the temperature by applying Wien's displacement law to the underlying Planck distribution of the emitted spectra as in this expression:

$$\lambda_{\max} T = C_3$$

where C_3=2897.6 μm•K.

Most of the test runs were configured for an Ocean Optics USB2000 photospectrometer to view the spectra though an optical fiber connected to a port in the anode block. Unfortunately, these attempts to obtain spectral data were thwarted by carbon immediately blocking the optical path through the hole. In an effort to circumvent this problem, a non-cooled anode block was coupled to the torch, and an optical fiber was mounted on a bracket to view the free jet exiting the truncated anode (Fig. 3.18). The molecular and atomic spectral peaks on top of the continuous blackbody distribution

Figure 3.18 Optical Fiber Mounted to View Spectra from Free Jet

obscure the precise peak wavelength. However by inspection, the peak of the distribution seemed to coincide with a wavelength of around 524 nm, corresponding to a temperature of 5530 K, for the entire range of torch operating currents. This estimated temperature is considered highly approximate. The true temperature measurands could probably range 500 K on either side of this estimated value. This temperature does not

necessarily represent the bulk temperature of the gas jet. It is plausible that some portion of the jet flow is at 5530 K, but probably not all of it.

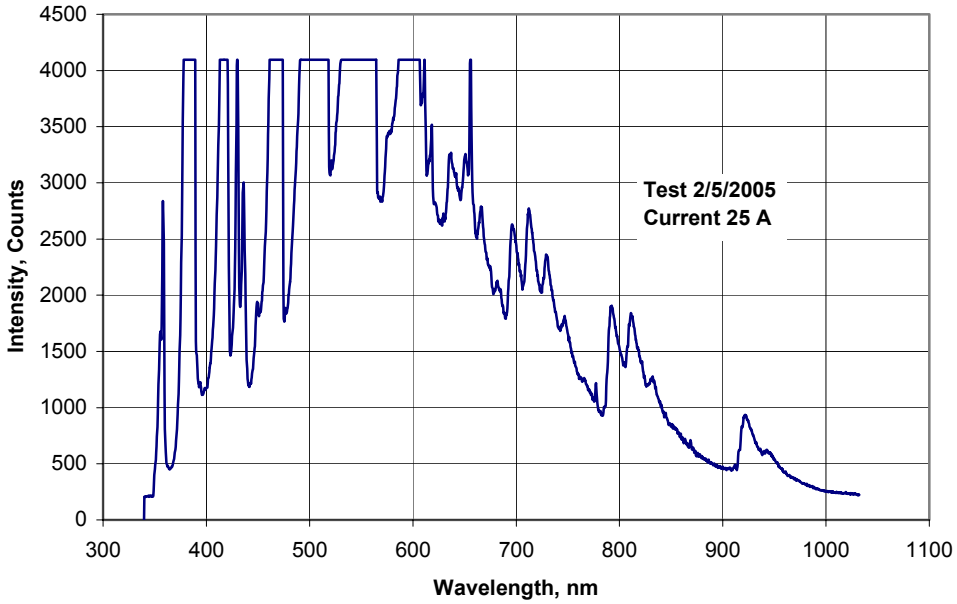

Figure 3.19 Emission Spectra from Free Jet

3.3 Technique for Chemical Analysis of Pyrolysis Products

Previous efforts to determine chemical composition relied on acquiring the emission spectra of the arc-heated gas emerging from the torch nozzle. However, photospectroscopic data tend to be much more informative in a qualitative rather than quantitative sense. Accordingly, a more suitable chemical analysis technique was sought. Mass spectroscopy was considered first; however, UTA's chemistry department does not have a mass spectrometer capable of detecting hydrogen. The most suitable technique available was found to be gas chromatography. Analyzing collected gas

samples using gas chromatography (GC) gives quantitative results and makes identifying chemical species much more straightforward. The primary disadvantage to this approach is that it does not indicate what species are present in the vicinity of the arc, but instead reveals the products after cooling has occurred. Chromatographic and spectrographic plots happen to look visually similar in that they consist of a series of sharp peaks along a horizontal axis. However, the two kinds of plots represent two entirely different phenomena. Chromatographic separation is the result of differences in the degree to which the components of a mixture are hindered in passing though an adsorptive media. For a successful separation, each component of a mixture will arrive at the detector at different time intervals, producing a peak on the signal trace from the detector. This time interval is called the retention time. The retention time for an unknown component of a mixture is compared with the retention time of a known substance (referred to as a standard) injected under the same conditions to determine the component identity. To determine the volume fraction of a component, the area under the detector output peak is compared to the area for a known volume of a standard.

Detecting hydrogen using gas chromatography does require some departure from the more commonly encountered GC set-ups. Hydrogen is not detectable by a flame-ionization detector, so the somewhat less sensitive thermal conductivity detector (TCD) must be used instead. The TCD measures the conductivity difference between a mixture of a sample component and the carrier gas with the conductivity of the carrier gas alone. The detector device is very similar to a hot-wire anemometer except that the heat transfer is altered by changes in gas conductivity rather than velocity. In regard to a

carrier gas, helium gives the best results for most analyses, but it produces anomalous detector output when mixed with hydrogen (Ref. 19). There is a detector signal polarity reversal in going from low to high concentrations of hydrogen in a helium carrier gas. Accordingly, the GC plot will show two small hills with a deep valley between them rather than a typical chromatography peak once a threshold concentration of hydrogen is exceeded. Because of this problem with a binary mixture of hydrogen and helium, argon was substituted for helium as the carrier gas. The large difference in thermal conductivity between argon and hydrogen provides excellent contrast for detecting hydrogen, but provides less sensitivity for other gases.

The UTA chemistry department provided access to a Gow-Mac Series 350 GCTCD (Fig. 3.20). In addition, approximately one hour of training was provided on the use of the chromatograph and paper plotter. All the chromatography analysis sessions were performed using an 8 ft. long column packed with HayeSep Q (divinylbenzene). Both the chromatograph and the foil sample bags have septums for accommodating gas syringe needles. A Hamilton 100 μL gas syringe was purchased for transferring gas samples from the bag to the chromatograph. This syringe features a small ball valve that may be closed to prevent gases from leaking out through the needle during the transfer. The flow rate of carrier gas was measured with a soap film meter and a stopwatch. This meter works simply by timing how long it takes a soap film membrane to move up one volume mark to another in a graduated tube with the carrier gas flowing into it.

Figure 3.20 Gow-Mac Series 350 Gas Chromatograph

To acquire the data in numerical form, a Dataq Instruments DI-194RS, RS-232-based portable data acquisition module was obtained. This inexpensive module ($25) was intended to be used only temporarily until a better data-recording device was

purchased. However, the Measurement Computing data module purchased as the intended replacement could not be readily configured to give adequate temporal resolution to record the GC peaks. Since this difficulty was never resolved, the DATAQ module was used for all the successful GC sessions because of its good temporal resolution and despite its poor 10-bit signal measurement resolution. It was necessary to amplify the detector signal 1000 times to effectively utilize the module's fixed –10 to 10V signal acquisition range. The Gow-Mac GC does feature a signal attenuation dial that was useful for adjusting the magnitude of the output signal. The height of the peak is also dependent on the amount of gas injected from the syringe. If the peaks are going off the scale, one can simply reduce the quantity of gas that is injected until the peaks fit into the available range.

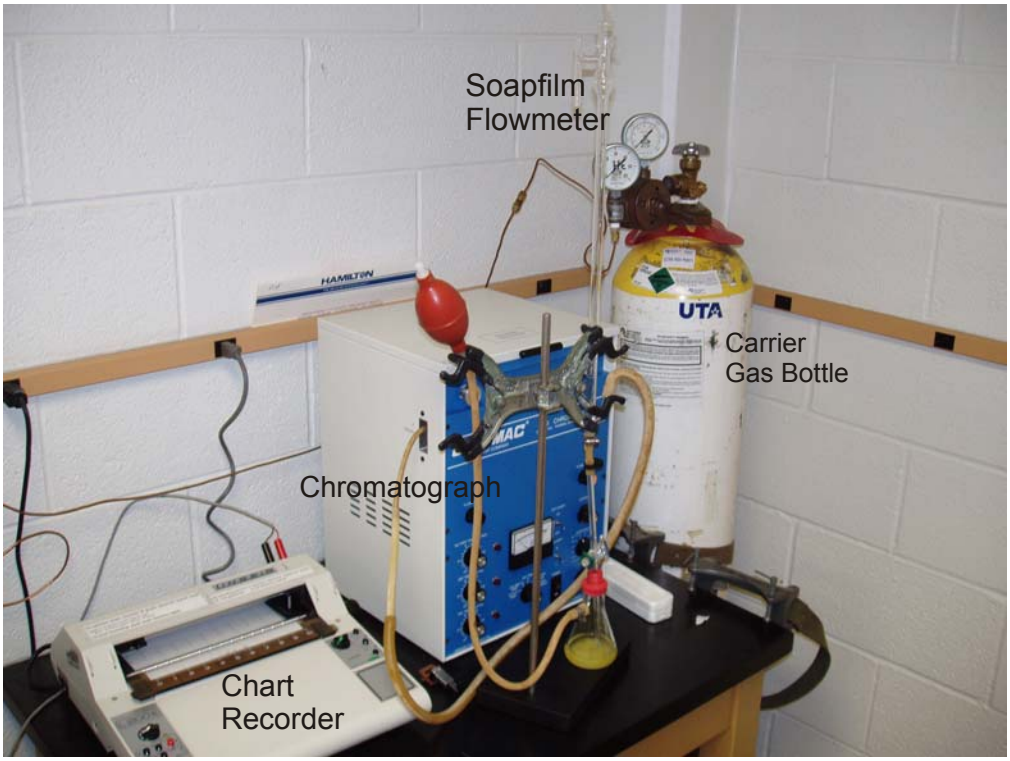

Figure 3.21 Gas Chromatography Set-Up with Soapfilm Flow Meter

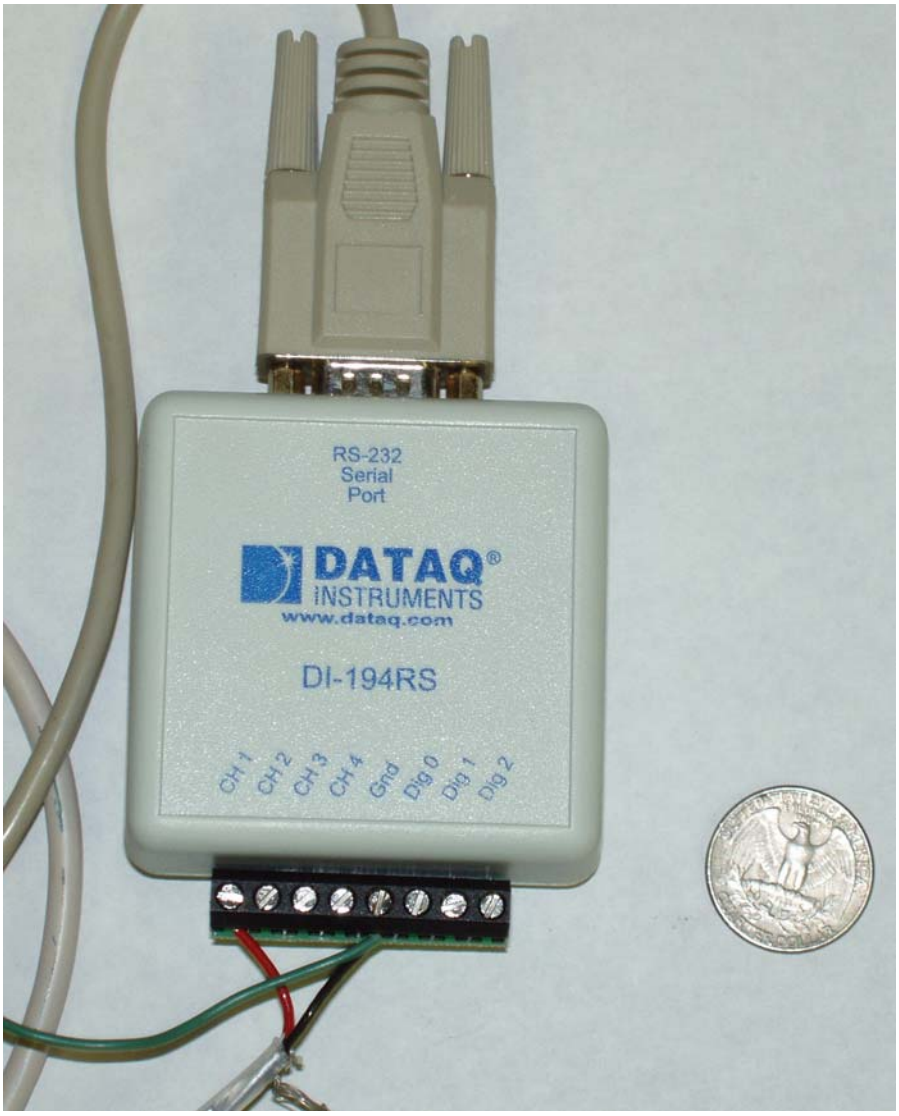

Figure 3.22 Portable Data Module

CHAPTER 4

RESULTS AND DISCUSSION

4.1 Composition of Gas Samples

For all the analysis runs of gas samples from methane pyrolysis, only three peaks were observed: a very prominent hydrogen peak followed by a barely detectable methane peak, and a small acetylene peak arriving much later (Fig. 4.1).

All of the successful GC analysis runs of the gas samples consistently produced plots that closely resemble Figure 4.1. Perhaps due to the limitations of making manual injections and/or the instrument, the methane peak always appeared on top of the tail of the hydrogen peak. Some effort was made in exploring different instrument settings in an attempt to improve the degree of component gas separation and optimize the detector output. However, none of the other settings that were tried worked any better than the settings selected for the second chromatography session which were the following: 72°C column temperature, 97°C detector temperature, and a flow rate of 20 mL/min. of argon carrier gas. Subsequent GC sessions in which data were collected had approximately these same settings. As shown in Figure 4.1, the identities of the gases creating the peaks were confirmed by injecting a known mixture of hydrogen, methane, and acetylene. When the plots of an unknown gas sample and the mixture standards are

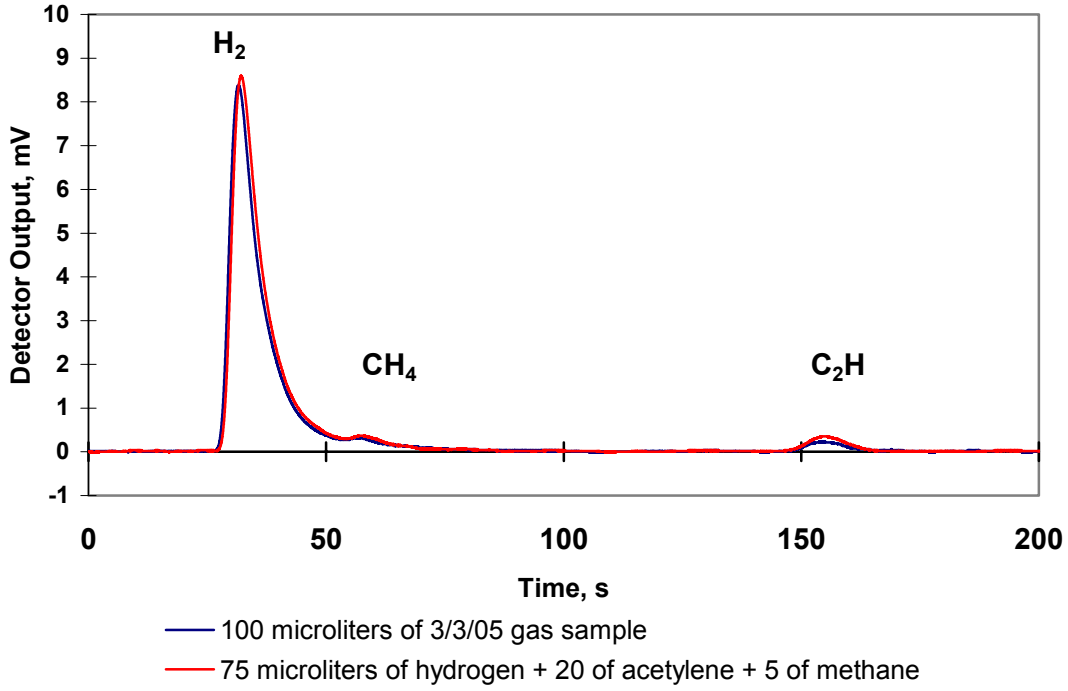

Figure 4.1 Gas Sample from 3/3/05 Test Run Compared with a Mixture of Standards

overlaid, the retention times match and the areas are similar. The acetylene standard was obtained from a cutting torch bottle and has some hydrogen and air contamination. This contamination artificially boosts the hydrogen peak when a mixture of standards is drawn into the syringe and injected. The hydrogen concentration data presented in this work were obtained using only hydrogen standards for comparison rather than a mixture of standards. Ten gas sample runs were made and these samples were analyzed during twelve chromatography sessions. The chromatograph was given typically three to four hours to warm-up to thermal equilibrium conditions; however, the column temperature

still tended to drift upward by a few °C during the data collection time period when samples were being injected.

The chromatograph output was recorded as a set of voltage values. A FORTRAN program called peakarea was written to process the GC data sets. Peakarea uses Simpson's rule to numerically integrate the areas under the chromatography peaks. The program also determines the retention time for the peaks as well as the height and width. The hydrogen composition of the samples ranged from 78 to 88 percent by volume (Table 4.1). The margin of error for a particular volume determination appears to be typically 2 to 5%. The concentration values presented in the data tables are generally averages from several injections often over many GC sessions. The volume

Table 4.1 Hydrogen Content of Gas Samples

Test Run	**Operating Point**		**Injection Pressure**	**H_2 Volume Fraction of Gas Sample**	**H_2 mole fraction of total products**
6/17/04	39.8 A	142V	55 psig	0.84	0.69
7/15/04	33.5A	171V	55 psig	0.80	0.72
8/17/04	37.9A	159V	50 psig	0.86	0.69
9/30/04	34A	? V	42 psig	0.78	0.72
11/29/04	32.4A	158V	50 psig	0.80	0.71
3/3/05	31.7A	150V	45 psig	0.82	0.70
3/22/05	28.2A	154V	40 psig	0.88	0.68
4/5/05-1	24.4A	148V	42 psig	0.86	0.69
4/5/05-3	40.2A	111V	42 psig	0.87	0.69
4/5/05-4	21.0A	91V	42 psig	0.85	0.72

concentrations of methane and acetylene could not be calculated accurately by peakarea due to the lowered sensitivity of the GCTCD using argon rather than helium as the carrier gas, and the low resolution of the portable data recorder that was used to acquire

the detector output. However, by inspecting the paper GC plots, it was not difficult to discern the approximate volume of methane or acetylene when injections of known standard volumes produced peaks both higher and lower than the unknown volume, effectively bracketing the unknown volume. The areas of the hydrogen standards for a particular section are plotted with the syringe volumes used to produce the areas. This plot is then curvefit to obtain a correlation for syringe volume as a function of the area

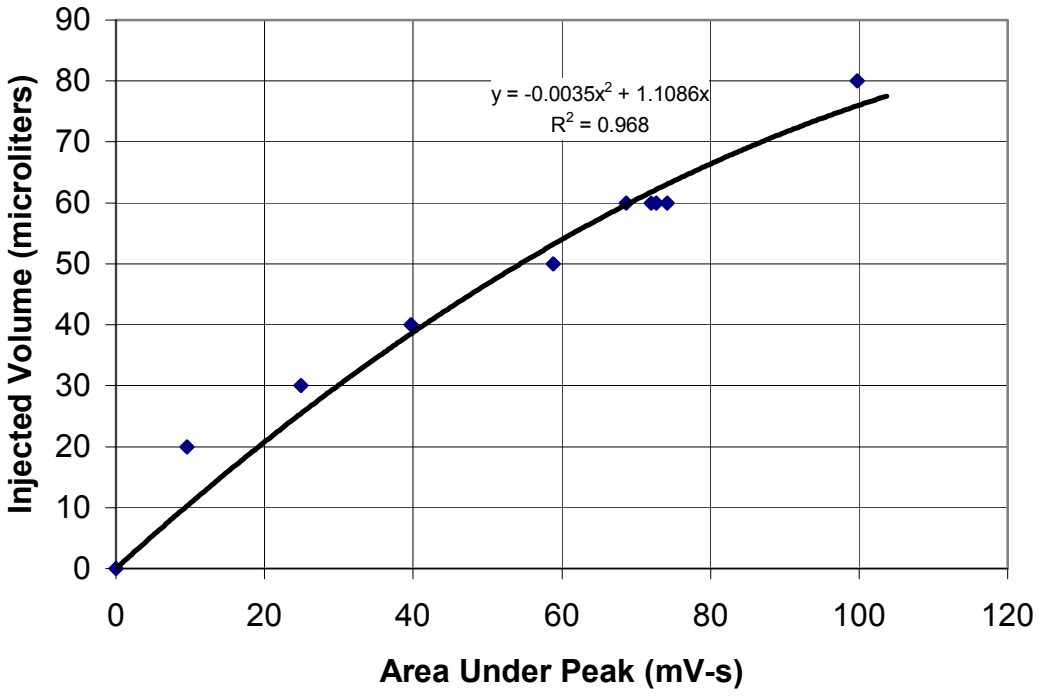

Figure 4.2 Hydrogen Standards Correlation for 4/8/2005 GC Session

under the peak (Fig. 4.2). Using this correlation, the hydrogen volume concentration in a test run sample may be determined based on the area under the peak.

To derive a reaction equation or product mole fraction estimates, methane was assumed to comprise only 2% of the gas sample volume, which appeared to be fairly typical for the samples analyzed. With this assumption for methane and having an accurate measurement of the hydrogen volume, the acetylene volume fraction was estimated by subtracting the hydrogen and methane volumes from the total injected volume. With the volume fraction of the test run samples known, the next step is to use these values to write a balanced reaction equation. One mole of methane is assumed to produce a certain number of moles of carbon, hydrogen, acetylene and methane.

$$CH_4 \xrightarrow{arc} aC + bH_2 + cC_2H_2 + dCH_4$$

Implicit in this reaction equation is the assumption that there are no hydrogen-containing species in the solid products. The solid products were not analyzed, so this assumption cannot be verified. From the gas sample analysis, the relative proportions of hydrogen, acetylene and methane are known. The reaction equation may be rewritten in terms of the volume fractions, f_{H_2}, $f_{C_2H_2}$, and f_{CH_4} thusly:

$$CH_4 \xrightarrow{arc} (1 - 2kf_{C_2H_2} - kf_{CH_4})C + k(f_{H_2}H_2 + f_{C_2H_2}C_2H_2 + f_{CH_4}CH_4)$$

This equation may be balanced on a hydrogen basis to solve for the constant *k*. For example: $4 = k(2f_{H_2} + 2f_{C_2H_2} + 4f_{CH_4})$

To give

$$k = \frac{4}{2f_{H_2} + 2f_{C_2H_2} + 4f_{CH_4}}$$

This value may now be substituted into the reaction equation to determine the product specie coefficients. Product mole fractions may be determined by dividing each coefficient by the sum of all the product coefficients.

The next step is to calculate the actual moles of hydrogen captured in the sample bag. The volume of the sample is determined by submerging the bag in a bucket of water and marking the level the water rises to. After the bag is removed, water is then added to the bucket with a graduated cylinder until the mark is reached. The amount of water added, minus the empty volume of the bag and the volume of the pusher (tool used to push the bag under water) is the volume of the sample gas. The ideal gas law may then be applied to calculate the moles of hydrogen where the conditions are ambient temperature and pressure.

$$n_{H_2} = \frac{P f_{H_2} V}{\tilde{R} T}$$

The sample bags were usually not completely filled, so the contents of the flexible bag were in pressure equilibrium with the atmosphere. The number of moles of reactant may be determined by multiplying the moles of hydrogen by the coefficient ratio of methane to hydrogen obtained from the balanced reaction equation.

$$n_{CH_4} = \frac{n_{H_2}}{b}$$

The reactant mass flow rate is calculated by multiplying the moles by the molecular weight and dividing by the sampling duration.

$$\dot{m} = \frac{MW_{CH_4} n_{CH_4}}{t_{sample}}$$

Not all of the test runs were successful. A gas sample was obtained on

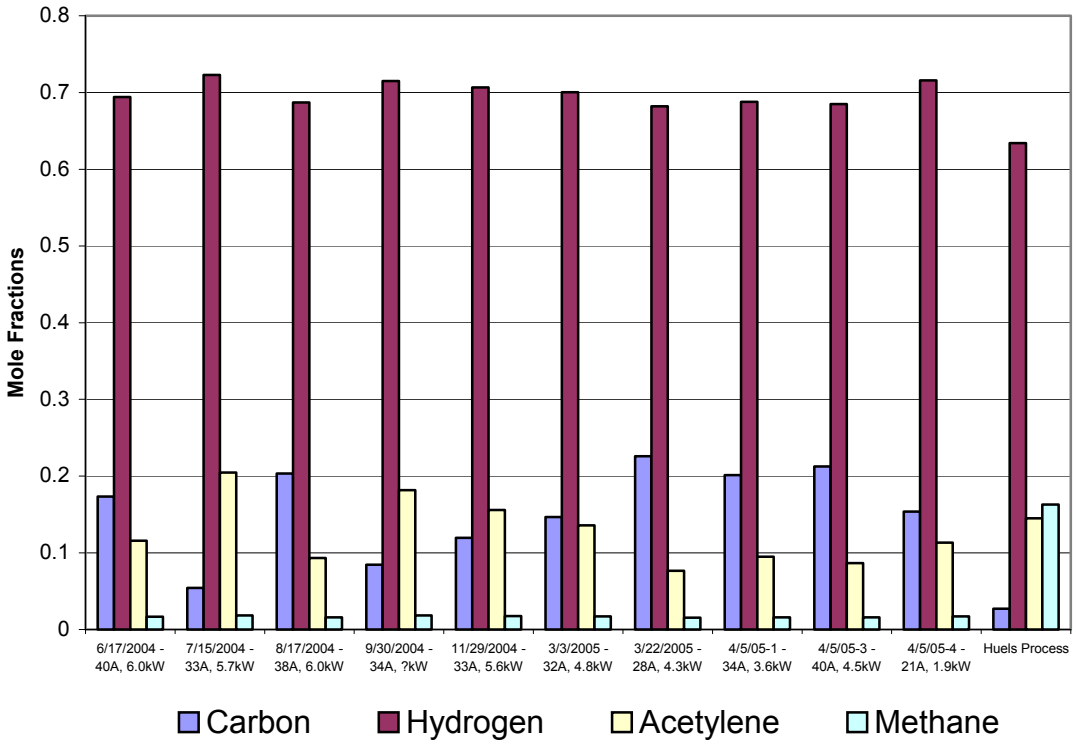

Figure 4.3 Summary of Chromatography Results with Comparison to Huels Process

9/30/2004 but the data were lost for this test run. Four test runs were conducted on 4/5/2005, but during the second test run the arc extinguished before the outlet gas sample was acquired.

The chromatography results were examined in an effort to find any trends indicating the influence of some factor. There appears to be no consistent effect of arc power or current on the gas sample composition. If there is an influential factor, then it

is minute enough to be hidden by the scatter in the data. This absence of an association is attributed to the arc heating the methane to temperatures well beyond what is required to thermally pyrolyze the flow. This overheating of the hydrocarbon was driven by the conditions required to form and sustain an arc. Other influential factors were considered as well, such as: the duration of the test run, the duration of the gas sampling, the time delay before the sample was taken, the mass flow rate and injection pressure.

4.2 Emission Spectra

Emitted photons result from changes in the quantum energy states of atoms or molecules. An atomic substance will emit light at discrete wavelengths as electrons go from high to low orbits. Accordingly, atomic emision is strictly due to changes in the electronic quantum state. On a spectrometer plot these appear as single sharp peaks called lines. For multi-atom species, there are rotational and vibrational energy modes in addition to the electronic modes. Because of the large number of possible rotational and vibrational states, molecular spectra appear as clusters of lines called bands. Identifying atomic lines can be as straightforward as looking-up the wavelength in a reference book table or database. Identifying molecular spectra is much more challenging, often requiring expertise and/or numerical simulation of the emitting modes.

As mentioned before, emission spectra were acquired from the pilot jet of the Hypertherm Torch shortly before MSE-TA's contract deadline. These were brief (100 ms) snapshots out of necessity because the arc would immediately extinguish after

being initiated. The spectral data did include a very prominant hydrogen alpha line, but most of the other atomic lines appeared to be from copper and hafnium. Because of the erosion of the cathode, which is made of copper with a hafnium insert (for electron emission), the presence of these atomic lines was hardly suprising. Moreover, when the emission spectra from plasma-heated methane were compared with the emision spectra from nitrogen and hydrogen, these metal lines were generally still present. These results from initial experiments are not presented, because better spectral data were subsequently acquired.

Although most of the test runs of the plasma torch apparatus were conducted with a spectrometer connected by a optical fiber to one of the anode ports, spectra were rarely observed due to carbon immediately blocking the light path. To circumvent this difficulty, an uncooled anode block was attached to the torch, and the optical fiber was mounted on a bracket to view the free jet exiting the anode. The primary interest was in getting some indication of the reaction temperature, however spectra were acquired that showed much less electrode metal contamination than the prior results (Fig. 4.4).

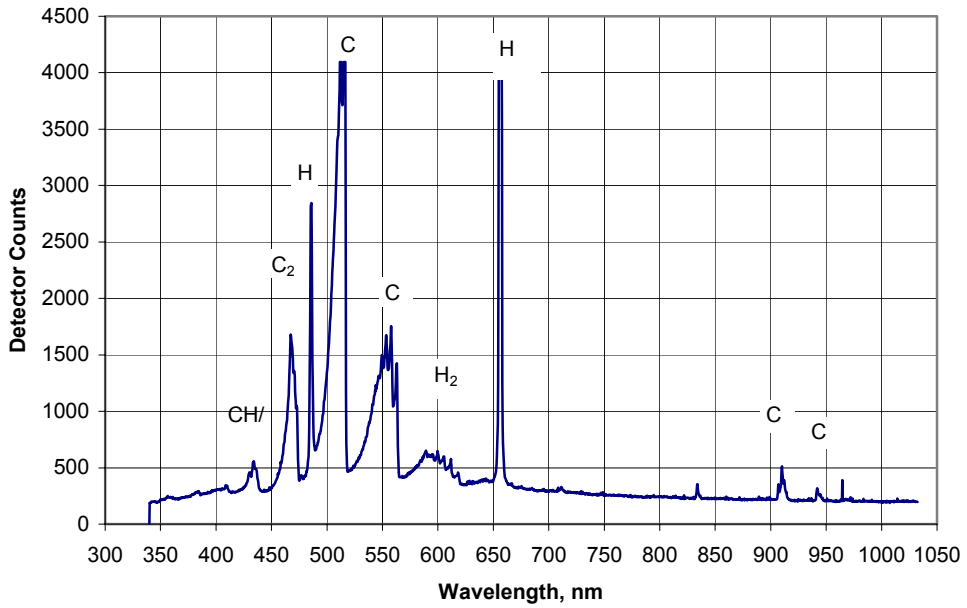

Figure 4.4 Spectra from Hypertherm Torch Running on Methane

The spectral plot also agrees with the plot given in Ref. 20 for the emission of a methane-fed plasma torch (Fig. 4.5). The plot from Ref. 20 goes to a shorter wavelength of 200 nm and is actually combined from the output of three spectrometers (Ocean Optics S2000s) for better resolution. For purposes of visual comparison, the data from this study and Ref. 20 are displayed together in Figure 4.6 over the range of wavelengths that they both cover. It should be noted that the torch in Ref. 20 is discharged into air, whereas the Hypertherm torch was always fired into a rough vacuum. Accordingly, the bands labeled CN on the plot from Ref. 20 do not appear on the plot from this investigation. The other bands all seem to match in shape but differ somewhat in intensity. The specie identifications given by Ref. 20 are assumed to be correct and were used in labeling the molecular bands in Figure 4.4. Virginia Tech has

been performing plasma torch research using spectrometers for more than a decade, so

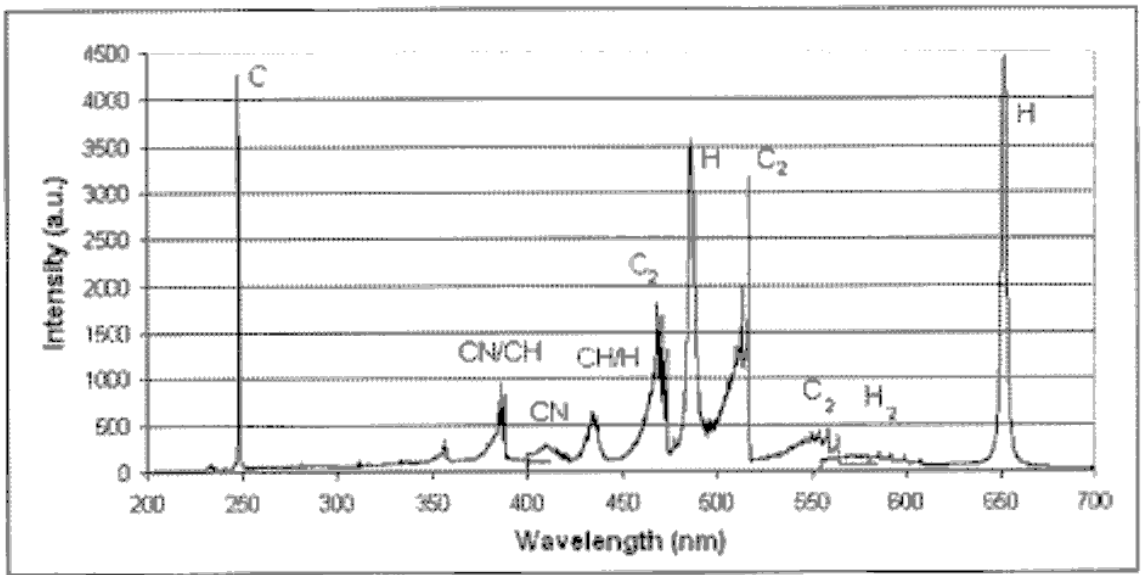

Figure 4.5 Spectra from Virginia Tech Plasma Torch

their identifications can probably be considered authoritative.

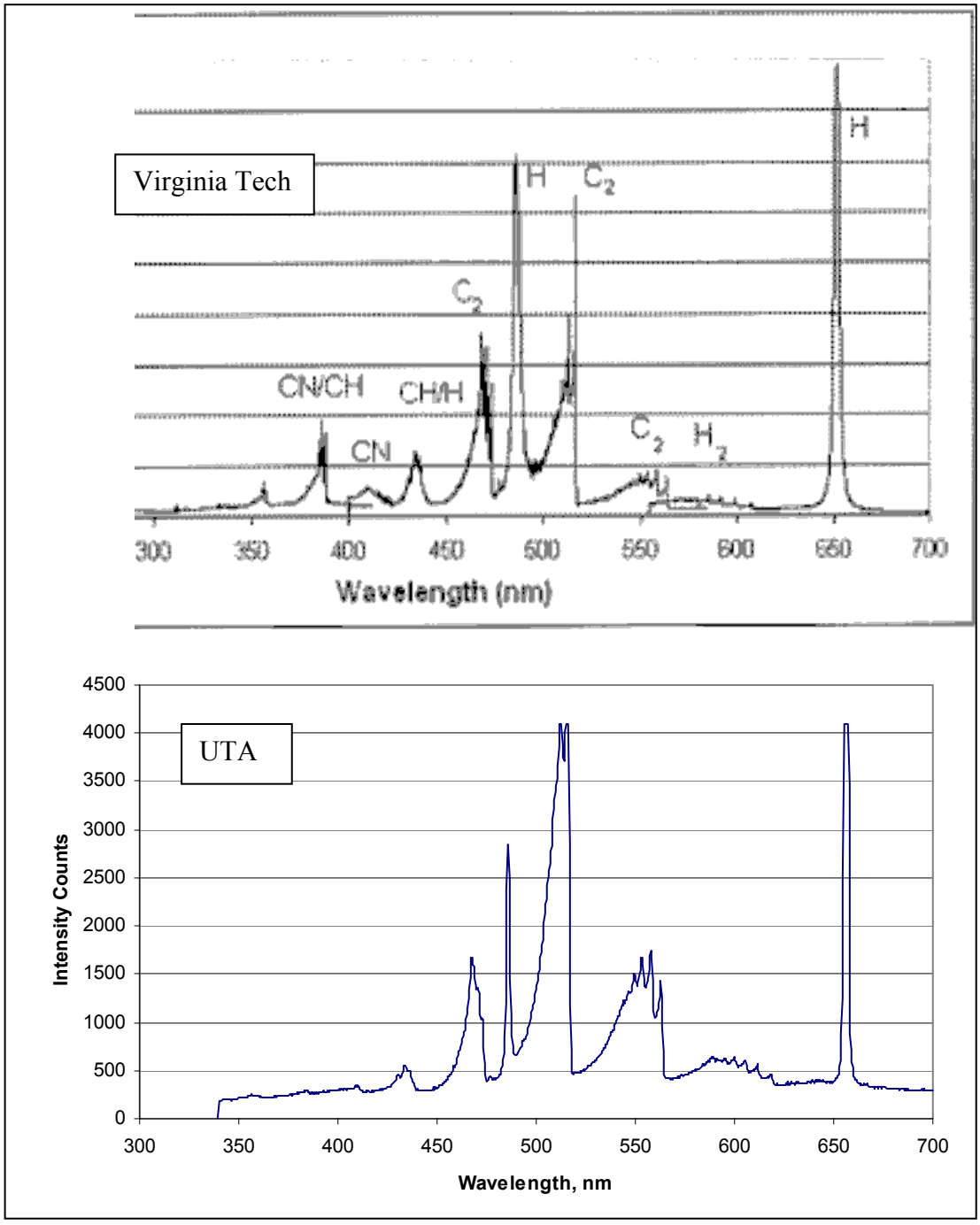

Figure 4.6 Side-by-Side Comparison of Emission Spectra

The emission spectra provides some indication of the temperature of the arc gas from the presence of C_2 bands. As the equilibrium diagram from Ref. 21 shows, C_2 does not form until the temperature exceeds 3400 °C. The spectra shown in Figures 4.4 and 4.6 are from a 25 A test run. The arc gas temperature for higher current test runs would be somewhat greater.

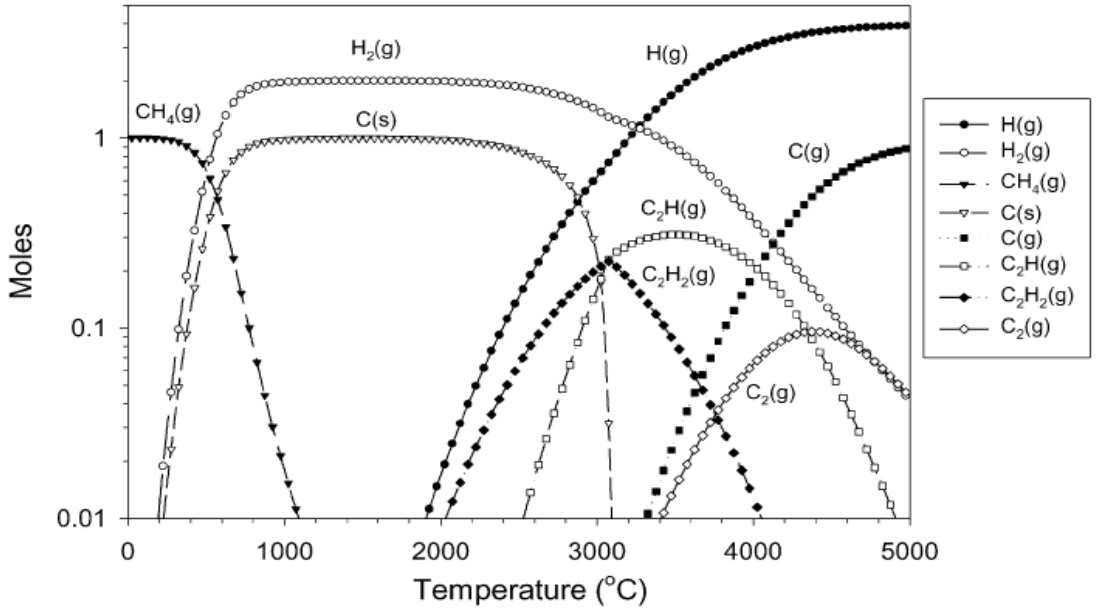

Figure 4.7 Simplified Equilibrium Diagram for Methane Decomposition

4.3 Comparison of Experimental Results with CEA Predictions

Methane pyrolysis simulations were conducted with the NASA Chemical Equilibrium Analysis (CEA) code for a range of temperatures and pressures relevant to the plasma torch experiments (Fig. 4.8). However, the GC results are not directly comparable to CEA predictions because the gas samples are at atmospheric temperature

and pressure rather than at the conditions specified for the CEA code reactions. As the specified reaction temperature is increased beyond 2500 K (for 3 atm), atomic hydrogen

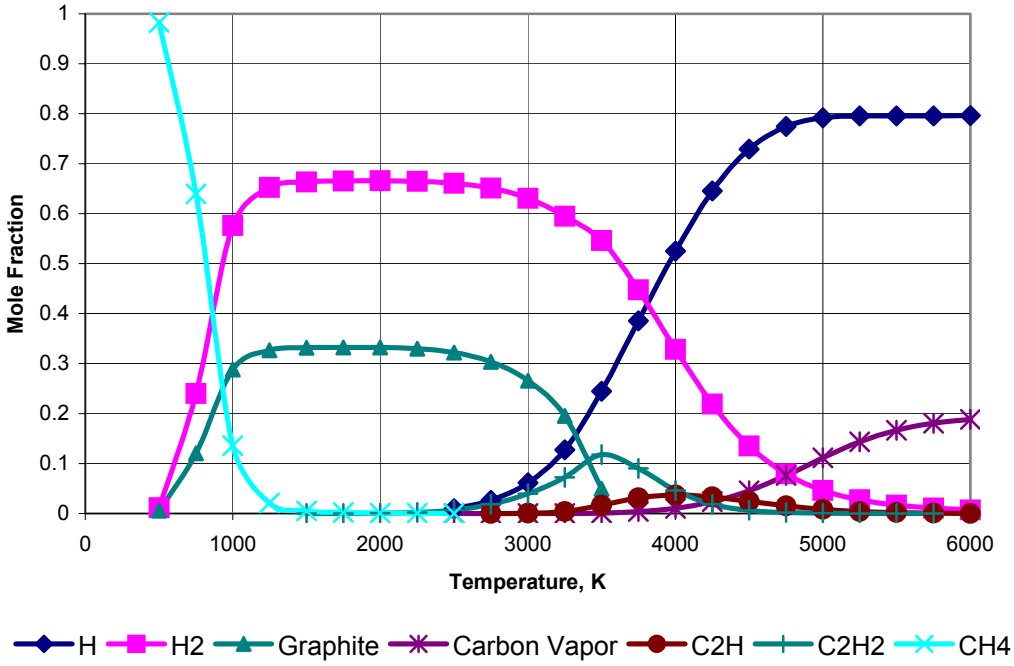

Figure 4.8 CEA Predictions of Methane Pyrolysis Products at 3 atm

and C_2H appear in the CEA predictions, which would not be present in a room temperature gas sample. The predictions in Figure 4.8 are consistent with Figure 4.7 excerpted from Ref. 21, which is expressed in relative moles rather than mole fractions. These figures show the temperature range in which carbon and diatomic hydrogen are formed.

For the purpose of making a more relevant comparison, the CEA predictions were extrapolated to account for atomic hydrogen recombining to form diatomic hydrogen and atomic hydrogen combining with C_2H to form acetylene (Fig. 4.9). This

extrapolation was performed by assuming that all the C_2H combines with an equal amount of atomic hydrogen to form additional acetylene. A similar assumption in regard to C_2H is made in Ref. 21. The remaining atomic hydrogen is then assumed to

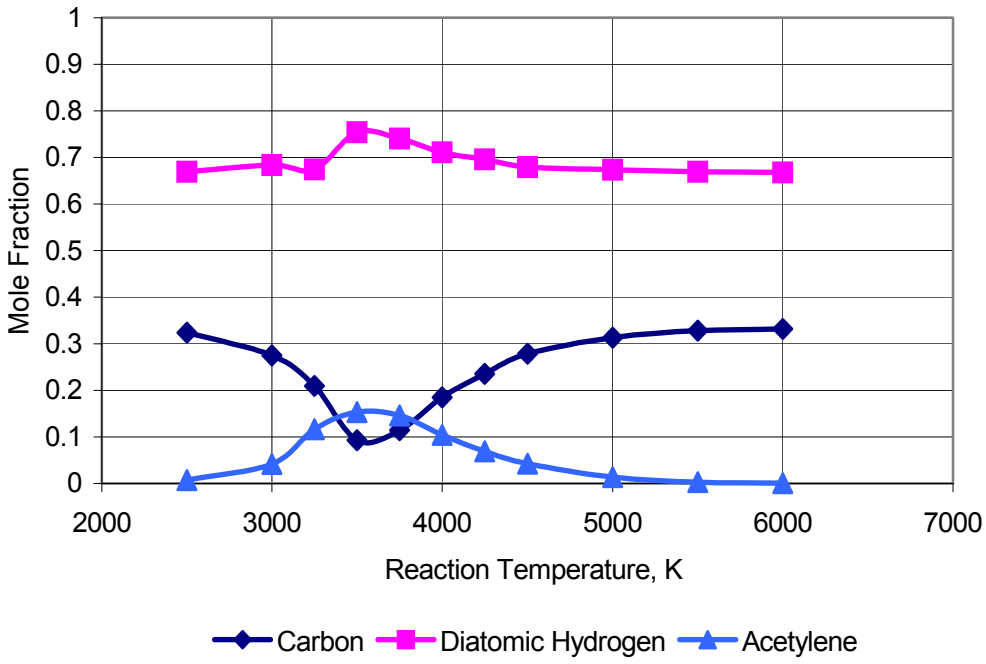

Figure 4.9 Methane Pyrolysis Products Assuming Recombination

recombine to form additional diatomic hydrogen. In addition, the multi-atom carbon species are arbitrarily added to the single carbon mole fraction, because these different carbon forms are not distinguished in the experimental analysis. Comparisons with the CEA calculations are further complicated by the fact that plasma torches do not produce a uniform flow temperature, but instead typically have a highly peaked temperature distribution, with the maximum temperature at the centerline often being twice the average temperature. Therefore, the reactions inside a plasma torch would actually occur over a wide range of temperatures rather than at a single characteristic

temperature. This issue is discussed in Ref. 22, in regard to the Huels acetylene production process. (This highly relevant paper was not discovered until after the completion of the test runs). The reaction zones in the Huels process are described as a set of concentric nested cylinders. However, the small plasma torch probably has a less pronounced temperature variation than a large Huels torch because the arc is very likely constricted within the small diameter nozzle orifice whereas in a Huels torch the arc only fills a small portion in the center of the inner chambers.

Further comparisons with CEA predictions were made for a set of specific test run conditions. First of all, the enthalpy of the gas exiting the nozzle was estimated based on an approximate arc-heating efficiency of 80%. According to test data from Hypertherm, the torch generally transfers about 80% of the electrical input to the arc gas with the remainder going into the airflow cooling the cathode (Fig. 4.10).

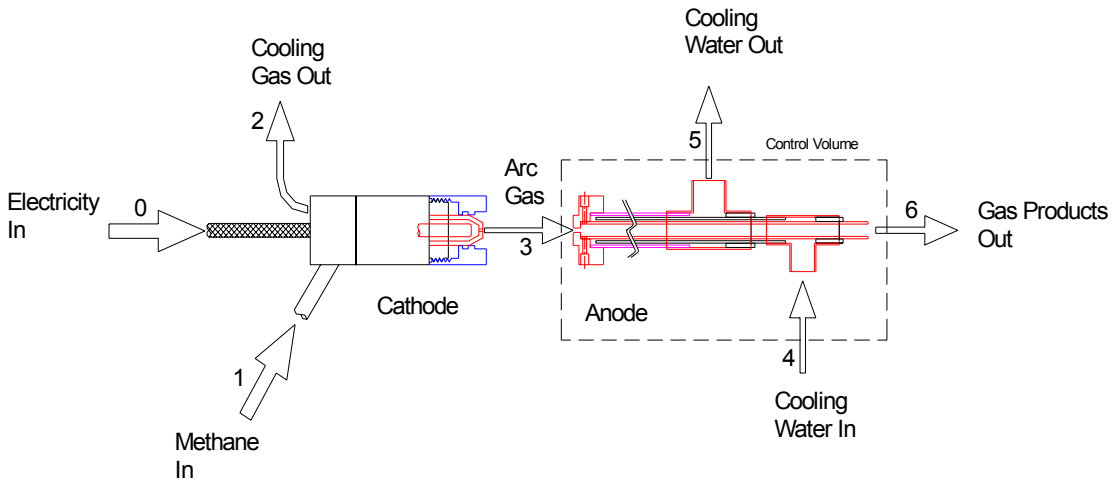

Figure 4.10 Thermodynamic Stations for Torch Apparatus

This given relationship stated in equation form is

$$(0.8)VI = \dot{m}_3(h_{T_3} - h_{T_1})$$

which may be solved for h_{T_3} .

$$h_{T_3} = \frac{(0.8)VI}{\dot{m}_3} + h_{T_1}$$

The mass flow of the arc gas is obtained from the GC analysis and sample bag volume. The gas entering at station one is assumed to be at room temperature (300 K) and 3 atm. The static enthalpy is obtained by assuming the flow exiting the nozzle orifice is choked and therefore at sonic velocity, so the kinetic energy term is subtracted from the total enthalpy as in this equation:

$$h_3 = h_{T_3} - \frac{a^2}{2}$$

This estimated value of h_3 and the measured pressure at the anode port are used to assign a thermodynamic state for the CEA input. The temperature and pressure input menu was used because it was not apparent how to simulate pyrolysis by directly inputting the enthalpy and pressure. Therefore, an iterative trial and error process was used to revise the temperature guesses until the target enthalpy and sonic velocity values were obtained.

Once the more noise-tolerant temperature sensors were installed in the water-cooled anode, calorimetric determinations of the state at station 3 could be made. The

enthalpies from the calorimetric measurements were compared to those obtained by assuming 80% of the input power is transferred to the nozzle flow (Fig. 4.11).

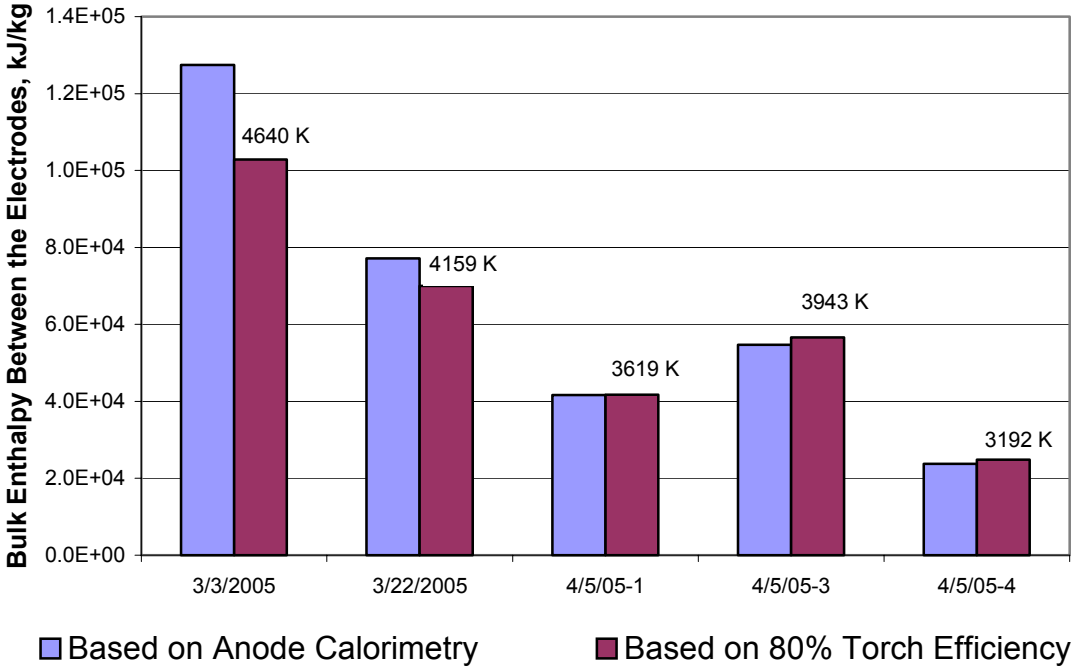

Figure 4.11 Bulk Enthalpy Estimates for Station 3

For the 7/15/2004, 8/17/2004, and the 11/29/2004 test runs, the pressure could only be roughly estimated from a coarsely graduated pressure gauge located well upstream of the torch. For these test runs, the pressure signal from the transducer connected to the anode port was obscured by electromagnetic interference. The later test runs had a pressure transducer installed with a much stronger signal on the anode port, giving a much more accurate indication of the pressure.

As expressed as a mole fraction, the hydrogen content is fairly insensitive to the range of test conditions for both the experimental results and the CEA predictions (Fig.

4.12 to 4.19). However, the proportions of acetylene and carbon do show a significant amount of variation. Because acetylene contains two carbon atoms, errors in determining the amount of acetylene from the gas sample analysis have the effect of magnifying the error in subsequently calculating the portion of carbon when balancing the reaction equation. Furthermore, the enthalpy values used for the CEA predictions have about a twenty percent uncertainty associated with them due to the difficultly in accurately determining the gas mass flow rate. Although there could have been some subtle experimental factors influencing the degree to which the results agree with the

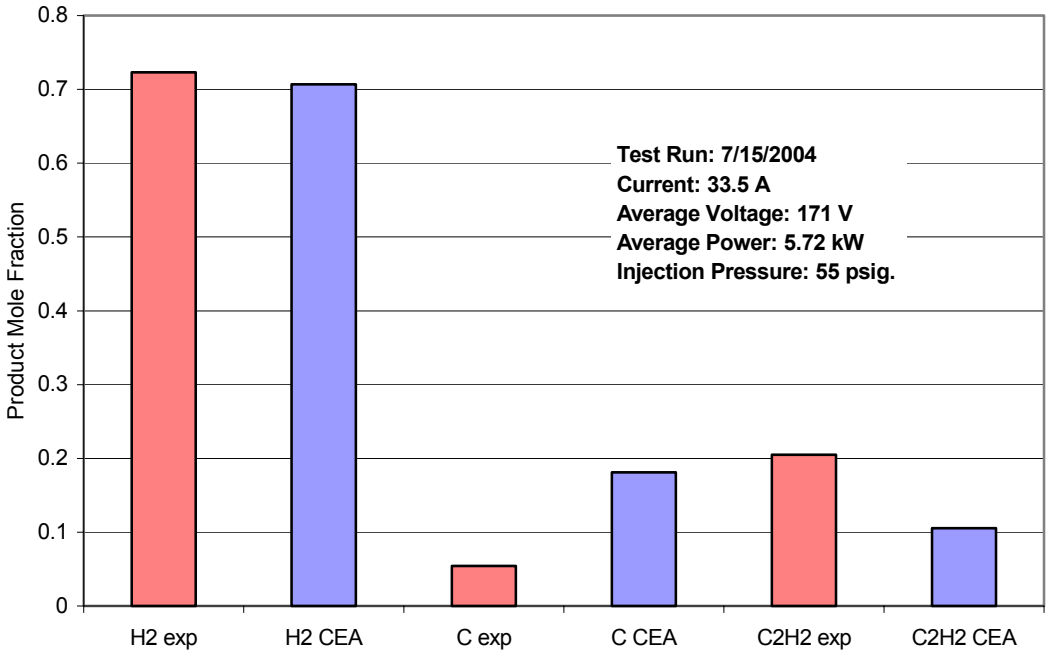

Figure 4.12 GC Results Compared with CEA Predictions for 7/15/2004 Test Run

predictions for a particular test run, this author attributes this randomness in the agreement primarily to the uncertainties in the measurements.

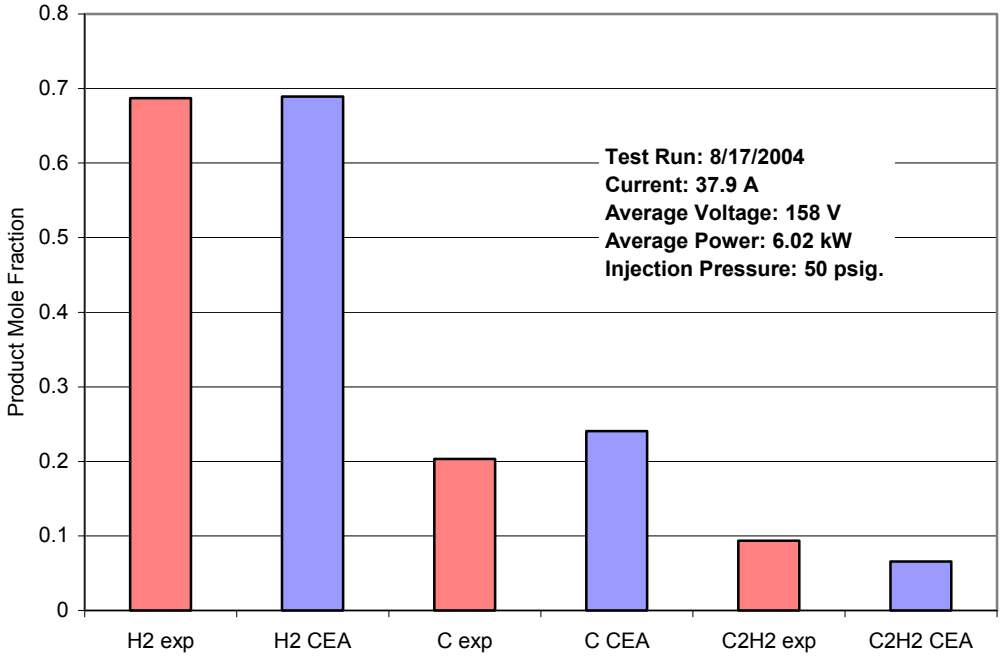

Figure 4.13 GC Results Compared with CEA Predictions for 8/17/2004 Test Run

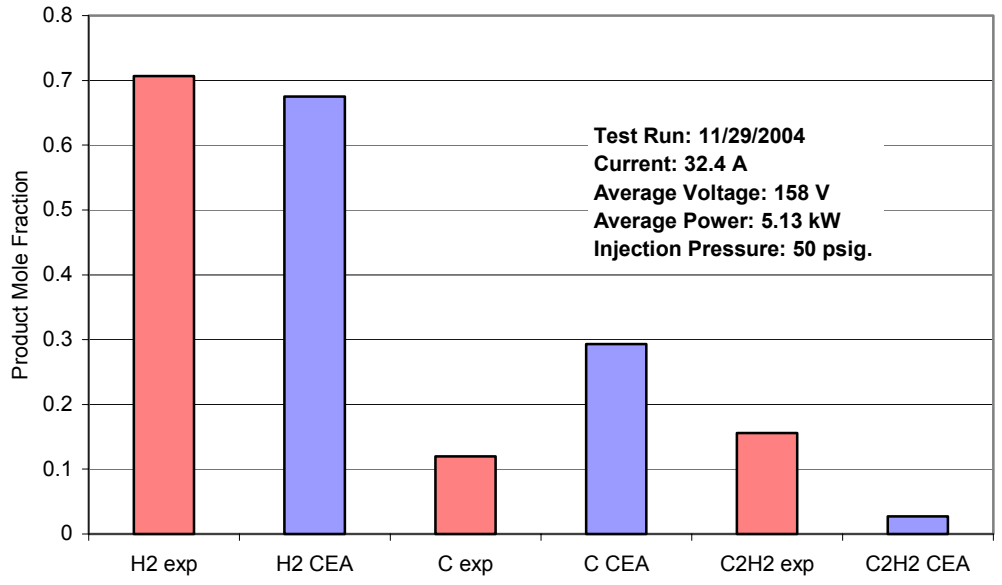

Figure 4.14 GC Results Compared with CEA Predictions for 11/29/2004 Test Run

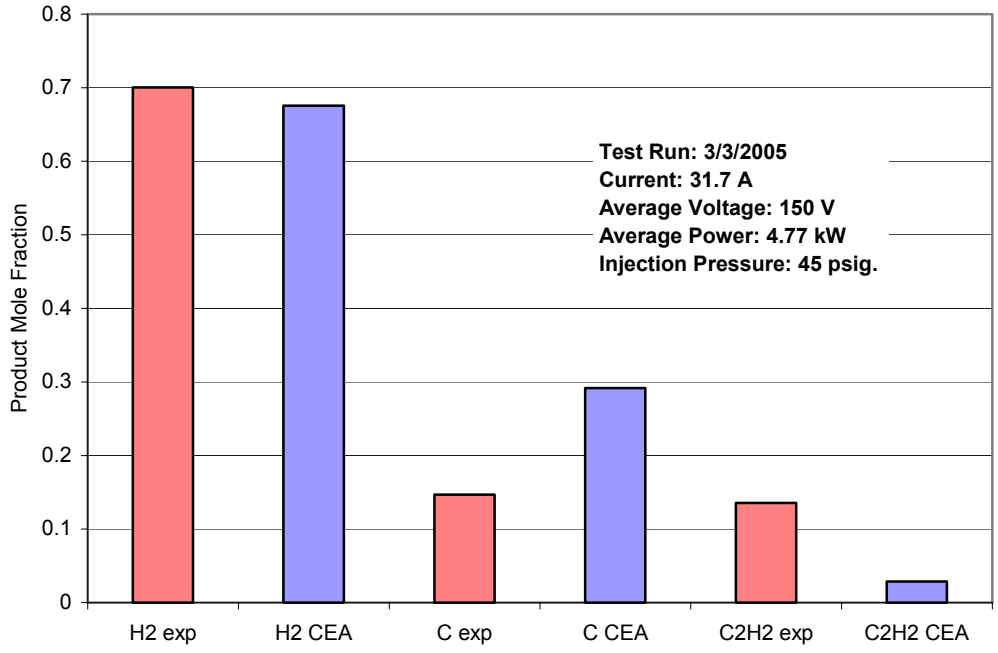

Figure 4.15 GC Results Compared with CEA Predictions for 3/3/2005 Test Run

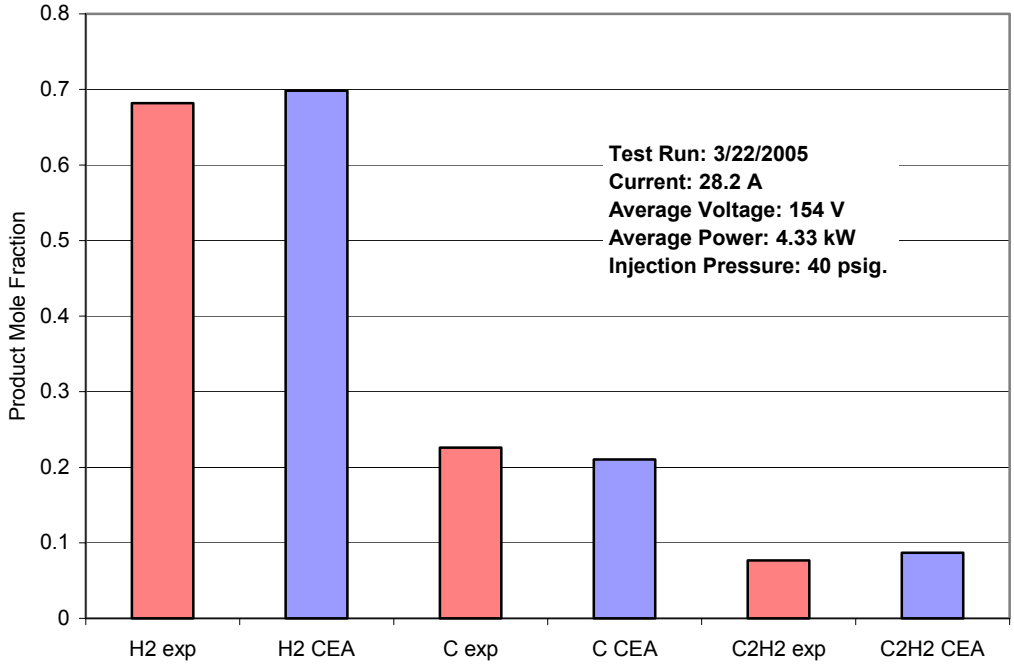

Figure 4.16 GC Results Compared with CEA Predictions for 3/22/2005 Test Run

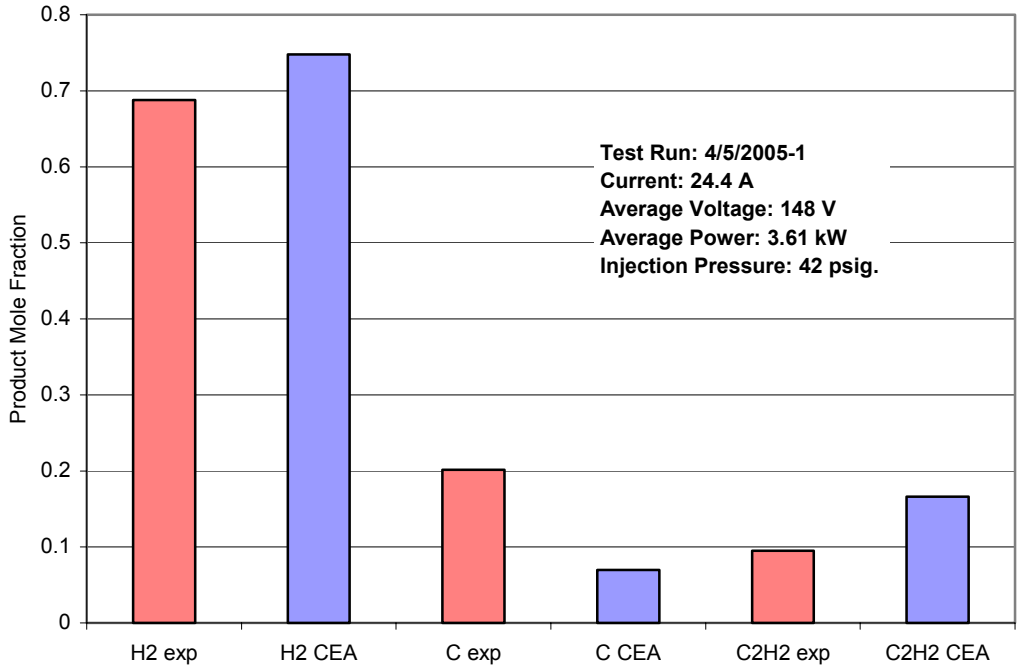

Figure 4.17 GC Results Compared with CEA Predictions for 4/5/2005-1 Test Run

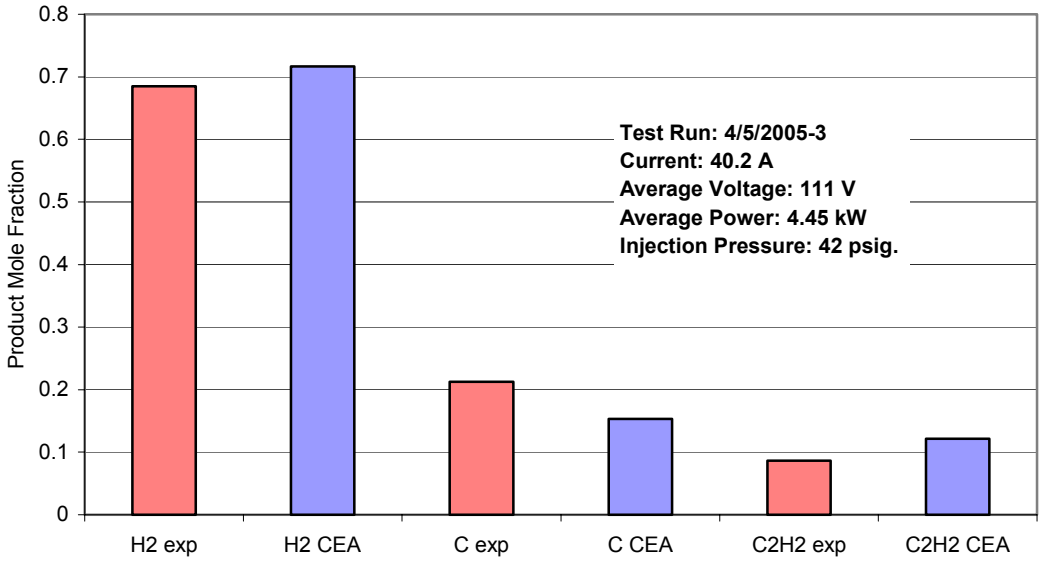

Figure 4.18 GC Results Compared with CEA Predictions for 4/5/2005-3 Test Run

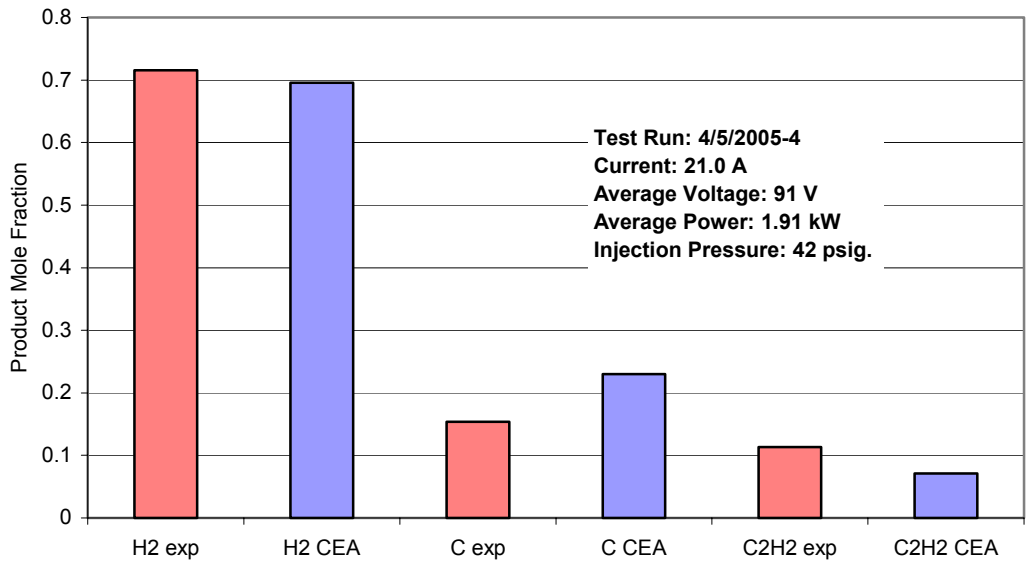

Figure 4.19 GC Results Compared with CEA Predictions for 4/5/2005-4 Test Run

4.4 Uncertainty Analysis

The main source of uncertainty in the pyrolysis experiments was the measurements of the gas sample volume, which contributed to most of the uncertainty in the mass flow rate and enthalpy determinations. Two different sizes of sample bags were used for the gas samples. Initially, three-liter capacity bags were used for the gas samples. Once it was discovered how much volume was actually needed for a 5 to 10 second duration gas sample, one-liter bags were purchased for subsequent test runs. The one-liter bags allowed a smaller, semitransparent bucket to be used for the volume

measurements. The volumes of the sample bags were generally measured at least twice if not three times. This repetition gave some indication of the variability of the measurements.

The main quantities of interest for the thermodynamic analysis are the mass flow rates and enthalpies. To determine the mass flow from the sample bag volume, the ideal gas law is applied, to first find the mole rate.

$$n = \frac{PV}{\tilde{R}T}$$

The partial volume, V, for a component of the sampled mixture is the volume fraction, f, determined from chromatography, times the total bag volume, V_{bag}.

$$V = fV_{bag}$$

The average mole rate of a component is the number of moles divided by the sampling duration, t.

$$\dot{n} = \frac{n}{t}$$

The mole rate may be calculated from:

$$\dot{n} = \frac{PfV_{bag}}{\tilde{R}Tt}$$

Following the approach given in Ref. 23, the uncertainty in the mole rate, $w_{\dot{n}}$, may be evaluated as a function of the partial derivatives with respect to each term and the individual uncertainties for each term.

$$w_{\dot{n}} = \left[\left(\frac{\partial \dot{n}}{\partial P} w_P \right)^2 + \left(\frac{\partial \dot{n}}{\partial f} w_f \right)^2 + \left(\frac{\partial \dot{n}}{\partial V_{bag}} w_{V_{bag}} \right)^2 + \left(\frac{\partial \dot{n}}{\partial T} w_T \right)^2 + \left(\frac{\partial \dot{n}}{\partial \tilde{R}} w_{\tilde{R}} \right)^2 + \left(\frac{\partial \dot{n}}{\partial t} w_t \right)^2 \right]^{1/2}$$

For the mole rate equation, the partial derivatives are the following:

$$\frac{\partial \dot{n}}{\partial P} = \frac{f V_{bag}}{\tilde{R} T t}$$

$$\frac{\partial \dot{n}}{\partial f} = \frac{P V_{bag}}{\tilde{R} T t}$$

$$\frac{\partial \dot{n}}{\partial V_{bag}} = \frac{P f}{\tilde{R} T t}$$

$$\frac{\partial \dot{n}}{\partial T} = -\frac{P f V_{bag}}{\tilde{R} T^2 t}$$

$$\frac{\partial \dot{n}}{\partial \tilde{R}} = 0$$

$$\frac{\partial \dot{n}}{\partial t} = -\frac{P f V_{bag}}{\tilde{R} T t^2}$$

Typical values for a hydrogen mole rate calculation are:

$f = 0.82$

$V = 0.6 \times 10^{-3}\ \mathrm{m}^3$

$P = 101{,}325\ \mathrm{N/m}^2$

$T = 300\,\mathrm{K}$

t=5 s

The corresponding uncertainties for these measurements are:

$w_f = 0.03$

$w_V = 0.1 \times 10^{-3}\ \mathrm{m}^3$

$w_P = 1{,}032.3\ \mathrm{N/m}^2$

$w_T = 1\ \mathrm{K}$

$w_t = 0.06\ \mathrm{s}$

Using these values to solve for the overall uncertainty in the mole rate gives $w_{\dot{n}} = 6.85 \times 10^{-7}\ \mathrm{kmol/s}$. When compared to the mole rate, $\dot{n} = 4.0 \times 10^{-6}\ \mathrm{kmol/s}$, the percentage uncertainty in the mole rate is 17%. The dominant factor in this overall uncertainty is the uncertainty in the sample bag volume measurement.

The mole rate of the reactant, methane, may be determined by multiplying the hydrogen mole rate by the ratio of moles of methane to hydrogen from the balanced reaction equation.

$$\dot{n}_{CH_4} = \frac{n_{CH_4}}{n_{H_2}} \dot{n}_{H_2}$$

Once the mole rate is determined, the mass flow rate may be calculated by multiplying by the molecular weight.

$$\dot{m}_{CH_4} = MW_{CH_4} \dot{n}_{CH_4}$$

Estimating the enthalpy from the assumed torch heating efficiency, η, uses the following given relationship:

$$h = \frac{\eta \mathrm{VI}}{\dot{m}_{CH_4}}$$

where V is the arc voltage and I is the arc current. Accordingly, the uncertainty in the enthalpy estimate is given by:

$$w_h = \left[\left(\frac{\partial h}{\partial \eta} w_\eta \right)^2 + \left(\frac{\partial h}{\partial \mathrm{V}} w_\mathrm{V} \right)^2 + \left(\frac{\partial h}{\partial \mathrm{I}} w_\mathrm{I} \right)^2 + \left(\frac{\partial h}{\partial \dot{m}_{CH_4}} w_{\dot{m}_{CH_4}} \right)^2 \right]^{1/2}$$

The efficiency, η, is treated as a constant although it is doubtful that this is precisely valid. For the case of the F-5000, the heating efficiency only varies by about 10% over its range of operation. Assuming constant efficiency the partial derivatives are:

$$\frac{\partial h}{\partial \eta} = 0$$

$$\frac{\partial h}{\partial \mathrm{V}} = \frac{\eta \mathrm{I}}{\dot{m}_{CH_4}}$$

$$\frac{\partial h}{\partial \mathrm{I}} = \frac{\eta \mathrm{V}}{\dot{m}_{CH_4}}$$

$$\frac{\partial h}{\partial \dot{m}_{CH_4}} = -\frac{\eta \mathrm{VI}}{\dot{m}_{CH_4}^2}$$

A nominal electric operating point is 150 V and 30 A. A typical methane mass flow rate is 5×10^{-5} kg/s. The heating efficiency was taken to be 0.8. The individual uncertainties are:

$w_V = 0.45\,\mathrm{V}$

$w_I = 0.3\,\mathrm{A}$

$w_{\dot{m}_{CH_4}} = 8.5\times10^{-6}\,\mathrm{kg/s}$

Evaluating the overall uncertainty in the enthalpy estimate gives $w_h = 1.23\times10^4\,\mathrm{kJ/kg}$. A midrange enthalpy value for the test runs is 6.44×10^4 kJ/kg, which would have an uncertainty of 19%. The primary influence on this uncertainty is the mass flow rate uncertainty, which was in turn dominated by the uncertainty in the sample bag volume measurement.

Although this level of uncertainty is substantial, it does not cast much doubt on the findings of this investigation in regard to hydrogen yield and the energy requirements of the experimental apparatus.

4.5 Discussion of Energy Requirements and Feasibility of On-Board Pyrolysis

The hydrogen yield does not seem to vary with power level or any other immediate parameter. If there is such an influencing factor, it is subtle enough to be hidden by the error scatter in the measurements and analysis. This lack of a correlation could be due to the flow being heated to the extent that an arc can be formed and sustained, which is considerably more than what is required to achieve complete

pyrolysis. Thermal pyrolysis only requires temperatures of 700 to 1200 °C, whereas the temperature of the arc plasma can be 12,000 °C or more (Ref. 15). All of the gas samples from successful test runs, in which the arc was sustained, revealed very near

Table 4.2 Apparatus Power Requirements

Test Run	**Methane Mass Flow Rate, kg/s**	**Heat Rate Available from Burning Methane, kW**	**Torch Power Input to Pyrolyze Methane, kW**
7/15/04	6.71×10^{-5}	3.36	5.65
8/17/05	5.62×10^{-5}	2.81	6.02
11/29/04	3.68×10^{-5}	1.84	5.13
3/3/05	2.92×10^{-5}	1.46	4.77
3/22/05	4.64×10^{-5}	2.32	4.33
4/5/05-1	6.23×10^{-5}	3.12	3.61
4/5/05-3	5.81×10^{-5}	2.91	4.45
4/5/05-4	5.18×10^{-5}	2.59	1.91

complete pyrolysis when analyzed. For the case of the Hypertherm torch, the proportion of gas actually being directly heated by the arc is much higher than what is typical for a Huels or segmented arc heater. For these arc heaters, only a small percentage of the total gas flow actually passes though the actual plasma arc; the great majority of the flow is heated indirectly by the arc. For example, the plasma core of the F-5000 is only 1/8” in diameter (at 800A) (Ref. 24), which is quite small as compared with the 1” anode barrel inside diameter and the 0.6875” diameter nozzle throat. In contrast, for the Hypertherm torch, the arc passes through the narrow 0.038” diameter nozzle orifice along with the entire flow subjected to the pyrolysis reaction.

Although these experiments demonstrated the feasibility of achieving almost complete pyrolysis in a very compact space, the power consumption was far above what

could be considered feasible for a flight vehicle. In only one test run (4/5/2005-4) was the torch power input lower than the amount of power that could be produced from burning the same mass flow of methane (Table 4.2). This direct manner of assessing feasibility is only valid if there are no means for the vehicle to recover some of the excess energy expended to accomplish the pyrolysis. A more fitting comparison for Table 4.3 may have been to list the combustion energy available from burning the hydrogen and carbon mixture resulting from pyrolysis. However, using reference book values, such a mixture of hydrogen and carbon will have a heating value of 54,900 kJ/kg, which is only 8% more output than the methane it was derived from (50,010 kJ/kg) (Ref. 25). The test run with the least power consumption was at a current of 21A. This particular run seemed to be close to the margin of the arc being extinguished rather than sustained, because a similar 20A run prior to this did fail to sustain the arc. This poor utilization of the input power for the apparatus is not surprising given that the design was improvised rather than being refined to minimize the power requirements. Furthermore, injecting additional methane downstream of the arc to exploit the high temperature of the arc-heated flow in order to thermally pyrolyze more methane was not attempted with this apparatus. (Injecting argon though the anode port, in order to keep a clear optical path for the spectrometer resulted in the arc being disrupted.) However, other plasma arc experiments and processes have been developed that show much more promising levels of power consumption (Table 4.3). For example, the Kaevner process used at the Karbomont facility reports energy consumption of 100.7 MJ per kg-mole of hydrogen (Ref. 26). The Kaevner device uses three-phase alternating current to form

arcs within a triangular array of carbon electrodes. Another technique, the GlidArc process, features an arc climbing between a pair of diverging electrodes in a "Jacob's Ladder" configuration (Ref. 27). In bench scale tests, the GlidArc process produced 1 mole of hydrogen and 0.22 mole of acetylene with 330 kJ (the author anticipated

Table 4.3 Energy Input for Various Hydrogen Generation Techniques

Data Source	**Energy Required to Produce a kg-mole of H_2, MJ/kmol**
7/15/04 Test Run	881.4
8/17/04 Test Run	1,015.1
11/29/04 Test Run	1,422.2
3/3/05 Test Run	2,917.4
3/22/05 Test Run	866.0
4/5/05-1 Test Run	685.0
4/5/05-3 Test Run	867.6
4/5/05-4 Test Run	432.1
Kvaener Process	100.7
Huels Process	280.6
Benchtop GlidArc	330
Prebola - Virginia Tech	40-75
Theoretical Water Electrolysis	285.8

considerable improvement with further development). However, the Kaevner and GlidArc devices appear much less suitable than an arc heater as a high discharge velocity fuel injector.

After the completion of the experiments for this investigation, a 1962 paper describing the Chemische Werke Huels' acetylene production process by DC arc was discovered (Ref. 22). During the Second World War, Germany depended on this chemical plant's process to supply acetylene as a precursor feed stock for producing synthetic rubber. In comparing the design of the Huels and Linde arc heaters, one can

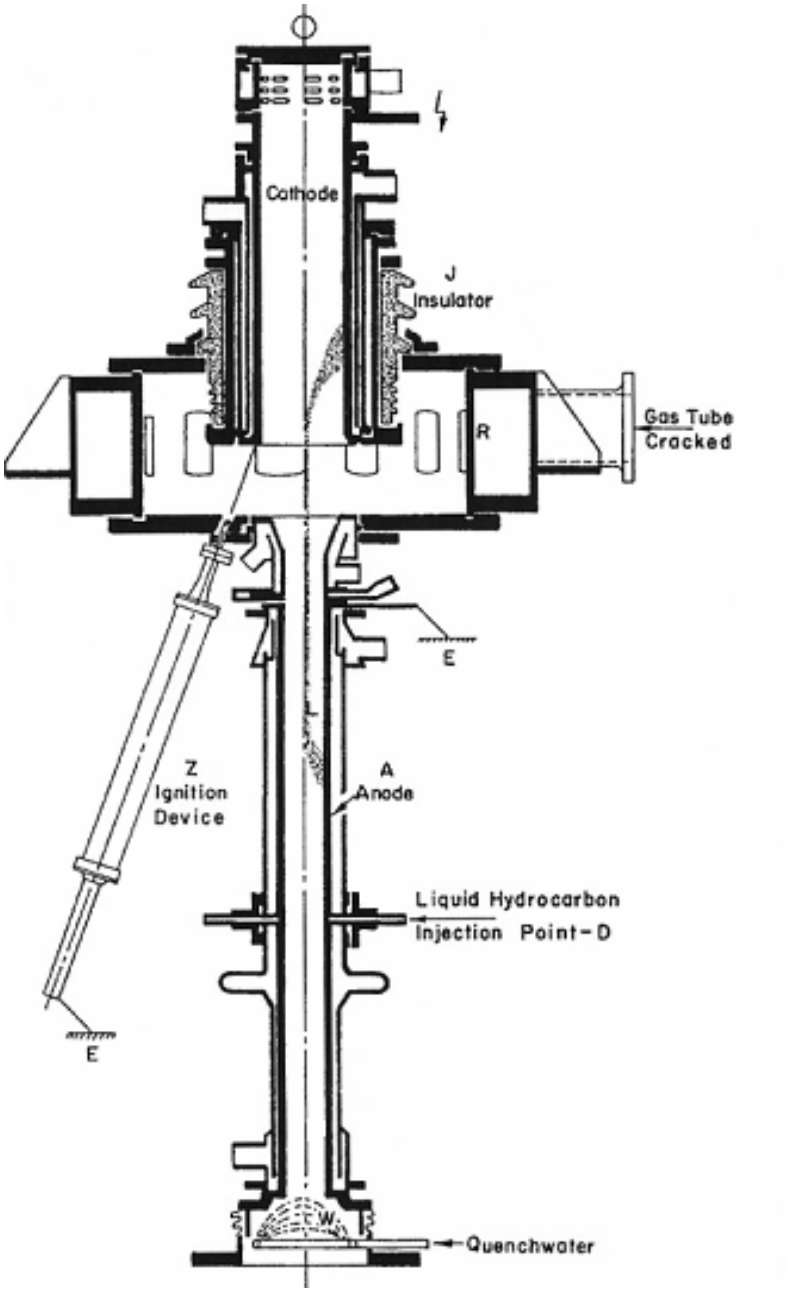

Figure 4.20 Huels Acetylene Production Arc Heater

introducing a hydrocarbon downstream of an arc to be thermally pyrolyzed in the "tail flame" of a different arc-heated gas. In this situation, the arc will be much more stable than in a hydrocarbon gas, and the hydrocarbon does not have to be excessively heated

in order to provide the conditions necessary to support an arc. As a case in point, the developers of the Kaevner process abandoned directly heating a hydrocarbon with the arc to arc-heating hydrogen and then injecting a hydrocarbon downstream. When using a tail flame to perform the pyrolysis, a Huels arc heater could prove to be even more competitive with the Kaevner and GlidArc processes in regard to energy consumption.

In 1986, Plasma Materials, Inc. (John Poole) patented a Huels-type plasma torch (Fig. 4.21) that demonstrated a 90% transfer of the arc energy to a hydrogen gas flow (with the remaining 10% heating the cooling water) (Ref. 28). On nitrogen, this torch is 75 to 80% efficient which is much better than the 50-55% efficiency of the F-5000. This

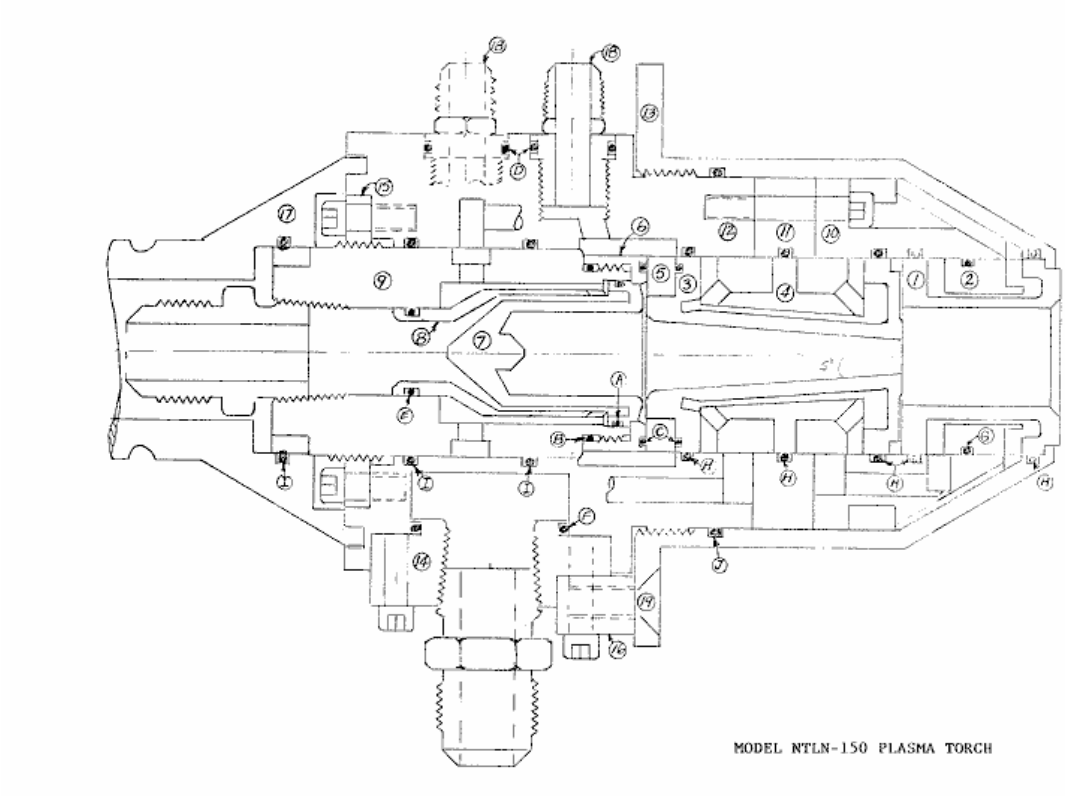

Figure 4.21 Plasma Materials Torch

In regard to the feasibility of using a pyrolysis process on board a flight vehicle, a simple case will be examined: Consider a liquid-methane fueled scramjet vehicle equipped with arc-heating fuel injectors. To provide electricity for the arc pyrolysis process, the vehicle has a 60% efficient gas turbine engine coupled to a generator. Using the Kvaener process as a representative value for the energy required for pyrolysis, results in an estimate of 12,600 kJ of energy to pyrolyze one kilogram of methane. With a 60% efficient electricity generation process, 20,900 kJ/kg out of the 54,900 kJ/kg total available combustion energy, would be utilized for pyrolysis. This leaves an effective heating value of the fuel of 34,000 kJ/kg for the vehicle. Multiplying this figure by the density of liquid methane gives an effective volumetric energy density of 14,360,000 kJ/m^3, which is still 70% greater than the energy density of liquid hydrogen (8,491,000 kJ/m^3). The unimaginative approach for this example is not intended as a technical suggestion, because it would be better to exploit the aerodynamic heating of the vehicle to drive the pyrolysis reactions.

Arc pyrolysis could probably be much better integrated into an AJAX vehicle as part of its overall thermodynamic system. For AJAX, there is great potential for recovering the energy used for fuel pyrolysis. The MHD generator extracts kinetic energy from the flow, which would otherwise appear as heat in the flow if it were compressed instead. In this sense, AJAX exploits the energy that would, for the case of a scramjet, only serve to heat the airframe and lessen the degree to which combustion energy could be injected into the flow.

The widely held belief that a non-hydrogen fuel will not burn with sufficient rapidity to be used in a supersonic combustor chamber of practical length may be faulty. Experiments have been reported in which liquid kerosene injected into a supersonic duct combusted in less length than hydrogen (Ref. 29). For these experiments, kerosene mixed much more readily with the air stream than hydrogen. However, the kerosene did contain an ignition-promoting additive: hydrogen. Arc-heating or any pyrolysis technique may be a less practical approach to utilizing a dense fuel in an air-breathing hypersonic vehicle than using ignition-promoting additives.

CHAPTER 5

CONCLUSIONS AND RECOMENDATIONS

5.1 Conclusions

This study experimentally demonstrated that methane may be pyrolyzed almost completely in a very compact space with a plasma torch, yielding a hydrogen mole fraction of approximately 0.7 of the total products. The power to mass flow ratio required to sustain an arc in the Hypertherm torch, resulted in the methane being heated to temperatures far beyond that required to thermally pyrolyze it. Based on enthalpy estimates for the station between the electrodes, the bulk temperature of the arc-heated products ranged from roughly 3000 to 5000K. The presence of C_2 bands in the emission spectra provides further evidence of products in this temperature range. The tubular electrode geometry of Huels torches seems to promote conditions that suppress carbon accumulation on the electrodes, which is a common problem for other plasma torch designs. A Huels torch is also likely to not heat the hydrocarbon feedstock to the excessive degree obtained with the Hypertherm torch. Some approximate agreement was observed between the experimental results and predictions from the NASA CEA code. However, this limited agreement is based on assuming that the predicted atomic hydrogen in the CEA predictions combines with C_2H to form additional acetylene and with itself to form additional diatomic hydrogen. Unfortunately, the pyrolysis torch apparatus required too much electric power to demonstrate any feasibility for within incorporation into a flight vehicle due to the necessity of heating the gas excessively in

order to sustain an arc. However, other researchers have demonstrated more feasible levels of power consumption for their arc pyrolysis devices, which suggests that a well-designed plasma torch could be a viable pyrolyzing fuel injector for a hypersonic air-breathing vehicle. If such a device proves to be feasible, then it could contribute substantially to lowering the cost and enhancing the practicality of hypersonic air-breathing vehicles.

5.2 Recommendations for Further Research

The F-5000 is much preferred over the modified Hypertherm torch in regard to suitability for pyrolysis research. However, a Huels configuration torch could be made for the Hypertherm power supply. John Poole's converging anode barrel design could be adopted. In addition, with the recent enhancement of the ARC's supersonic wind tunnel, a small scale Huels torch could be tested as a fuel injector discharging into a supersonic stream. (Virginia Tech has been doing this for years, but with a non-Huels geometry.)

The heating value of the arc-pyrolysis products should be investigated. There are claims that it is much higher than what has been stated in reference texts.

Injecting additional fuel downstream of the arc would certainly produce more pyrolyzed products per unit energy input. The Arc-Heated Wind Tunnel facility is well poised for experimenting with this technique once it becomes operational again. The anode barrel includes auxiliary injection ports, there are two plenum chamber injection

segments on hand, and there is an operational secondary gas injection system. Moreover, liquid hydrocarbons could readily be injected downstream of the arc.

Arc pyrolysis has potential in regard to helping implement the "hydrogen economy". Localized conversion of natural gas into hydrogen and carbon would sidestep the difficulty and expense of implementing a hydrogen distribution and storage infrastructure. In this author's opinion, efficient arc pyrolysis units could probably be made as small as a household refrigerator, so large conversion facilities would not be required. Moreover, it is possible that the first application of on-board fuel reformation may be for a truck or automobile rather than a flying vehicle. In contrast to carbon dioxide, the solid carbon produced by pyrolysis does not need to be sequestered from the atmosphere, but merely gathered for storage or disposal. However, the carbon probably could be better utilized in carbon-oxygen fuel cells or structural products.

APPENDIX A

DATA REDUCTION PROGRAM FOR PLASMA TORCH EXPERIMENTS

```
c      pstorch.f
c      last revison 4/7/05
c
c
      real t(2200),sample(2200),waterdt(2200),
     x anodewf(2200),current(2200),hanode(2200),
     x gast(2200),apress(2200),rapress(2200),
     x baratron(2200),voltage(2200),tpress(2200)



          real lkc1,lkc2,lkc3,lkc4,lkc5,lkc6,lkc7,lkc8,lkc9
      real lasttime,scannum,anodewdt(2200),ranodedt(2200)


      integer day,year,runnum,startpoint,endpoint,nscans

      character*12 filein,fname,fname2, gas
          write(*,*)' pstorch.f - reduction program for small'
          write(*,*)' plasma torch with RTD and temp ICs'
          write(*,*)
          write(*,222) 'Enter name of file of HP3852 vector values: '
          read(*,*) filein
          write(*,*)
      write(*,222) 'Enter name of output file of converted data: '
222       format('  ',a\)
      read(*,*) fname
          write(*,222) 'Enter name of run summary file: '
          read(*,*) fname2
      open(3,file=filein,status='old')

      open(4,file=fname,status='new')

          open(8,file=fname2,status='new')


333       format(1x,12(a11,','))

          write(*,*)
          write(*,*)
      write(*,222) ' Enter month: '
      read(*,*) month
          write(*,*)
          write(*,*)
```

```
      write(*,222) ' Enter day: '
      read(*,*) day
           write(*,*)
           write(*,*)
      write(*,222) ' Enter year (yyyy): '
      read(*,*) year
           write(*,*)
           write(*,*)
      write(*,222) ' Enter run number: '
      read(*,*) runnum
           write(*,*)
           write(*,*)
           write(8,*)
           write(8,15) month,day,year,runnum
15    format(' (',i2,'/',i2,'/',i4,')   run:',i2)
           write(8,*) ' Converted values written to: ', fname
           write(*,*)
           write(*,*)
           write(*,222) ' Enter gas used in run: '
           read(*,*) gas
           write(*,*)
           write(*,*)
      write(*,222) ' Enter number of scans: '
      read(*,*) nscans
           write(*,*)
           write(*,*)
      write(*,222) ' Input scan time: '
      read(*,*) scantime
           write(*,*)
           write(*,*)
           write(*,222) ' Enter arc current dial setting: '
           read(*,*) dial
           write(*,*)
           write(*,*)
           write(*,222) ' Enter gas injection pressure: '
           read(*,*) regpress
      write(*,*)
           write(*,*)
           write(*,222) ' Enter gas RTD position from anode contriction: '
           read(*,*) tcposition
           write(*,*)
           write(*,*)
           write(*,222) ' Enter barometric pressure (mm of Hg): '
           read(*,*) patm
```

```
      atm=patm/51.75
      scannum=nscans*1.0
    timeinc=scantime/scannum
    lasttime=0.0
    write(8,*) ' Echo of keyed-in informtion: '
      write(8,*) ' Number of multiplexer scans = ',nscans
    write(8,*) ' Duration of scan = ',scantime,' s'
      write(8,*) ' Arc current dial setting: ',dial,' amps'
      write(8,*) ' Gas injection pressure: ',regpress,' psi'
      write(8,*) ' Gas used in run: ',gas
    write(8,*) ' Gas RTD position from constriction:',tcposition,'in'
      write(8,*) ' Barometric pressure = ',atm,' psia'
      write(8,*) ' Calculated results: '
c     type T thermocouple polynomial coef. voltage in microvolts
c     temperature in degrees C
    tc1=2.5928e-2
    tc2=-7.602961e-7
    tc3=4.637791e-11
    tc4=-2.165394e-15
    tc5=6.048144e-20
    tc6=-7.293422e-25
c     type K t/c polynomial coef. voltage in microvolts (> 20644 microvolts)
c     temperature in degrees C (500 to 1372 C range)
    hkc0=-1.318058e2
      hkc1=4.830222e-2
      hkc2=-1.646031e-6
      hkc3=5.464731e-11
      hkc4=-9.650715e-16
      hkc5=8.802193e-21
      hkc6=-3.110810e-26
c     type K t/c polynomial coef. voltage in microvolts (< 20644 microvolts)
c     temperature in degrees C (0 to 500 C range)
      lkc1=2.508355e-2
      lkc2=7.860106e-8
      lkc3=-2.503131e-10
      lkc4=8.315270e-14
      lkc5=-1.228034e-17
      lkc6=9.804036e-22
      lkc7=-4.413030e-26
      lkc8=1.057734e-30
      lkc9=-1.052755e-35
c      specific heats
      cpw=4.184
      cpn2=1.0416
```

```
c
      ch5last=0.0
      ch6last=0.0
           ch7last=0.0
           ch12last=0.0
      ch13last=0.0
      ch14last=0.0
      ch15last=0.0
      ch16last=0.0
      ch17last=0.0
      ch18last=0.0
      ch19last=0.0
      ch20last=0.0
      ch21last=0.0
      ch22last=0.0
      ch23last=0.0

           write(*,*)
           write(*,*)
      write(*,*) 'Going to read input file'
111    format(g14.7)

       do 100 i=1,nscans
         t(i)=lasttime+timeinc
         lasttime=t(i)

c      read and calculate upstream water temp with AD592
               read(3,*) ch5
c              if    (ch5 > 11.0) ch5=ch5last
c          ch5last=ch5
c                    uswt(i)=ch5*1000.0

c          read and calculate water delta temp with AD592s (50mV/C)
               read(3,*) ch6
               if    (ch6 > 11.0) ch6=ch6last
           ch6last=ch6
                    waterdt(i)=(ch6-0.0275)*20.0

c          read and calculate (unamplified, redundant) anode port press
               read(3,*) ch7
               if (ch7>11.0) ch7=ch7last
               ch7last=ch7
               rapress(i)=ch7*2000.0
```

```
            read(3,*) ch8
            read(3,*) ch9
            read(3,*) ch10
            read(3,*) ch11

c     read and calculate anode water flow rate in gpm
          read(3,*) ch12
           if (ch12>11.0)  ch12=ch12last
           ch12last=ch12
          anodewf(i)=(ch12-0.154)*53.54*60.0/6679.6
c           read and calculate anode pressure - Motorola Transducer
          read(3,*) ch13
              if    (ch13>11.0) ch13=ch13last
              ch13last=ch13
              apress(i)=22.5927*ch13-4.1207

c     read and calculate arc current
          read(3,*) ch14
           if (ch14>11.0)  ch14=ch14last
           ch14last=ch14
          current(i)=10.06*ch14-0.7546
c     read and calculate water delta T with 1000x amp type T T/C
          read(3,*) ch15
           if (ch15>11)  ch15=ch15last
                     if (ch15<-9) ch15=ch15last
           ch15last=ch15
c          convert to microvolts
              ch15m=1.0e3*ch15
              anodewdt(i)=tc1*ch15m+tc2*ch15m*ch15m+tc3*ch15m**3+
     x     tc4*ch15m**4+tc5*ch15m**5+tc6*ch15m**6
c     read and calculate gas T from  1000 ohm RTD
c     signal is conditioned by ADT70 10mV/C
          read(3,*) ch16
           if (ch16>9.9)  ch16=ch16last
                if (ch16<-1.0) ch16=ch16last
           ch16last=ch16

              gast(i)=100.0*(ch16)

          read(3,*) ch17


          read(3,*) ch18
```

```
          read(3,*) ch19

c          is gas sample being taken? yes=4.5 volts
          read(3,*) ch20
               sample(i)=ch20

c      read and calculate test section pressure in psi
          read(3,*) ch21
            if (ch21>11.0)  ch21=ch21last
            ch21last=ch21
c          convert to mmHg then to psi
          baratron(i)=100.0*ch21/51.75
c     read and calculate arc voltage
          read(3,*) ch22
            if (ch22>11.0)  ch22=ch22last
            ch22last=ch22
          voltage(i)=65.232*ch22-2.1506

c           read and calculate upstream torch pressure
c           Omega transducer on filter amp #5 output=(signal*100)
c           transducer 200psi=100mV before amplification
          read(3,*) ch23
                if(ch23>11.0) ch23=ch23last
                     ch23last=ch23
               tpress(i)=ch23*20.0

           write(*,*) i
c
c          waterdt(i)=dswt(i)-uswt(i)
c
c2345 789
100     continue
      write(*,*)
           write(*,*)
           write(*,*) 'read input file '
c
c       write converted values to output file
      write(4,333) 'time','anodeP','waterflow','current','waterdT',
     x  'gasT','tsP','voltage','torchP','ranodeP','sample',
     x  'anodewdT'
      write(4,333) 'sec.','psi','gpm','amps','C','C','psia','volts',
     x  'psig','psig','volts',' C'
```

```
c     write array
      do 200 i=1,nscans
      write(4,444)t(i),apress(i),anodewf(i),current(i),waterdt(i)
     x ,gast(i),baratron(i),voltage(i),tpress(i),rapress(i),
     x sample(i),anodewdt(i)
444       format(1x,12(g11.4,','))
200   continue
      write(*,*) 'wrote converted values to ',fname
c
c2345 7
c      get mass flow rates
c     water flow rates (normally) do not vary during run
      anodesum=0.0
           do 300 i=1,nscans
        anodesum=anodewf(i)+anodesum

300   continue
c       solve for average flow rate and convert gpm to kg/s
c     1m^3/s=1.5859e4 gpm, density of water = 997.0 kg/m^3
      mdotanode=(anodesum/scannum/1.5859e4)*997.0

      write(*,*)   '  determine test window '
       j=1
350       if (current(j)>1.5) then
            startpoint=j+25
c                       allow about half a second for starting transients
            starttime=t(startpoint)
                 goto 360
          else
            j=j+1
            goto 350
         endif
360        j=2200
370      if (current(j)>1.5) then
            endpoint=j
            endtime=t(endpoint)
                 goto 375
          else
            j=j-1
            goto 370
         endif
375    write(*,*) ' found startpoint and endpoint'
```

```
c     calculate enthalpies for plasma torch
c
c     determine anode enthalpy
      call avg(waterdt,endpoint,startpoint,atempavg)
      call standev(waterdt,atempavg,endpoint,startpoint,adtdev)
      call chauv(waterdt,atempavg,adtdev,endpoint,startpoint,ranodedt)
      do 410 i=startpoint,endpoint
         waterdt(i)=ranodedt(i)
410   continue
      call lsf(t,waterdt,endpoint,startpoint,atempm,atempb)
      do 420 i=startpoint,endpoint
        hanode(i)=(atempm*t(i)+atempb)*cpw*mdotanode
420   continue
c     calculate inlet N2 enthalpy

c     calculate jet bulk total enthalpy

c     month, day, year, time to file

c     calculate avg enthalpy of cooling water

          call avg(hanode,endpoint,startpoint,ahanode)
          write(*,*)
          write(*,*) ' Avg Power to cooling water =',ahanode,' kW'
          write(8,*)
          write(8,*) ' Average Power to cooling water =',ahanode,' kW'

c     calculate avg current to arc heater
      call avg(current,endpoint,startpoint,acurrent)
          write(*,*)
          write(*,*) ' Average current to Plasma Torch =',acurrent,' Amps'
          write(8,*)
          write(8,*) ' Average current to Plasma Torch =',acurrent,' Amps'
c     calculate avg voltage to arc heater
      call avg(voltage,endpoint,startpoint,avoltage)
          write(*,*)
          write(*,*) ' Average voltage to Plasma Torch =',avoltage,' Volts'
          write(8,*)
          write(8,*) ' Average voltage to Plasma Torch =',avoltage,' Volts'
c     calculate avg power to arc heater
      apower=acurrent*avoltage/1000
```

```
      write(*,*)
      write(*,*) ' Average power to Plasma Torch =',apower,' kW'
      write(8,*)
      write(8,*) ' Average power to Plasma Torch =',apower,' kW'

c     calculate average anode barrel pressure
      call avg(apress,endpoint,startpoint,aapress)
    write(*,*)
      write(*,*) ' Average anode barrel pressure =',aapress,' psig'
      write(8,*)
      write(8,*) ' Average anode barrel pressure =',aapress,' psig'
c     calculate average injection pressure
      call avg(tpress,endpoint,startpoint,atpress)
    write(*,*)
      write(*,*) ' Average injection pressure =',atpress,' psig'
      write(8,*)
      write(8,*) ' Average injection pressure =',atpress,' psig'
c     calculate average leaving gas temperature
      call avg(gast,endpoint,startpoint,agast)
    write(*,*)
      write(*,*) ' Average leaving gas temp =',agast,' C'
      write(8,*)
      write(8,*) ' Average leaving gas temp =',agast,' C'
c     print average water delta T
      write(*,*)
      write(*,*) ' Average water delta T =',atempavg,' C'
      write(8,*)
      write(8,*) ' Average water delta T =',atempavg,' C'

c   calculate run duration
      durat=t(endpoint)-t(startpoint-25)
      write(*,*)
      write(*,*) ' Run duration =',durat,' seconds'
      write(8,*)
      write(8,*) ' Run duration =',durat,' seconds'




    close(3)
    close(4)
      close(8)
    stop
    end
```

```
      subroutine avg(y,epoint,spoint,yavg)
       real y(2200),yavg,points
       integer epoint,spoint
       sumy=0.0
        do 20 i=spoint,epoint
          sumy=y(i)+sumy
20      continue
       points=(epoint-spoint)*1.0
       yavg=sumy/points
      return
          end

      subroutine standev(y,yavg,epoint,spoint,sdev)
       real y(2200),yavg, sdev
       integer epoint,spoint
       sumd=0
        do 40 i=spoint,epoint
          sumd=(y(i)-yavg)**2+sumd
40      continue
       pop=(epoint-spoint)*1.0
       sdev=sqrt(sumd/pop)
      return
          end



      subroutine chauv(y,yavg,sdev,epoint,spoint,yr)
       real y(2200),yavg,sdev,yr(2200)
       integer epoint,spoint
       crit=3.5*sdev
        do 50 i=spoint,epoint
          dev=abs(y(i)-yavg)
           if (dev.gt.crit) then
              yr(i)=yavg
           else
              yr(i)=y(i)
           endif
 50      continue
      return
          end

c2345 7890123
       subroutine lsf(x,y,epoint,spoint,slope,b)
```

```
      dimension x(2200),y(2200)
      real slope,b
      integer epoint,spoint
c
      sumx=0.0
      sumx2=0.0
      sumxy=0.0
      sumy=0.0

c
      do 10 i=spoint,epoint
        sumx=x(i)+sumx
        sumx2=x(i)*x(i)+sumx2
        sumxy=x(i)*y(i)+sumxy
        sumy=y(i)+sumy
10      continue
      xavg=(x(epoint)-x(spoint))/2.0
      start=spoint*1.0
      endpoint=epoint*1.0
      yavg=sumy/(endpoint-start)
      slope=(sumxy-sumx*yavg)/(sumx2-sumx*xavg)
      b=yavg-slope*xavg
     return
        end
c2345 78
```

APPENDIX B

REDUCTION PROGRAM FOR GAS CHROMATOGRAPHY DATA

```
C       peakarea.f
C          last revision 7/2/04
        real t(32000),y(32000),area(20),p(20),tp(20)
        real basewidth(20)
        real sum
        integer iflag
        character*12 filein, fname
        character*80 line1, line2, line3, line4
        write(*,*)
        write(*,222) 'Enter name of GC data file: '
        read(*,*) filein
        write(*,*)
        write(*,222) 'Enter name of output file: '
222     format(' ',a\)
        read(*,*) fname
        open(3,file=filein,status='old')
        open(4,file=fname, status='new')
        write(*,*)
c       write(*,222) 'Enter number of data rows: '
c       read(*,*) nrows
        read(3,*)
        read(3,*)
        read(3,*)
        read(3,*)
        npts=0
10      read(3,*,end=20)
                npts=npts+1
c           write(*,*) npts
        goto 10
20      continue

    close(3)
        open(3,file=filein,status='old')
        read(3,*) line1
        read(3,*) line2
        read(3,*) line3
        read(3,*) line4
        write(4,*) line1
        write(4,*) line2
        write(4,*) line3
        write(4,*) line4
        write(*,*) line1
        write(*,*) line2
```

```
      write(*,*) line3
      write(*,*) line4
      sum=0.0
c     read(3,*)
c     read(3,*) t,a1
c     read(3,*) t,a2
c     read(3,*) t,a3
c     baseline=(a1+a2+a3)/3.0
c     npts=npts-4
       do 30 i=1,30
         read(3,*) t(i),y(i),b,c,d
         sum=sum+y(i)
         write(*,*) sum
30     continue
      baseline=sum/30.0
      deltat=t(2)-t(1)
c     baseline=0.0
      write(*,*) 'baseline =',baseline
      write(4,*) 'baseline =',baseline
      thres=baseline +0.15
      sum=0.0
      peak=baseline
      iflag=0
      k=0
c      do 40 j=1,30
c        backspace 3
c        write(*,*) 'backspace'
40     continue
       do 100 i=31,npts
       read(3,*) t(i),y(i),b,c,d
c      write(*,*) t(i)
        if (y(i)>thres) then
          if (iflag.eq.0) then
            istart=i
            iflag=1
          endif
          sum=sum+y(i)-baseline
          if (y(i)>peak) then
            peak=y(i)
            peaktime=t(i)
          endif
        else
          if (iflag.eq.1) then
                    iend=i
```

```
            k=k+1
            area(k)=sum*deltat
            p(k)=peak
            tp(k)=peaktime
            basewidth(k)=t(iend)-t(istart)
            peak=baseline
            sum=0.0
            iflag=0
           endif
         endif

100    continue
         do 200 j=1,k
           write(*,333) ' area(',j,')=',area(j),' mV-s'
           write(*,*)
                write(4,333) ' area(',j,')=',area(j),' mV-s'
           write(4,*)
                write(*,333) ' peakheight(',j,')=',p(j),' mV'
           write(*,*)
           write(4,333) ' peakheight(',j,')=',p(j),' mV'
           write(4,*)
           write(*,333) ' peaktime(',j,')=',tp(j),' seconds'
           write(*,*)
           write(4,333) ' peaktime(',j,')=',tp(j),' seconds'
           write(4,*)
           write(*,333) ' basewidth(',j,')=',basewidth(j),' seconds'
           write(*,*)
           write(4,333) ' basewidth(',j,')=',basewidth(j),' seconds'
           write(4,*)
200    continue
333      format(a,i2.2,a,g14.7,a)
       close(3)
       close(4)
       stop 'finished'
       end
```

APPENDIX C

GAS SAMPLE TEST RUN DATA

Test Run Date	Arc Current, A	Arc Voltage, V	Arc Power, kW	Injection Pressure, psig
6/17/2004	39.83	141.8	5.65	55
7/15/2004	33.48	170.7	5.72	55
8/17/2004	37.94	158.8	6.02	50
9/30/2004	34	?	?	42
11/29/2004	32.44	158.1	5.13	50
3/3/2005	31.72	150.3	4.77	45
3/22/2005	28.15	153.7	4.33	40
4/5/2005-1	24.42	147.7	3.61	42
4/5/2005-3	40.19	110.7	4.45	42
4/5/2005-4	20.98	90.9	1.91	42

Test Run Date	Gas Sample Volume, L	Hydrogen Fraction of Sample	Acetylene Fraction of Sample	Methane Fraction of Sample
6/17/2004	?	0.84	0.14	0.02
7/15/2004	0.71	0.795	0.185	0.02
8/17/2004	0.943	0.863	0.1173	0.02
9/30/2004	1.468	0.7813	0.1987	0.02
11/29/2004	0.715	0.803	0.177	0.02
3/3/2005	0.62	0.821	0.159	0.02
3/22/2005	0.853	0.881	0.099	0.02
4/5/2005-1	0.66	0.861	0.119	0.02
4/5/2005-3	0.79	0.87	0.11	0.02
4/5/2005-4	0.76	0.846	0.134	0.02

Test Run Date	Methane Inlet Mass Flow Rate, kg/s	Test Run Duration, s	Gas Sample Duration, s	Delay of Gas Sample after Test Run Start, s
6/17/2004	?	8.566	?	?
7/15/2004	6.71E-05	7.565	3.580	1.85
8/17/2004	5.62E-05	8.022	5.580	2.23
9/30/2004	?	9.8	?	?
11/29/2004	3.68E-05	8.758	6.470	1.17
3/3/2005	3.55E-05	7.975	5.590	0.7682
3/22/2005	4.64E-05	10.037	6.110	2.187
4/5/2005-1	6.23E-05	8.647	4.377	2.52
4/5/2005-3	5.81E-05	8.86	5.440	1.247
4/5/2005-4	5.18E-05	8.765	5.910	1.509

Test Run Date	Maximum Cooling Water ΔT, °C	Cooling Water Mass Flow Rate, kg/s	Leaving Gas Temperature, °C	Pressure at Anode Port, psig.
6/17/2004	7	0.155	?	?
7/15/2004	?	0.155	?	?
8/17/2004	?	0.155	?	?
9/30/2004	?	0.155	?	?
11/29/2004	?	0.153	?	?
3/3/2005	6.99	0.155	68.3	22.86
3/22/2005	5.48	0.155	141	35.86
4/5/05-1	3.98	0.155	172.4	34.25
4/5/05-3	7.46	0.101	200	38.65
4/5/05-4	2.90	0.100	166.3	39.17

Test Run Date	Weight of Empty Sample Bag, g	Weight of Filled Sample Bag, g	Weight Reduction Due to Buoyancy, g	Net Weight of Sampled Gas, g
7/15/2004	30.439	29.795	0.912	0.268
8/17/2004	30.356	29.55	1.211	0.405
9/30/2004	32.213	31.04	1.885	0.712
11/29/2004	31.704	30.923	0.918	0.137
3/3/2005	21.866	21.423	0.796	0.353
3/22/2005	22.306	21.47	1.245	0.409
4/5/05-1	21.667	21.175	0.847	0.355
4/5/05-3	21.962	21.308	1.014	0.360
4/5/05-4	22.455	21.903	0.976	0.424

Test Run Date	Weight of Extracted Carbon, g	Deposition Rate of Carbon, g/s
6/17/2004	0.089	1.04E-02
7/15/2004	0.039	5.16E-03
8/17/2004	0.062	7.73E-03
9/30/2004	0.104	0.010612
11/29/2004	0.083	9.48E-03
3/3/2005	0.047	5.89E-03
3/22/2005	0.138	1.37E-02

REFERENCES

1. Sweetman, B., *Aurora, The Pentagon's Secret Hypersonic Spyplane*, Motorbooks International, p. 73, 1993.

2. Emanuel, G., "The Role of Stagnation Pressure for Air-Breathing Hypersonic Propulsion," AIAA Paper 2003-6928, 2003.

3. Sutton, G., *Rocket Propulsion Elements*, 6th Ed., John Wiley & Sons, Inc., p. 254, 1992.

4. Miller, J., *Lockheed Martin's Skunk Works*, Midland Publishing Ltd., 1995.

5. Bruno, C., and Czysz, P., "Magnetohydrodynamic Coupled Ramjet Propulsion System: A Perspective," ISABE-2001-1230, 15th International Symposium on Air Breathing Engines, Bangalore, India, September 2001.

6. Lee, Y-M., Czysz, P., and Petly, D., "Magnetohydrodynamic Energy Bypass Applications for Single Stage-to-Orbit Vehicles," AIAA Paper 2001-1901, 2001.

7. Prebola, J., "Performance of a Plasma Torch With Hydrocarbon Feedstocks for Use in Scramjet Combustion," Master's Thesis, Virginia Polytechnic Institute & State University, August 1998.

8. Kuranov, A.L., Korabelnikov, A.V., Kuchinsky, V.V., and Sheikin, E.G., "Fundamental Techniques of the AJAX Concept," AIAA Paper 2001-1915, 2001.

9. Ganiev, Y.C., Gordeev, V.P., Krasilnikov, A.V., Lagutin, V.I., Otmennikov, V.N., and Panasenko, A.V., "Aerodynamic Drag Reduction by Plasma and Hot-Gas Injection," *Journal of Thermophysics and Heat Transfer*, Vol. 14, No. 1, January-March 2000.

10. Rizkalla, O., Chinitz, W., and Erdos, J., "Calculated Chemical and Vibrational Nonequilibrium Effects in NASP-Type Nozzles," AIAA paper 88-3263, 1988.

11. Rittenhouse, L.E., Whoric, J.M., and Wilson, D.R., "Experimental and Theoretical Results Obtained with a Linear MHD Accelerator Operated in the Hall Current Neutralized Mode," AEDC TDR 67-150, November 1967.

12. Boonjue, S., "Arc Heater Performance, Calibration, and Data Correlation," Master's Thesis, University of Texas at Arlington, August 1997.

13. Taylor, D., "Ejector Design for a Variety of Applications," Agardograph #163, November 1972.

14. Pope, A., and Goin, K., *High Speed Wind Tunnel Testing*, John Wiley & Sons, Inc, pp. 87-91, 1965.

15. MacDermott, W.N., Horn, D.D., and Fisher, C.J., "Flow Contamination and Flow Quality in Arc Heaters Used for Hypersonic Testing," AIAA paper 92-4028, July 1992.

16. Grey, J., "Thermodynamic Methods of High-Temperature Measurement," *ISA Transactions*, Vol. 4, No. 2, April 1965, pp. 102-115.

17. Boonjue, S.B., Roseberry, C.M., and Wilson, D.R., "Results from the Initial Operation of a Continuous-Flow Arc-Heated Hypersonic Propulsion Test Facility," AIAA Paper 96-4505, 1996.

18. Hruby, V., Kolencik, J., Annen, K.D., and Brown, R.C., "Methane Arcjet Experiments," AIAA paper 1997-2427, 1997.

19. Snavely, K., and Subramaniam, B., "Thermal Conductivity Detector Analysis of Hydrogen Using Helium Carrier Gas and HayeSep D Columns," *Journal of Chromatographic Science*, Vol. 36, April 1998.

20. Gallimore, S.D., Jacobsen, L.S., O'Brien, W.F., and Schetz, J.A., "Spectroscopic Investigations of Hydrocarbon- and Nitrogen-Based Plasmas for Supersonic Ignition," AIAA paper 2002-5247, 2002.

21. Anderson, R.P., Finke, J.R., and Taylor, C.E., "Conversion of Natural Gas to Liquids via Acetylene as an Intermediate," *Fuel,* Vol. 81, No. 7, pp. 909-925, May 2002.

22. Gladisch, H., "How Huels Makes Acetylene by DC Arc," Hydrocarbon Processing and Petroleum Refining, Vol. 41, No. 6, pp. 159-164, June 1962.

23. Holman, J.P., *Experimental Methods for Engineers*, 4th Ed., McGraw-Hill, pp. 50-57, 1984.

24. Poole, J., Personal Correspondance to Author

25. Dorf, R.C., Editor, *The Engineering Handbook*, CRC Press & IEEE Press, p542, 1996.

26. Palm, T., Buch, C., Kruse, B., and Sauar, E., “Green Heat and Power,” Bellona Report 3:1999.

27. Czernichowski, A., “Production of Hydrogen from CH_4, CO, or H_2S in Gliding Electric Discharges,”

28. Poole, J., Plasma Materials, Inc., Manchester, NH, US patent US4570048: “Plasma jet torch having gas vortex in its nozzle for arc constriction.” Issued February 11th, 1986.

29. Dessornes, O., and Bouchez, M., “Combustion Experiments of Liquid Kerosene and Hydrogen/Methane Mixing in a Dual Mode Ramjet,” AIAA paper 2005-3400, 2005.

BIOGRAPHICAL INFORMATION

Christopher Roseberry received a B.S. in Mechanical Engineering from Texas Tech University in 1988. He went on to perform low-speed wind tunnel experiments to investigate the airflow entering the frontal cooling openings of automobiles. His thesis reporting this investigation was titled "Automotive Cooling Airflow Correlations." In 1990, Christopher earned a Master of Science degree in Mechanical Engineering from Texas Tech University. He is licensed as a professional engineer in Texas. For more than a decade, he has been a full member of the American Society of Mechanical Engineers, and the American Institute of Aeronautics and Astronautics. In addition, he has been a primary author for three technical papers and secondary author for three others. His interest in aerodynamics began during his childhood. However, his interests have broadened over the years to include thermodynamics and materials. Christopher intends to develop inventions and technology to help make life better for humanity.